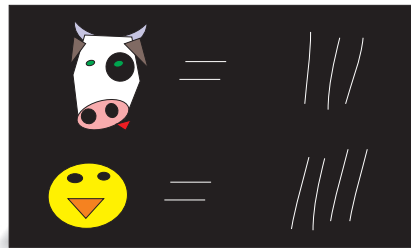


# Nanopores and Nanochannels Fabrication and Applications in Analytical Biochemistry and Colloid Science

Institute of Microtechnology,  
University of Neuchâtel, Switzerland

I am the *first*  
protein counting  
nanopore in  
silicon, next!



I am ovalbumin.

I am bovine  
serum albumin.

Anpan Han

2006



*... results indicate the high potential of this investigation method e.g. for label-free immunoassays ...*  
*Prof. Urs Staufer, Uni. Neuchâtel*



*... surface micromachining technology is exploited to create nanochannels with excellent channel uniformity...*  
*Prof. Thomas R. Ward, Uni. Neuchâtel*



*... les travaux de M. Anpan Han sont d'une grande originalité et d'un très haut niveau scientifique ...*  
*Prof. Nico de Rooij, Uni. Neuchâtel*



*... in particular the work of protein translocation and the experiment with antigen-antibody binding is very innovative and opens new perspective in the field of molecular recognition assay...*  
*Prof. Philippe Renaud, EPFL*

*... more work is needed but the first results are exciting ...*  
*Prof. Cees Dekker, Delft Uni. of Tech.*



# IMPRIMATUR POUR LA THESE

## Nanopores and Nanochannels - Fabrication and Applications in Analytical Biochemistry and Colloidal Sciences

**Anpan HAN**

---

UNIVERSITE DE NEUCHATEL

FACULTE DES SCIENCES


La Faculté des sciences de l'Université de Neuchâtel,  
sur le rapport des membres du jury

MM. U. Stauffer (directeur de thèse),  
N. de Rooij, T. Ward,  
C. Dekker (Delft NL)  
et P. Renaud (EPF Lausanne)

autorise l'impression de la présente thèse.

Neuchâtel, le 31 octobre 2006

UNIVERSITE DE NEUCHATEL  
FACULTE DES SCIENCES  
Le doyen  
Secrétariat-décanat de la faculté  
Rue Emile-Argand 11 - CP 158  
CH-2009 Neuchâtel



J.-P. Derendinger

### **Key words**

*Biotechnology, nanotechnology, nanofabrication, molecular probes, lab-on-chip,  
DNA analysis, protein analysis, single molecule analysis, immunoassay, coulter  
counter,  
electrophoresis, electroosmosis, colloid science, molecular interactions, capillary  
force, porous materials,  
electronbeam lithography, surface micromachining,  
silicon, silicon dioxide, silicon nitride,  
nanofluidics, nanopores, nanochannels*

### **Mots clés**

*Biotechnologie, nanotechnologie, nanofabrication, sondes moléculaires,  
laboratoire-sur-chip,  
analyse d'ADN, analyse de protéines, analyse de molécules isolées, immunoassay,  
compteur Coulter,  
électrophorèse, electroosmose, science colloïdale, interactions moléculaires, force  
capillaire, matériaux poreux,  
lithographie par faisceau d'électrons, microusinage de surface,  
silicium, oxyde de silicium, nitrure de silicium,  
nanofluidiques, nanopores, nanocanaux*



## Preface – thesis outline

In this thesis, a presentation of nanopores and nanochannels will be given with the emphasis on fabrication as well as applications. Nanopores and nanochannels are the basic building blocks of fluidic devices with dimensions in the nanometer range. The major applications of such nanofluidic devices are to study and carry out analysis of biological molecules such as DNA and proteins. Taking the advantage of having comparable dimensions as single biomolecules, new and outperforming devices based on nanofluidics could be constructed to study and analyze one molecule at a time. A motivation and brief literature overview on single molecule experiments and analysis will be given. To have an idea of the physical forces and transport mechanisms inside nanopores and nanochannels, selected models will be presented and discussed in the framework of this thesis.

Despite the similar dimensions, the development of nanopores and nanochannels has been very different. The research and development of nanopore based devices accelerated after Meller et al. showed that DNA with different sequence could be distinguished (Meller, 2000). The investigators proposed that there was a possibility to sequence DNA using just one molecule. The drive to sequence DNA using nanopores also showed that they are very powerful single molecule probes. A short communication reports for the first time the interactions between synthetic nanopores and proteins (Chapter 4). A manuscript under preparation describes such interaction under different environmental conditions. To illustrate the capabilities of nanopore sensing, a protein-protein affinity assay which did not require any labeling was demonstrated (Chapter 5). The nanopore fabrication process developed at IMT is included in the above paper and manuscript and critical steps are described in detail in the appendix.

Unlike nanopores, the development efforts of nanochannels have been broader and acquired a more diversified application profile. An introduction is given in single molecule analytical biochemistry and the other promising application of nanofluidic devices - colloid science. Recent developments in nanofabricated devices present a new experimental platform for colloid science, which was previously unavailable. A part of the author's work at IMT was a subject in colloid science; the filling of nanochannels by capillary force (Chapter 7). The nanochannel fabrication process developed at IMT is also presented (Chapter 8).

To be able to have a good understanding of the contents of this thesis basic knowledge in microfabrication (Madou, 2002) and cell biology (Alberts, 1998) is recommended.

*whole day without eating,  
and the whole night without sleeping,*

*thinking did I,  
waste,  
to learn is wiser.*

*elements of the analects of Confucius  
understood and translated by Anpan Han*

# Table of Contents

<b>CHAPTER 1 : INTRODUCTION.....</b>	<b>1</b>
NANOPORES AND NANOCHANNELS .....	1
SINGLE MOLECULE EXPERIMENTS AND ANALYSIS.....	2
<b>CHAPTER 2 : SELECTED MODELS IN NANOFUIDICS.....</b>	<b>4</b>
LAMINAR FLOW .....	4
THE ELECTRIC DOUBLE LAYER.....	4
ELECTROPHORESIS, ELECTROOSMOSIS.....	6
<b>CHAPTER 3 : DRIVE AND DEVELOPMENT OF NANOPORES .....</b>	<b>7</b>
COULTER COUNTERS - RESISTIVE PULSE SENSING .....	7
ION CHANNELS AND PATCH CLAMPING .....	7
DETECTING DNA MOLECULES USING ION CHANNELS - DNA SEQUENCING .....	8
SYNTHETIC NANOPORES .....	9
NANOPORES AS A MOLECULAR PROBE - MOLECULAR COULTER COUNTER .....	10
<b>CHAPTER 4 : PAPER 1, SENSING PROTEIN MOLECULES USING NANOFABRICATED PORES.....</b>	<b>13</b>
<b>CHAPTER 5 : MANUSCRIPT UNDER PREPARATION, DETECTING DIFFERENT PROTEIN MOLECULES USING SYNTHETIC NANOPORES AND APPLICATIONS IN LABEL-FREE MEASUREMENT OF MOLECULAR INTERACTIONS.....</b>	<b>17</b>
<b>CHAPTER 6 : NANOCHANNEL DEVICES – APPLICATIONS AND FABRICATION .....</b>	<b>35</b>
SINGLE MOLECULE ANALYSIS .....	35
APPLICATIONS IN COLLOID SCIENCE .....	36
<i>Filling of nanochannels by capillary force.</i> .....	37
FABRICATION STRATEGIES.....	37
<i>Surface machining</i> .....	37
<i>Bulk machining</i> .....	38
<b>CHAPTER 7 : PAPER 2, FILLING KINETICS OF LIQUIDS IN NANOCHANNELS AS NARROW AS 27NM BY CAPILLARY FORCE .....</b>	<b>39</b>
<b>CHAPTER 8 : PAPER 3, DESIGN AND FABRICATION OF NANOFUIDIC DEVICES BY SURFACE MICROMACHINING .....</b>	<b>47</b>
<b>CHAPTER 9 : SUMMARY AND OUTLOOK.....</b>	<b>54</b>
<b>APPENDIX, CRITICAL STEPS OF NANOPORE FABRICATION .....</b>	<b>56</b>
LPCVD Si <sub>3</sub> N <sub>4</sub> .....	56
PRETREATMENT OF Si <sub>3</sub> N <sub>4</sub> BEFORE PMMA SPINNING: .....	56
E-BEAM WRITING PROCESS. ....	56
PATTERN TRANSFER FROM PMMA TO Si <sub>3</sub> N <sub>4</sub> BY REACTIVE ION ETCHING .....	57
<b>REFERENCES .....</b>	<b>59</b>
<b>LIST OF PUBLICATIONS .....</b>	<b>63</b>
<b>A NON-STANDARD ACKNOWLEDGEMENTS .....</b>	<b>64</b>
<b>BIOGRAPHY.....</b>	<b>66</b>

*is it not pleasant to learn and practice?*

*is it not delightful to have friends coming from distance?*

*not disturbed by the absence of recognition, a true gentleman.*

## Chapter 1 : Introduction

In the talk “There’s Plenty of Room at the Bottom” of 1959, the Nobel Laureate Richard P. Feynman described how miniaturization, the process of making things smaller, would influence our daily life, and that this process would continue until we have the control over the atoms. Indeed, miniaturization has an extreme impact on computer and information technology. Fueled by Moore’s Law, brave inventions and powerful tools developed side by side with semiconductor industry have enabled mankind to build structures on few tens of nanometers. Semiconductor based technology is finally approaching the dimensions of nature’s information storage, DNA, and nanometer-sized machines, proteins. The question is then, could we somehow investigate and analyze nature’s building blocks on a single molecule level using our man made counterparts.

### **Nanopores and nanochannels**

Since DNA and many proteins are in aqueous solutions in their native environment, the intuitive approach is to construct nanosystems which would allow fluids. The simplest closed fluidic system is a tube with a diameter,  $d$ , and length,  $l$ . Tubes could be divided into two categories, pores and channels. A channel has a large length to diameter ratio (Figure 1-1 a) and a pore has a ratio of about unity (Figure 1-1 b). In the case of pores, since it is often embedded in a membrane, the length of the pore will be equal

to the thickness of the membrane. Channels with circular geometry are ideal systems to model; however, most nanochannel fabrication technologies yield channels with a rectangular cross-section (Figure 1-1 c). Due to the nanometer dimensions, fabricating nanotubes could be extremely challenging and difficult. For example, nanopores have been constructed in silicon nitride using ion-beam sculpting or drilled in silicon oxide by high energy electrons (Li, 2001; Storm, 2003). As for nanochannel systems, advanced techniques such as nanoimprinting lithography have been used (Cao, 2002; Han, 2000). Despite the difficulties of nanotube fabrication, experiments in nanochannels and nanopores proved to be very promising.

To answer our question, indeed, nanofluidic systems allow the investigation and the analysis of nature’s building blocks. For example, nano-

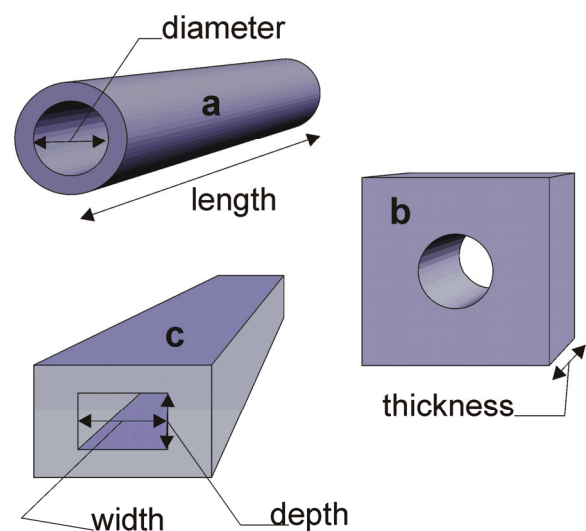


Figure 1-1. Illustration of channels with circular (a) and rectangular cross-section (c). A pore imbedded in a membrane (b).

channel devices could unfold natively coiled DNA, which enables the investigator to measure the length of single DNA molecules (Tegenfeldt, 2004) and study the binding sites of gene regulating proteins (Wang, 2005b). Using nanopore experiments, Meller et al. could distinguish single DNA molecules based on their sequence alone (Meller, 2000). Wang et al. reported a technology that integrates nanochannels into microfluidic devices, which could concentrate dilute protein solutions up to one million fold (Wang, 2005a). This technology could increase the detection limit of biochemical analysis by six orders of magnitude. Lower detection limits could be used to make diagnostics of disease at a very early stage, which then gives the physician longer time for intervention. Not only are nanofluidic devices a promising and powerful tool to analyze single biomolecules, they have great potential as a new technological platform in many biotechnology applications.

### ***Single molecule experiments and analysis***

To understand the general philosophy and advantages of single molecule experiments and analysis, we go back in time. In the year 1674, for the first time, Anton Van Leeuwenhoek looked at and described the life inside a drop of water using a light microscope. About 200 years later, in the fairy tale story “A Drop of Water” by the Danish writer H. C. Andersen, life in a drop of water was not as harmonic and

common as seen by the naked eye. The Magician showed his friend, the Troll, through the magnifying glass a drop of water from the pond. In the drop of water people-like creatures were grabbing, stealing, and eating each other, a true chaos. Unaware of the function of the magnifying glass and that he was looking inside a drop of water; the Troll thought that it was a live picture of the City of Copenhagen.

Today, more than 300 years after the discovery of the light microscope, we constantly strive to look at life on a smaller scale - the scale of molecules. Powerful techniques such X-ray crystallography and nuclear magnetic resonance imaging are able to give atomic resolution of protein structures in three dimensions. Like most average measurements these techniques together with light scattering and gel electrophoresis give a picture of the average protein. The question is now, does the average protein represent well the ensemble of proteins. For large biomolecules such as DNA and proteins, the large degree of freedom of the internal molecular organization could cause subpopulations, or highly heterogeneous systems. Indeed, several studies showed that large DNA molecules show highly individual behavior. Using fluorescence single molecule imaging techniques, the unfolding of genomic  $\lambda$ -phage DNA in elongational flows showed large diversity (Perkins, 1994; Perkins, 1997; Smith, 1998). The investigators explained that due to that long DNA molecules can fold into many energetically favorable states, the unfolding of such

molecules will also need many different energies.

Apart from unmasking inhomogeneities in ensembles, experiments on the single molecule level have also given insight to the detailed operation mechanism of complex protein machines. Methods such as scanning force microscopes (SFM), optical and magnetic tweezers are used to directly probe intermolecular and intramolecular forces on a single molecule level (Bustamante, 2000). For example, using optical traps, Davenport et al. followed the movement of single *Escherichia coli* RNA polymerase proteins (Davenport, 2000) during DNA transcription. They observed that the movement was not continuous and uniform, but it included pauses and as wells as different speeds. Noji et al. showed the ATP hydrolysis mediated rotation of single F1-ATPase motor proteins, which ended the widely disputed question, if the motor-like protein could perform rotational movement (Noji, 1997). Using magnetic tweezers, it was proven that the same motor protein is also able to convert mechanical to chemical energy (Itoh, 2004). By measuring the fluorescence resonance energy transfer between two single fluorescent molecules attached to different parts of a protein, it is possible to determine the distance between the fluorescent molecules. This allows the study of how proteins are folded and their energy landscape (Weiss, 2000).

Indeed, investigating apparently pure and homogenous biomolecules using single mole-

cule techniques, we see the less chaotic H. C. Andersen picture of a droplet of water: a multitude of inhabitants working in their different way and personality. Although we must keep in mind that in many situations, the information on the single molecule level does not perfectly reflect the collective behavior of the ensemble. For example depending on the intermolecular organization of collagen proteins and its surrounding matrix, the collagen protein could form cartilage with different mechanical properties. The mechanical properties of cartilage on the micrometer scale is also different from the nanometer scale (Stolz, 2004)

The original idea formed at the IMT, was to construct a sophisticated nanofluidic device, which both included nanopores and nanochannels. This device would benefit from the advantages provided by the two. The main application of such a device was to analyze single biological molecules. As the reader will discover in the following chapters the fabrication technologies for the nanopores and nanochannels are very different which makes an integrated device very complicated and difficult to realize. However, as the work at IMT progressed, the main challenge became the understanding of what is happening at the nanoscale. The integrated device was never realized. Nevertheless, like many other investigators, efforts in nanopores and nanochannels at the IMT showed that nanofluidics have great potentials both in single molecule analysis and colloid science.

## Chapter 2 : Selected models in nanofluidics

Before entering the fabrication and experiment details in nanofluidic devices, I believe that it is necessary to have an idea of the physics and chemistry taking place inside such devices. Much of the theory involving interactions in liquids on the nanometer scale have been developed in the field of colloid science. Referring to Shaw (Shaw, 1989), Probst (Probst, 2003) and Hunter (Hunter, 1981), in this section, I selected and summarized relevant models to describe different transport mechanisms and forces acting on biomolecules inside nanofluidic devices.

All fluidic systems modeled in this section are idealized by making the *continuum approximation*: the liquids, surfaces, and molecules modeled are continuous and indefinitely divisible. Since this thesis involves phenomena in the nanometer range, where structures and fluids are only a few hundred to few thousand layer of molecules, one could question the continuum approximation. The threshold of the transition between continuum and discrete is not clear. According to a review by Eijkel and van den Berg (Eijkel, 2005), idealized systems above 2 nm could be modeled using the continuum approximation. Indeed, continuum theory has successfully been used to model colloidal systems, which dimensions are comparable to those in this thesis.

### **Laminar flow**

The nature of flow inside a tube filled with a liquid with the density  $\rho$ , viscosity  $\eta$ , moving with the speed  $v$ , could be determined by calculating the dimensionless Reynolds number

$$\text{Re} = \frac{\rho v d}{\eta} \quad (\text{Eq. 1})$$

For Reynolds numbers below unity the flow is laminar, and for high values the flow has a turbulent nature. For a water filled tube with a diameter of 100 nm, to have a Reynolds number above one, the average flowrate has to be larger than 1 m/s. A flow could be generated by the application of a pressure difference. Poiseuille's equation relates the hydrostatic pressure drop,  $\Delta P$

$$\Delta P = \frac{32\eta l v}{d^2} \quad (\text{Eq. 2})$$

Assuming an average flowrate of 1 m/s and a tube length of 100 nm the pressure drop is equivalent to 30 bars. Hence, under atmospheric pressure conditions, flows in nanotubes have a laminar nature.

### **The electric double layer**

In many nanofluidic experiments aqueous buffers are used as the solvent and silicon dioxide ( $\text{SiO}_2$ ) is used to construct the fluidic device. At the interface an *electric double layer* (EDL) is formed. At pH 7 upon contact with water, the  $\text{SiO}_2$  surface exposing silanol groups becomes negatively charged. To maintain overall charge-neutrality the surface charges attract ions of the



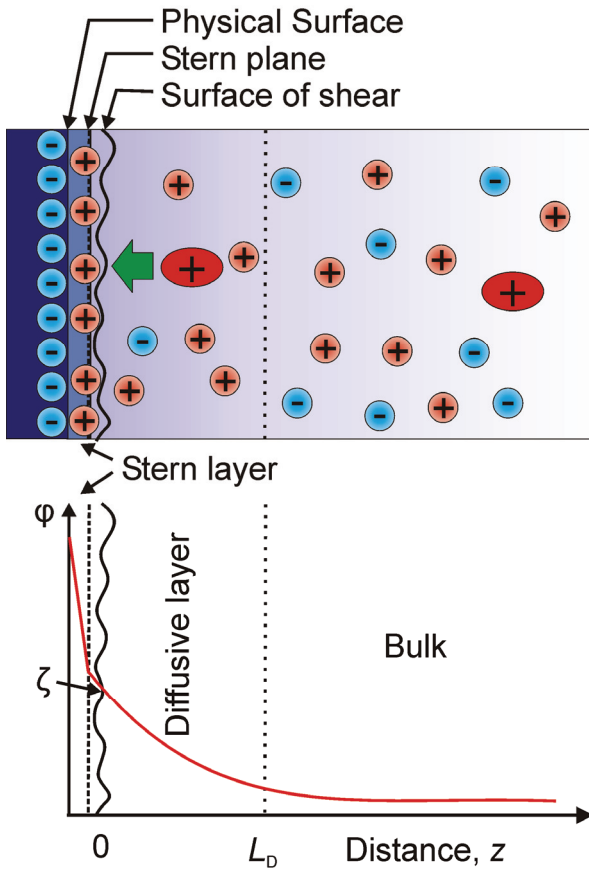


Figure 2-1. Schematic representation of the structure of the electric double layer. Redrawn from “Introduction to Colloid and Surface Chemistry” by D.J. Shaw (Shaw, 1989)

opposite valence, cations in the case of  $\text{SiO}_2$ . As more cations balance the negatively charged surface, the electrostatic force decreases. The EDL is the layer of water containing an excess of either cations or anions which balance the surface charge. A schematic drawing of the double layer is given by Shaw (Figure 2-1). It is divided into two layers, the *Stern layer*, which is the molecular layer of cations adsorbed to the negatively charged surface, and the *diffusive layer* which expands into the solution. The distribution of charges generates an electric

potential,  $\phi$ . The Debye-Hückel approximation for  $\phi$  is given by,

$$\phi = \frac{\sigma L_D}{\epsilon} \exp(-z/L_D) \approx \zeta \exp(-z/L_D) \quad (\text{Eq. 3})$$

Where  $\sigma$  is the surface charge density, which depends strongly on the pH,  $z$  is the distance from the surface (Stern plane),  $\epsilon$  is the dielectric permittivity, and  $L_D$  is the thickness of the double layer, also referred as the Debye length.  $\zeta \approx \sigma L_D/\epsilon$  is the *zeta potential*, which is defined as the potential at the location where the molecules could “slip” or flow past the charged surface; the *surface of shear* (Figure 2-1). The Debye-Hückel approximation states that the potential decreases exponentially from the surface with a decay constant of  $L_D$ , i.e. the electrostatic force between a charged biomolecule and a surface is strongest if the distance between the two is less than  $L_D$ . This force could be neglected if the molecule is far, i.e. several  $L_D$  away from the surface. For an aqueous solution containing ion pairs with the same number of charges, e.g. KCl ( $\text{K}^+$ ,  $\text{Cl}^-$ ), the Debye length is given by,

$$L_D = \left( \frac{\epsilon R T}{2 F^2 q^2 c} \right)^{1/2} \quad (\text{Eq. 4})$$

Where  $c$  is the concentration,  $q$  is charge number,  $R$  is the gas constant,  $T$  is the absolute temperature and  $F$  is the Faraday constant.  $L_D^2$  is inversely proportional to the ion concentration of the liquid. For KCl; 1M:  $L_D = 0.3$  nm, 100 mM:  $L_D = 1$  nm, 10 mM:  $L_D = 3$  nm, 1mM:  $L_D = 10$  nm.

### **Electrophoresis, electroosmosis**

Apart from transport of material inside a tube by pressure driven flow, if the liquid is an aqueous solution the transport could also be facilitated by applying an external electric field tangential to the tube wall - *electrophoresis and electroosmotic flow* (EOF). Electrophoresis is defined as the movement of a charged surface relative to a stationary liquid, while EOF is the flow of liquid relative to a stationary charged surface. Hence, only the choice of reference differs electrophoresis from electroosmosis (Shaw, 1989).

Starting with electrophoresis, for small molecules with radius,  $r_m$ , significantly smaller than  $L_D$ , molecules could be considered as point charges. The electrostatic force acting on the molecule is given by  $F_L = qe_0 E_x$ , where  $E_x$  is the external field and  $e_0$  is the elementary charge. The force acting on the molecule creates a movement, and since the molecule moves relatively to a viscous medium, a drag counteracts this displacement. In the steady state situation, the electrostatic force is balanced by the Stokes drag. Assuming that the molecule has the shape of a sphere and that the flow is of non-slip nature, the drag is given as  $F_{drag} = -6\pi\eta r_m v_e$ , where  $v_e$  is the electrophoretic velocity of the molecule. Balancing the electrostatic force and the Stokes drag, solving the velocity yields the Hückel equation.

$$v_e = \frac{qe_0}{6\pi\eta r_m} E_x = \mu_e E_x \quad (\text{Eq. 5})$$

Where  $\mu_e$  is the electrophoretic mobility, which could also be expressed in terms of the zeta potential,  $\mu_e = \epsilon\zeta/1.5\eta$ . In the case of very large molecules, where the Debye length is very small compared to the radius of the moving object, the velocity  $v_{EOF}$  of is given by the *Helmholtz - Smoluchowski* equation

$$v_{EOF} = \frac{\epsilon\zeta}{\eta} E_x \approx \frac{\sigma L_D}{\eta} E_x \quad (\text{Eq. 6})$$

The velocity is proportional to the surface charge density of the molecule, which is strongly dependent on the pH. At the isoelectric point, the surface charge density and the  $v_{EOF}$  would be zero. This is true for proteins with diameters in the range of 5-10 nm, dissolved in a 1 M KCl solution ( $L_D = 0.3$  nm).

Changing the reference frame, the walls of a tube filled with water are used as the stationary charged surface; the external electrical field displaces the mobile ions in the EDL. The moving ions drag the water molecules and create a flow parallel to the walls: electroosmotic flow (EOF). The direction of the EOF is determined by the polarity of the surface charge on the walls. In the case of  $\text{SiO}_2$ , at pH 7, the direction of EOF would be towards the negatively biased electrode, because cations which balance the negative silanol groups are driven towards the negatively biased electrode. The flow profile of the EOF inside a tube can be solved numerically. Far away from the double layer the EOF velocity is given by (Eq. 6). This is not surprising due to the symmetry of electrophoresis and electroosmosis.

## **Chapter 3 : Drive and development of nanopores**

Chapter 1 introduced the nanopore as a platform to make analysis on the single molecule level, and discussed the advantages of single molecule analysis. In this chapter a literature overview will be given on the drive and development of nanopores and their applications, from the Coulter counter, patch clamping, the first ion channel-DNA interactions, to the possible application as an economical way to sequence DNA. Its potentials as a single molecular probe will also be discussed. The development of nanopores has been driven by technological progress as well as social and public interest. Please also refer to a review by Bayley and Martin (Bayley, 2000) for more information on this subject.

### ***Coulter counters - resistive pulse sensing***

The simple and elegant idea of detecting particles passing through a pore has its origin from the Coulter Counter device invented in the 1950's (Coulter, 1953; Lines, 1992). An aperture, which size is slightly larger than the particle of interest, separates two chambers filled with buffer solution. The immersed electrodes in the two chambers create a current of ions through the aperture. As a particle passes through the aperture, the probe, the ionic current is partially blocked and this perturbation is measured. Commercial systems are available from Beckman Coulter, and they have been

used as a standard method to analyze the size distribution of particles above 400 nm. One of the greatest advantages of the Coulter Counters is that it could determine the volume of individual particles. The Coulter Counter is a single particle analyzer. In common with single molecule analysis it could obtain information that is not possible by average measurements. In the 1970s, by using sub-micrometer diameter pores prepared from nuclear track etched polymer sheets, Deblois and Bean, reported the detection of polystyrene particles with diameter of 60 nm (Deblois, 1970). The investigators named their technology "Nanopar Analyzer". A comparative study involving electron microscopy, Nanopar analysis, and light scattering spectroscopy of different virus particles was made (Deblois, 1978). While light scattering spectroscopy only yield average virus size, the resistive pulse sensing could resolve different sub-populations in a virus sample, which was in accordance with electron microscopy. This study showed the strength of the resistive sensing principle compared to average measurements.

### ***Ion channels and patch clamping***

The size of the molecule that could be detected using the resistive pulse sensing technique depends on the size of the aperture and the sensitivity of the current measurement technique. To detect biomolecule with dimensions below 10 nm, very small pores and sensitive

current measurement techniques are needed. With the advance in molecular biology and electrophysiology new tools are available to detect even smaller molecules.

Ion channels, being a few nm in inner diameter and similar in length, carry out vital functions for cells such as complex transport of different ions. (For an introduction to cell-membrane biology please refer to *Essential Cell Biology* (Alberts, 1998)). Sakmann and Neher received the Nobel Prize in 1991 for their discoveries concerning the function of single ion channels in cells. To do this they developed the *patch clamping* technique. The idea is to collect a very small piece, *patch*, of cell membrane using a micro-pipette, and then measure the current of ions passing through the ion channels under different stimuli. (For an introduction to patch clamping please refer to *Patch Clamping* (Molleman, 2003) and *The Axon Guide*, (Sherman-Gold, 1993).) Hence, both a new kind of pore, very small in diameter, and ultra sensitive current monitoring equipment is available to detect still smaller molecules using the Coulter approach.

### **Detecting DNA molecules using ion channels - DNA sequencing**

There are several variations of the patch clamping technique; one of them is the *lipid bilayer* setup. In lipid bilayer experiments a synthetic bilayer with a diameter of about 100  $\mu\text{m}$  is suspended in a holder, which separates two liquid reservoirs. Purified ion channel proteins are

added to one of the liquid reservoirs and they self-assemble into the bilayer. The embedded ion channel could then be studied. The first nanopore experiments were based on such bilayer experiments, where the ion channel functioned as the aperture or probe. Studies by Kasianowicz showed that a single stranded DNA molecule, ssDNA, which passed through an  $\alpha$ -hemolysin ion channel, perturbed the ion current through the pore (Kasianowicz, 1996). As the DNA is translocated through an ion channel, the ion current will decrease due to the DNA partially blocking the pore for a short period of time. The current and blockage time will depend on the size of the molecule and its chemistry. Experiments by Meller et al. showed that the signature depended on the sequence of the DNA (Meller, 2000). Based on these promising results and the Human Genome Project receiving great public interest, the idea to use the nanopore for DNA sequencing strongly promoted its further development.

The public interest for DNA sequencing, i.e. reading genetic information is tremendous. Genetic disease and other inherited features are encoded in DNA. The ultimate information for a physician and the pharmaceutical companies would be to design and select drugs for an individual based on the genes of that individual. However, the cost of sequencing would have to be drastically reduced. The goal is to bring the cost down to \$1000 (Constans, 2003) using novel technologies such as nanopores. Hence, enormous efforts have been dedicated to

achieve this goal. The success of these efforts will revolutionize medical diagnostics, the pharmaceutical industry as well as all life-related sciences.

### **Synthetic nanopores**

Biological pores have been used as probes in the first nanopore measurements. However, they have certain disadvantages such as instability and the requirement of difficult preparation steps. The idea is to implement a semiconductor device with a pore, which mimics the biological ion channel, while at the same time being more robust (Li, 2001; Storm, 2003). As discussed in Chapter 1, using semiconductors as the basis, advanced electronics from the computer industry could be added. Several approaches were used to fabricate such nanometric pores in synthetic materials (Table 1). Listed in Table 1 are the year of publication, the technology, the material of the pore, the

smallest diameter that was reported using the technology, and the length of the pore. The first synthetic pore, that was able to detect DNA, was reported by Li et al. (Li, 2001). The pore fabrication process is based on closing an existing pore by sputtering with feedback control (Li, 2001; Stein, 2004b). Using high energy electron beams (200 keV) it is also possible to drill 2 nm holes in 20-nm-thick silicon dioxide or silicon nitride membranes (Ho, 2005; Krapf, 2006; Storm, 2003; Wu, 2005). Organic materials have also been used, e.g. similar to the Nanopores (Deblois, 1970), Siwy et al. reported an improved fabrication of polyimide membranes with a single nuclear track etched pore (Siwy, 2003). Mara et al. then used these pores to detect DNA (Mara, 2004), and later Heins et al. detected porphyrin molecules (Heins, 2005). Ito et al. embedded multi-walled carbon nanotubes in epoxy resin to serve as pores (Ito, 2004; Ito, 2003). However, due to the relatively large in-

**Table 1. Nanopore fabrication technologies**

	<b>Year</b>	<b>Technology</b>	<b>Material</b>	<b><i>d</i> (nm)</b>	<b><i>l</i> (nm)</b>	<b>Reference</b>
<b>A</b>	1996	biological pore	$\alpha$ -hemolysin	1.5	5	(Kasianowicz, 1996)
<b>B</b>	2001	ion-beam sculpting	$\text{Si}_x\text{N}_y$	1	20	(Li, 2001)
<b>C</b>	2003	300keV TEM shrink	$\text{SiO}_2$	1	40	(Storm, 2003)
<b>D</b>	2003	300keV TEM drill	$\text{SiO}_2$	6	10	(Storm, 2003)
<b>E</b>	2003	SEM assisted hydrocarbon deposition	$\text{Si}_x\text{N}_y$	10	30	(Schenkel, 2003)
<b>F</b>	2003	preferential ion track etch	polyimide	2	-	(Siwy, 2003)
<b>G</b>	2004	FIB drill	$\text{Si}_x\text{N}_y$	25	10	(Tong, 2004)
<b>H</b>	2004	200 keV TEM drill	$\text{Si}_x\text{N}_y$	1	10	(Heng, 2004; Ho, 2005)
<b>I</b>	2004	alumina coating of nanopores	$\text{Al}_2\text{O}_3$	1	10	(Chen, 2004)
<b>J</b>	2006	200 - 300keV TEM drill	$\text{Si}_x\text{N}_y$	1	30	(Krapf, 2006)
<b>K</b>	2005	200 - 300keV TEM drill	$\text{Si}_x\text{N}_y/\text{SiO}_2$	1	40	(Wu, 2005)

ner diameter of the carbon nanotubes, sensitivity is less impressive. Nevertheless, if single walled carbon nanotubes are used, sensitivity could be increased. Common for all reported nanopore fabrication technologies listed in Table 1, one pore is fabricated at a time, which is often labor intensive and time consuming.

### ***Nanopores as a molecular probe - molecular Coulter Counter***

The development of synthetic nanopores has been driven by the goal of DNA sequencing using a single molecule. Research efforts also showed that nanopores proved to be a powerful tool as a molecular probe - *a molecular Coulter Counter*. There is a clear advantage of nanopore measurements compared to fluorescence or SFM measurements (Chapter 1): the requirement of labeling of the molecule being investigated is made superfluous. For fluorescence and SFM measurements the labeling procedure is critical. For example the labeling of antibodies could remove their binding capability (Kricka, 2005). For many SFM experiments random labeling is used. In this case, it is very difficult to know how many molecules are attached to the label. Another important advantage of the nanopore approach is the simplicity of the measurement setup. To detect single fluorescence molecules sophisticated and expensive microscopes are needed. For nanopore experiments the measurement setup only requires sensitive electronics. The

removal of the label and less expensive measurement setup greatly reduce the time and cost.

The molecule which has been subjected to numerous studies is, to no surprise, DNA. Both ssDNA (Fologea, 2005a) and double stranded DNA, dsDNA, (Li, 2003a; Mara, 2004; Storm, 2005a) have been probed by artificial nanopores. Li et. al. observed, that depending how DNA was folded while entering the pore, different current signatures were obtained (Li, 2003a). Storm et al. reported longer DNA molecules needed more time to pass through the pore (Storm, 2005a; Storm, 2005b). Studies on how experimental conditions affect the translocation have been reported. Measurement, made under different ion concentrations, showed that the conductivity change due to the translocation of DNA molecules could be both negative and positive (Chang, 2004; Smeets, 2006). Chang et al. and later Smeets et al. explained this phenomenon (Chang, 2004; Smeets, 2006); the current change observed during the translocation is the sum of two effects. Firstly, the DNA inside a nanopore blocks the ion current. Secondly, the positive ions, that screen the negative charges of the DNA backbone, are also introduced into the pore. At high ion concentrations the first effect dominates, and a decrease in current was observed. As the ion concentration decreases, the introduced screening ions surpass the blocked ions, which results in a net current increase. Fologea et al. showed that the translocation time could be increased by a factor of ten by changing the environmental conditions



(Fologea, 2005b). The increase of the viscosity by adding glycerol increased the translocation time. The temperature had a minor effect while the driving electrical field had a strong influence. However, increasing the translocation time often came at the sacrifice of signal to noise ratio.

Several future applications have been proposed apart from DNA sequencing. Storm et al. suggested that since the translocation time depended on the length of DNA, nanopores could be used as an alternative to gel electrophoresis to determine DNA size. Another interesting observation is made by Wang et al.: ssDNA translocations showed larger variations if ssDNA was chemically treated or stored over a long period of time (Wang, 2004). Wang et al. proposed that this could be for example used as a method to access the quality of ssDNA.

Other small molecules have also been detected (Table 2). In the same table the pore fabrication technology are also included. From Table 2, DNA with molecular weight ( $M$ ) between 15 kDa to 4.5 MDa could be detected using artificial nanopores. The time resolution, which is the inverse of the low-pass filter bandwidth  $B$ , and the relative current drop,  $\Delta I/I$ , are inferior to experiments using biological pores. Fologea et al. showed that if signals with shorter duration than  $1/B$  are filtered with the bandwidth  $B$ , the magnitude of the signal will be attenuated, but the duration will remain correct. Nevertheless, for most experiments the

time resolution has been ten times smaller than the typical translocation time,  $T$ .

One of the missing family of molecules in Table 2 is the proteins. One could imagine that nanopores are ideal to study the micro-heterogeneity of proteins. The origin of the heterogeneity of protein is attributed to their size and synthesis. Proteins have molecular weight between a few kg/mol (kD) e.g. lysozym and several hundreds of kD e.g. catalase. The hydrodynamic diameters of proteins are typically between 1 and 10 nm, although, large protein complexes could be significantly larger. Larger molecules have larger probability to exist in several energetically favorable conformations. Proteins are synthesized through a cascade of process, variations can not be avoided. An introduction to the synthesis of proteins from a template DNA could be found in “Genes VII” (Lewin, 2000).

In this thesis, efforts have been put into the fabrication of nanopores with the specific purpose to detect globular protein molecules on the single molecule level: a molecular Coulter Counter for proteins. The initial findings are described in Chapter 4. In Chapter 5, we detected five different proteins using an optimized nanopore design. Experiments were carried out at different pH showed micro-heterogeneity, in apparent pure samples. The size of proteins was reproducibly determined. Finally, we illustrated unique applications of nanopores by a proof-of-concept antibody-antigen binding assay, which did not require any labels or amplification steps.

**Table 2. Molecules probed using different technologies**

<b>Molecule</b>	<b>Reference</b>	<b>Year</b>	<b>Tech</b>	<b>M(kD)</b>	<b><i>d</i> (nm)</b>	<b><i>l</i> (nm)</b>	<b><math>\Delta I/I</math></b>	<b><math>1/B</math> (<math>\mu</math>s)</b>	<b><i>T</i> (ms)</b>
ssDNA	(Kasianowicz, 1996)	1996	A	40	1.5	5	0.5	40	1
ssDNA	(Meller, 2000)	2000	A	33	1.5	5	0.5	10	1
ssDNA	(Wang, 2004)	2004	A	23	1.5	5	0.25	10	1
ssRNA	(Butler, 2006)	2005	A	23	1.5	5	0.25	20	1
Peptides	(Sutherland, 2004)	2004	A	0.5	1.5	5	0.5	100	6
dsDNA	(Li, 2003a)	2003	B	2000	3	10	0.1	100	1
dsDNA	(Storm, 2005a)	2005	C	4500	10	20	0.05	100	0.1-6
dsDNA	(Mara, 2004)	2004	F	660	4	-	0.5	100	5
Porphyrin	(Heins, 2005)	2005	F	15	4.5	-	0.01	100	100
ssDNA, dsDNA	(Heng, 2004)	2004	H	16	1	10, 30	0.5	100	3
ssDNA	(Fologea, 2005a)	2005	B	2000	4	10		100	0.1-1
dsDNA	(Peng, 2004)	2004	I	2000	15	40		100	1
dsDNA	(Smeets, 2006)	2006	J	29000	10	20	0.05	100	1



## **Chapter 4 :**

### **Paper 1,**

## **Sensing Protein Molecules Using**

## **Nanofabricated Pores**

A. Han, G. Schürmann, G. Mondin, R. Bitterli, N. Hegelbach, N. F. de Rooij, and U. Staufer

Applied Physics Letters, 2006, 88, 093901

Reproduced from Applied Physics Letters. 88, 093901, copyright 2006,

American Institute of Physics

*to know what you know*

*and*

*to know what you do not know*

## Sensing protein molecules using nanofabricated pores

Anpan Han, Gregor Schürmann, Giampietro Mondin, Roland Andreas Bitterli, Nicole G. Hegelbach, Nico F. de Rooij, and Urs Staufer<sup>a)</sup>

*Institute of Microtechnology, University of Neuchâtel, Rue Jaquet-Droz 1/C.P. 3, CH 2007 Neuchâtel, Switzerland*

(Received 23 August 2005; accepted 18 January 2006; published online 28 February 2006)

We report the detection of protein molecules with nanofabricated pores using the resistive pulse sensing method. A 20-nm-thick silicon nitride membrane with a nanofabricated pore measuring about 55 nm in diameter separated an electrolyte cell into two compartments. Current spike trains were observed when bovine serum albumin (BSA) was added to the negatively biased compartment. The magnitude of the spikes corresponded to particles 7–9 nm in diameter (the size of a BSA molecule) passing through the pore. This suggests that the current spikes were current blockages caused by single BSA molecules. The presented nano-Coulter counting method could be applied to detect single protein molecules in free solution, and to study the translocation of proteins through a pore. © 2006 American Institute of Physics. [DOI: 10.1063/1.2180868]

The resistive pulse sensing method, also referred to as the Coulter principle,<sup>1</sup> is one of the standard methods to size and count particles. An aperture, which size is slightly larger than the particles of interest, separates two chambers filled with buffer solution. The electrodes in the two chambers create a current of ions through the aperture. As a particle passes through the aperture the ionic current is blocked and this perturbation is measured.<sup>2</sup> Commercially available systems are able to detect particles down to 400 nm.<sup>3</sup> The same approach was used to detect single deoxyribonucleic acid (DNA) molecules. Since the size of the aperture must be comparable to the DNA molecules both membrane proteins<sup>4–6</sup> and nanofabricated pores with diameter below 10 nm (Refs. 7–11) have been employed. Theoretical models and molecular dynamic simulations have been used to study the translocation mechanism.<sup>12,13</sup> The translocation of the much larger and more complex group of biomolecules, proteins, is observed in protein conducting channels situated, e.g., in the nuclear membrane and endoplasmic-reticulum.<sup>14,15</sup> To our knowledge, sensing of unlabelled proteins in the size range of 10 nm using a synthetic nanopore has not been reported. In this letter, we report the observation of current spikes caused by the interaction of BSA with a nanopore. We also show strong evidence that the spikes are caused by the translocations of single molecules.

The nanopore fabrication is different from previous reported work.<sup>9,10,16,17</sup> We started with coating a 100 mm diameter, <100>, double-side polished silicon wafer on both sides with a 20-nm-thick layer of silicon nitride (Si<sub>3</sub>N<sub>4</sub>). The pores were defined using electron-beam lithography into a poly(methyl methacrylate) layer spun onto the front side and then transferred into the under laying Si<sub>3</sub>N<sub>4</sub> with reactive ion etching. Finally, potassium hydroxides etch from the back side created a free-standing membrane with one, two, four, or nine pores. The pore, observed using transmission electron microscopy, had an elliptical shape with, respectively, a major and minor diameter of 58 and 50 nm. Each membrane was situated in the middle of an 8 × 8 mm chip. To reduce

the noise during current measurements, a 300- $\mu$ m-thick polydimethylsiloxane (PDMS) sheet with a 200- $\mu$ m-diameter hole was prepared and sealed onto the silicon chip such that the membrane was under the hole in the PDMS sheet.<sup>17</sup>

A chip was then mounted into a homebuilt holder (Fig. 1), and the Ag/AgCl electrodes were connected to a patch clamp amplifier (Axopatch 200B, Axon Instruments). The data acquisition was done using a data acquisition card from National Instruments, and LABVIEW software was used to control the data acquisition card and signal processing.

The resistance of a chip is the sum of the resistance of the silicon nitride membrane with pores embedded and the access resistance, which depends, e.g., on the electrodes. By measuring and fitting the resistance of chips with different number of pores, we obtained the access resistance (230 k $\Omega$ ) and the resistance per pore (2.29 M $\Omega$ ). Using the model reported by DeBlois *et al.*<sup>18</sup> and Ito *et al.*,<sup>17</sup> the resistance,  $R$ , of a pore, having length  $l_p$  and diameter  $d_p$  filled with saline solution with conductivity  $\kappa$ , is given by

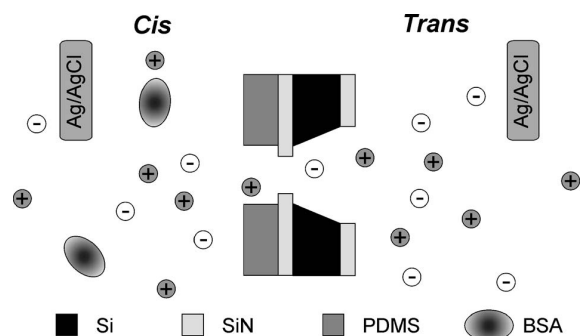


FIG. 1. Cross-sectional illustration of the experimental setup. The nanofabricated chip in the middle of the figure separates the *cis* and the *trans* chambers filled with 1 M KCl, 10 mM Tris, pH 8. Using Ag/AgCl electrodes connected to a patch clamp amplifier, an electric field can be applied across the membrane in which a single nanopore was embedded. The current was recorded as BSA was added to the *cis* chamber. Note that the illustration is not drawn to scale.

<sup>a)</sup>Author to whom correspondence should be addressed; electronic mail: urs.staufer@unine.ch

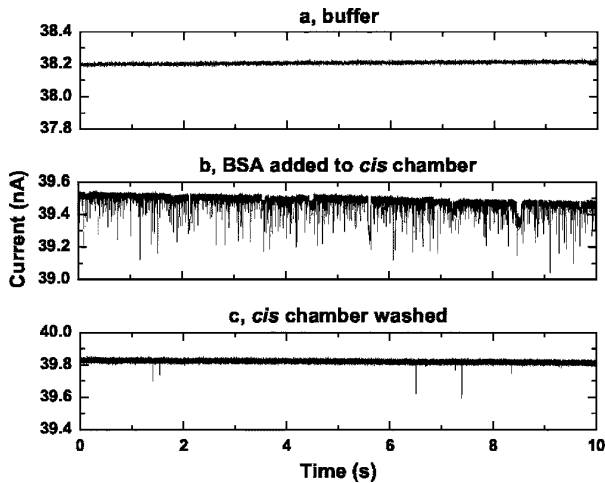


FIG. 2. Ionic current measurements through a nanopore at 100 mV. Figure (a) shows the current when both chambers were filled only with buffer. In (b), BSA was added to the *cis* chamber, and in (c) BSA was removed by washing.

$$R = \frac{4(l_p + 0.8d_p)}{\kappa\pi d_p^2}. \quad (1)$$

Using the above model a resistor of 2.3 M $\Omega$  corresponds to a pore 57 nm in diameter and 20 nm thick filled with our buffer (Conductivity: 110 mS), which is in good agreement with the pore dimensions measured by transmission electron microscopy. This also confirmed that the currents we measured were indeed through the nanopore and not caused by, e.g., leakage in the setup.

Using a chip with a single pore, we made an experiment comprising of three sequences; first, we filled both reservoirs (0.3 mL) with buffer solution, then we added bovine serum albumin (BSA) to the *cis* chamber, and finally we removed the BSA by washing the *cis* chamber. After each sequence, we measured the current through the nanopore when the voltage between the *trans* and *cis* electrodes was set to  $-100$  mV, and then 100 mV. When the reservoirs were filled with buffer the current through the nanopore at 100 mV was measured to about 40 nA [Fig. 2(a)], and  $-40$  nA if the voltage was set to  $-100$  mV. Upon addition of BSA, such that the concentration in the *cis* chamber was 1.5  $\mu$ M, and setting the voltage to 100 mV, we observed current transients with magnitudes up to  $-400$  pA [Fig. 2(b)]. For  $-100$  mV, we observed a few spikes with a lower magnitude of about 50 pA. After rinsing the chip in buffer, only a few spikes were observed [Fig. 2(c)].

We extracted the amplitudes and the duration of spikes which blocked more than 100 pA of current and were less than 4 ms long. We selected the threshold to be  $-100$  pA for two reasons; first, the spike should be significantly larger than the background noise, and second the magnitude is larger than the few small spikes observed when the *trans* chamber was negatively biased. Similar events in DNA translocation measurements are interpreted as collisions between DNA molecules and the nanopore.<sup>4</sup> Statistical analysis of 548 events (Fig. 3) showed that 85% of the current transient lay between  $-100$  and  $-200$  pA and the duration of most spikes (80%) are in the range below 0.5 ms. To reduce the noise level, we used a low-pass filter at 5 kHz, which gave a time resolution of 0.5 ms. Hence, the shape of spikes with

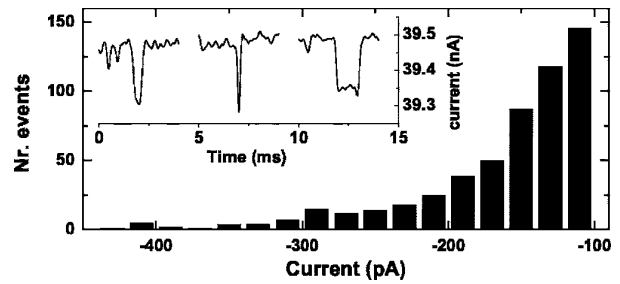


FIG. 3. Spikes counted during 30 s, with magnitude of above  $-100$  pA and duration of less than 4 ms. Inset shows three current spikes with different shapes at high time magnification.

durations less than 0.5 ms would be seriously distorted. Current transients longer than 1 ms often showed the characteristic well-shape with a flat bottom (Fig. 3 inset), which is frequently observed in DNA translocation measurements.<sup>4,5,11</sup> However, current transients shorter than 1 ms do not have a flat bottom, which is probably due to the filtering. Limiting the statistical analysis to a subset of peaks longer than 0.5 ms showed that 80% of them had a magnitude between  $-100$  and  $-200$  pA, which is identical to the distribution of the entire data set.

If the spikes we observed were due to translocations of single BSA molecules, the current drop,  $\Delta I$ , could be used to estimate the diameter,  $d_m$ , of the BSA molecules. DeBlois *et al.*<sup>18</sup> reported that

$$d_m^3 = s \frac{\Delta I}{I} (l_p + 0.8d_p) d_p^2, \quad (2)$$

where  $I$  is the baseline current and the constant  $s$  is close to unity. Current drops of between 100 and 200 pA would correspond to particles between 7 and 9 nm in diameter, which is commensurate with the size of a BSA molecule.<sup>19</sup>

Based on the above results, we suggest that the current transients were caused by the interaction of BSA with the nanofabricated pore, and we propose the hypothesis that some of the current transients were caused by the translocation of single BSA proteins through the nanopore. The results shown in Fig. 2 indicate that the spikes in the current measurements are caused by the addition of BSA. Current transients were only present if the electrode in the *trans* chamber is positively biased. This agrees well with our interpretation. Since at pH 8 BSA, in its *N* form, has 18 negative charges in total,<sup>19</sup> and the negatively charged protein will be electrophoretically driven to the positively biased electrode. After the washing step, we observed only a few current transient, further supporting our interpretation that current transients were caused by BSA-pore interactions. Using Eq. (2), we estimated that current drops of 100–200 pA correspond to particles 7–9 nm passing through a 57 nm pore, which supports our hypothesis that some of the current transients are caused by single BSA molecules passing through a nanopore. A further support of our hypothesis stems from occasional base-line shifts of about  $-100$  to  $-200$  pA in magnitude, which could be caused by a single BSA molecule temporarily adsorbed to the inner wall of the pore (data not shown). However, we estimated that after the translocation measurements the BSA concentration in the *trans* chamber was extremely low (about 60 000 BSA molecules or  $3 \times 10^{-16}$  mol/L after 1 h of measurement), such that to di-

rectly verify the existence of BSA molecules would have been very challenging in itself. This issue will still have to be investigated in future. For DNA translocation measurements, such direct verification is done by using polymerase chain reaction, which is an extremely sensitive and selective method.<sup>5,9</sup>

In conclusion, for the first time, we could show the interaction of a protein (BSA) and a nanofabricated inorganic pore. By recording the ionic current through a nanopore, we observed current transients when we added the protein to one side of the pore. Current spikes were only observed when a positive potential was applied, which was expected, since BSA molecules are negatively charged at *pH* 8. The magnitude of the spikes corresponded to particles 7–9 nm in diameter passing through a nanopore.<sup>17,18</sup> This results suggest that some of the current spikes we observed were current blockage caused by a single BSA molecule passing through a nanopore. If indeed the current spikes were caused by single protein molecules passing through the pore, the Coulter principle could be applied to detect and screen unlabelled and unattached single proteins under physiological conditions.

The authors would like to thank the technical staff of ComLab, the joint IMT-CSEM clean room facility. Anpan Han also acknowledges the Danish Research Agency for the financial support (Grant: Internationaliseringsstipendium) for his PhD studies at IMT, University of Neuchâtel.

- <sup>1</sup>W. H. Coulter, U.S. Patent No. 2.656.508 (October 20, 1953).
- <sup>2</sup>R. W. Lines, in *Particle Size Analysis*, edited by N. G. Stanley-Wood and R. W. Lines (The Royal Society of Chemistry, Cambridge, 1992), p. 350.
- <sup>3</sup>H. Bayley and C. R. Martin, *Chem. Rev. (Washington, D.C.)* **100**, 2575 (2000).
- <sup>4</sup>A. Meller, L. Nivon, E. Brandin, J. Golovchenko, and D. Branton, *Proc. Natl. Acad. Sci. U.S.A.* **97**, 1079 (2000).
- <sup>5</sup>J. J. Kasianowicz, E. Brandin, D. Branton, and D. W. Deamer, *Proc. Natl. Acad. Sci. U.S.A.* **93**, 13770 (1996).
- <sup>6</sup>T. C. Sutherland, Y. T. Long, R. I. Stefureac, I. Bediako-Amoa, H. B. Kraatz, and J. S. Lee, *Nano Lett.* **4**, 1273 (2004).
- <sup>7</sup>A. J. Storm, C. Storm, J. Chen, H. Zandbergen, J.-F. Joanny, and C. Dekker, *Nano Lett.* **5**, 1193 (2005).
- <sup>8</sup>H. Chang, F. Kosari, G. Andreadakis, M. A. Alam, G. Vasmatzis, and R. Bashir, *Nano Lett.* **4**, 1551 (2004).
- <sup>9</sup>J. B. Heng, C. Ho, T. Kim, R. Timp, A. Aksimentiev, Y. V. Grinkova, S. Sligar, K. Schulten, and G. Timp, *Biophys. J.* **87**, 2905 (2004).
- <sup>10</sup>A. Mara, Z. Siwy, C. Trautmann, J. Wan, and F. Kamme, *Nano Lett.* **4**, 497 (2004).
- <sup>11</sup>J. L. Li, M. Gershow, D. Stein, E. Brandin, and J. A. Golovchenko, *Nat. Mater.* **2**, 611 (2003).
- <sup>12</sup>S. T. Cui, *Mol. Phys.* **102**, 139 (2004).
- <sup>13</sup>P. G. de Gennes, *Proc. Natl. Acad. Sci. U.S.A.* **96**, 7262 (1999).
- <sup>14</sup>S. M. Simon and G. Blobel, *Cell* **65**, 371 (1991).
- <sup>15</sup>J. O. Bustamante, J. A. Hanover, and A. Liepins, *J. Membr. Biol.* **146**, 239 (1995).
- <sup>16</sup>J. Li, D. Stein, C. McMullan, D. Branton, M. J. Aziz, and J. A. Golovchenko, *Nature (London)* **412**, 166 (2001).
- <sup>17</sup>T. Ito, L. Sun, and R. M. Crooks, *Anal. Chem.* **75**, 2399 (2003).
- <sup>18</sup>R. W. Deblois and C. P. Bean, *Rev. Sci. Instrum.* **41**, 909 (1970).
- <sup>19</sup>D. C. Carter and J. X. Ho, in *Advances in Protein Chemistry* (Academic, San Diego, 1994), Vol. 45, p. 153.

## Chapter 5 :

**Manuscript under preparation,**

**Detecting Different Protein Molecules Using Syn-**

**thetic Nanopores and Applications in Label-free**

**Measurement of Molecular Interactions**

Anpan Han, Marc Creus<sup>†</sup>, Gregor Schürmann, Vincent Linder, Thomas Ward<sup>†</sup>, Nicolaas F. de Rooij and Urs Staufer\*.

Institute of Microtechnology, University of Neuchâtel, Rue Jaquet-Droz 1, P.O. Box 526, CH-2002 Neuchâtel, <sup>†</sup>Department of Chemistry, University of Neuchâtel, Av. de Bellevaux 51 / C.P. 2, CH-2000 Neuchâtel, Switzerland.

\*Corresponding author. E-mail: urs.staufer@unine.ch. Phone: +41 (0) 32 7205357. Fax: +41 (0) 32 7250711

### **Abstract**

Nanofabricated pores in 20-nm-thick silicon nitride membranes were used to detect five different proteins. A pore about 28 nm in diameter separated an electrochemical cell into two compartments, and the ion current through the pore was recorded. Addition of proteins to the chamber on one side of the pore, caused current perturbations that correlated with the size and charge of the proteins. In specific, the diameters of proteins were reproducibly determined with sub-nanometer accuracy. We illustrate the potential for unique applications of this novel nanotechnology with a proof-of-concept, ultra-sensitive protein-protein binding assay without any need for labels or amplification steps.

Detection of single biological molecules has become accessible in many laboratories using ultra-sensitive fluorescence microscopy (1-3), which, together with scanning probe microscopy (4), is able to reveal unique and hidden, inter- and intra molecular interactions and structural information, e.g. the rotational motion of F1-ATPase (5, 6). Nanopores offer an alternative for detection of single-molecules (7, 8). The principle of nanopore detection is known as resistive pulse sensing or Coulter principle (9). Commercially-available instruments can size and count particles down to 400 nm (10). An aperture only slightly larger than the particles of interest separates two chambers of an electrochemical cell. The immersed electrodes in the two chambers create an ion current through the aperture; as a particle passes through the aperture the ion current is partially blocked. The magnitude of the perturbation is proportional to the volume of the particle. Compared to fluorescence and scanning probe microscopy, nanopore sensing has certain unique and keen advantages: labeling of the molecules is unnecessary and the setup and instrumentation is simpler and more economical since no microscopes with active moving parts are needed.

Using the biological pore  $\alpha$ -hemolysin, Meller et al. could distinguish DNA which only differ in sequence (11). However, biological pores have practical limitations due to operating pH, temperature and fixed pore diameter; synthetic counter-parts, in contrast, are less affected by these parameters (8, 12-14). In spite of the apparent simplicity and elegance of the molecular Coulter counter, the only molecules that have been detected are DNA and porphyrin (15). Recently, we reported for the first time the detection of the protein bovine serum albumin (BSA) using nanopores fabricated by e-beam lithography (16). The initial findings did not answer our main important questions, which we address in this report; could we differentiate proteins? What happens at different pH? If we could sense size difference, it is then possible to detect molecular interactions, where a protein binds to another molecule?

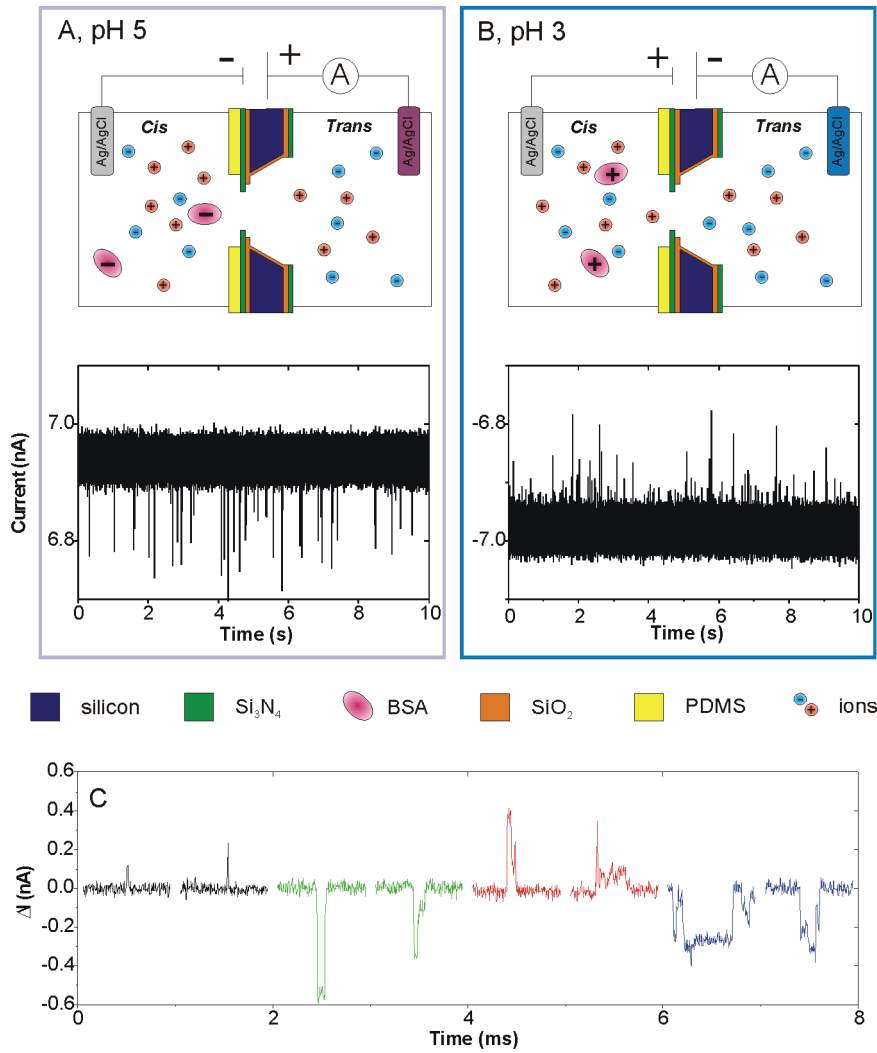


Fig. 1. Illustration of the experiment. After the insertion of a chip with an embedded nanopore, buffer solution (1M KCl buffered using 100 mM citrate or bis-tris propane) was added into both chambers, and the ion current was measured using a low-noise current amplifier. Measurement bandwidth was 100 kHz, at 10 kHz most spikes were not resolved. **(A)** at pH 5 BSA was added to the *cis* chamber, and valleys were observed in the current transient when the *trans* electrode voltage was set to 50 mV. Very few peaks were observed at -50mV. **(B)** at pH 3 we observed the contrary, peaks dominated at -50 mV compared to valleys at 50 mV. **(C)** High time resolution current trace of selected perturbation. Black line, BSA, pH 3, -50 mV, Green line: BSA, pH 5, 100 mV. Red line: streptavidin, pH 5, -100 mV. Blue line: streptavidin, pH 5, 100 mV.



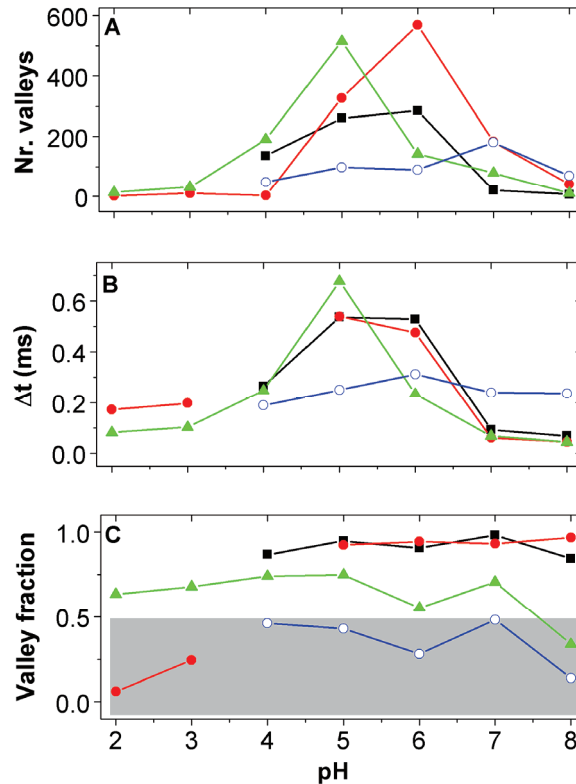


Fig. 2. (A) Number of valleys counted during 1 min for ovalbumin (black squares), BSA (red disc), streptavidin (green triangles) and avidin (blue circles) at different pH. Average duration  $\Delta t$  of spikes (B) Valley fraction,  $f_v$ , is given in (C) (see supporting materials).

In our previous report the magnitude of the current perturbations caused by the proteins were low, and the observed current transients had shorter duration than our time resolution (16); we therefore addressed these issues by increasing the general sensitivity of our system.

According to our estimation, at pH 8 a BSA molecule will pass through a 20 nm long nanopore in 2  $\mu$ s (see supporting materials). To measure 2  $\mu$ s current perturbations the necessary measurement bandwidth should be at least 1 MHz, which is 100 times higher than reported experiments using synthetic nanopores (13, 17, 18). To increase the time resolution we improved our nanopore design such that our measurement bandwidth increased from 5 kHz to 100 kHz, i.e. 10 times better time resolution compared to previous reports (13, 17, 18). Still, this improvement only provided a practical time resolution of 40  $\mu$ s. To further increase the resolution of translocation events we decreased the electrophoretic mobility ( $\mu_e$ ) of the protein by operating at a pH closer to the isoelectric point (pI) of the protein, where it has zero net-charge. We carried out measurements at various pH for four different proteins: ovalbumin (OA), avidin (AV) from egg white, BSA and recombinant streptavidin (SAV) from *Escherichia coli* (19). After adding a protein to the *cis* side of



the pore, current was recorded when the *trans* electrode was biased at +50mV and then at -50mV (an example for BSA is show in Fig. 1 A, B). We refer to spikes measured at positive voltage bias as *valleys* and spikes at negative voltage bias as *peaks*. Zooming in onto some of the spikes (Fig. 1 C), we observed that the spikes had different shapes. For BSA, at pH far away from the pI, most spikes were very sharp and the duration of such peaks was often less than 40  $\mu$ s. Hence, the true shape of the current perturbations could not be resolved at pH values far from the pI, whereas at pH closer to the pI, spikes had well shapes or more complex structures.

The number of detected valleys was plotted against the pH (Fig. 2 A). Each data point was based on the average value of three experiments made in three different pores. In total 12 different pores were used for the experiments in Fig. 2. Fig. 2 A shows the number of valleys counted during 1 min normalized to the protein concentration in the *cis* chamber ( $\mu$ g/ml). We did not have data for all pH, since at pH 2 and 3 OA and AV were not soluble (not shown). In Fig. 2 B we plotted the average duration of spikes ( $\Delta t$ ). To compare the number of peaks and valleys observed at the same pH, we plotted the fraction of spikes that were valleys,  $f_v = n_v / (n_p + n_v)$ , where  $n_v$  is the number of valleys and  $n_p$  is the number of peaks (Fig. 2 C).

We postulate that the spikes are caused by single protein molecules translocating through the pore. As the protein passes through the pore, ions are blocked, decreasing the absolute current and causing peaks in the current trace. Protein molecules with a negative net-charge will be driven to the positively biased *trans* electrode and then cause a current drop (a valley); conversely, positively charge proteins will be driven towards the negatively biased electrode. According to our postulation if  $f_v = 1$  then all proteins in a sample are negatively charged, if  $f_v = 0$ , then all proteins are positively charged, and if  $f_v = 0.5$  then half of the proteins are positively charged and the other half is negative. Our observations using BSA supported our interpretation that current perturbations are caused by translocating proteins, and they also justify our initial concerns that we must slow down the protein to be able to detect them. Firstly, the longest average spike duration for BSA were observed around the pI, where the proteins should have the lowest mobility; this observation was confirmed with OA. Secondly, at low  $\mu_e$  our electronics was then fast enough to detect protein translocations, therefore, we counted more spikes close to the pI. At pH far from the pI we only detect a fraction of the protein translocations. Fig. 2 shows for BSA that most spikes were detected at pH 6, while for high and low pH less spikes were observed. Also the average spike duration was largest for pH 5 and 6. At high pH, over 90 % of the spikes were valleys, whereas we observed mostly peaks at pH 2 and 3. We omitted the data for BSA at pH 4 because we only detected less than 10 spikes, since the confidence in these data was comparably low. Our results and interpretations for BSA agreed well

with previous reports; BSA is negatively charged at pH above 4.25 while positively charged below this pH (20, 21). The fact that the switch of polarity did not take place at pH 5.3, the pI measured by isoelectric focusing, is explained by BSA having high affinity towards anions (20-22). According to Scatchard et al. and Menon and Zydney at pH 5, while being slightly positively charged at 1 mM  $\text{Cl}^-$ , BSA binds up to 8  $\text{Cl}^-$  ions at 50 mM  $\text{Cl}^-$  resulting in a negative net-charge. Consequently, we interpret that at pH 4 BSA carried almost zero net-charge and was therefore marginally affected by the applied electric field, which agrees well with our observation that at pH 4 only few spikes were detected. From Fig. 2 A and using a 10  $\mu\text{g/ml}$  protein concentration, we found that the number of translocation events were about 5000 molecules/min, or 50 attomoles ( $10^{-18}$  moles)/hr; to our knowledge, unlike PCR for DNA, direct detection of such small amounts of protein remains a technical challenge. At present, we do not have a direct proof for protein translocations as in the case of DNA translocations experiment, where this was achieved by polymerase chain reaction (PCR) amplification of the DNA collected from the other side of the pore (7).

We expected AV, with a pI of 10.5, to be positively charged across the whole pH range. However, according to our results, AV only clearly showed a positive charge at pH 8, and the ratio  $f_v$  was about 0.5 for pH between 4 and 7. Although this finding was initially surprising, it may be explained by the fact that the avidin we used was highly heterogeneous both in terms of molecular weight and glycosylation (23), leading to a protein population with both positive and negative charge at the same pH. Homogeneous, nonglycosylated recombinant SAV (19) would be expected to switch polarity at pH 6 or 7 (calculated pI), but, puzzlingly, most SAV molecules appeared to maintain an over-all negative charge across the whole pH scale. Although our SAV was initially judged pure by SDS-PAGE and ESI-TOF mass spectrometric analysis, we then carried out isoelectric focusing experiments to measure the pI of SAV; to our great surprise, as with egg AV, this recombinant SAV contained several species with varying pI. Our results with avidin and streptavidin suggest that analysis based on the Coulter principle in nanopores is exquisitely sensitive to protein micro-heterogeneity, as measured in solution under non-denaturing conditions. Statistical analysis of the current change  $\Delta I$  of the valleys, i.e. depth of the valleys at pH 6 (Fig. 3) showed one clear maximum for OA and BSA, while the distribution for SAV was more broad. On average BSA caused a larger current drop than OA. This observation also supports our interpretation that each spike corresponded to a single protein translocation, since according to the Coulter principle larger molecules gives a larger current drop. We make statistical analysis for each experiment and the most frequent current drop  $\Delta I_{mf}$  were obtained, which was used to calculate the diameters ( $d_m$ ) of BSA and OA (Table 1). However, the values (7.3 nm and 8.6 nm) were significantly larger than those obtained from sedimentation equilibrium studies (5.4 nm and 7.1 nm)

(24),. The reason for these differences remain unexplained, but note that in our calculations we approximated that  $\Delta I_{mf}$  was directly proportional to  $d_m^3$ , and that the current drop we measured was the maximal current drop (see supporting materials). Nevertheless, we observed good reproducibility between experiments performed using different pores on different days. The variation of  $\Delta I_{mf}$  is equivalent to the upper limit of the variation of  $d_m^3$ . The 10%  $\Delta I_{mf}$  variation for a proteins 5.4 nm in diameter (OA) corresponds to just 0.2 nm variation in diameter. Hence, we could reproducibly determine the diameter of BSA and OA with an accuracy of 0.2 nm.

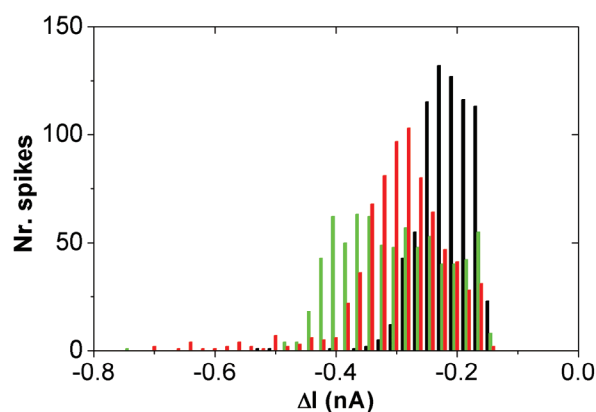


Fig. 3. Statistical analysis of current drop distribution of OA (black), BSA (red) and SAV (green) at pH 6. Driving voltage 100 mV, 750 events for each protein.

**Table 1. Base line current and current drop data, calculated values for pore and protein diameter.**

Pore	Protein	I (nA)	$d_p$ (nm)	$\Delta I_{mf}$ (nA)	$d_m$ (nm)
A	OA	10.7	21.9	0.21	7.1
B	OA	10.8	22.0	0.25	7.5
C	OA	14.0	26.3	0.23	7.3
D	BSA	14.0	26.4	0.31	8.6
E	BSA	14.5	26.5	0.27	8.7
F	BSA	15.9	28.9	0.31	8.8

\* Calculated values of pore diameter (see supporting materials)

Having established that several proteins could be detected using our nanopore and having investigated the detection characteristics according to protein size, pH/pI and micro-heterogeneity, we next explored a critical aspect of our research: are there any applications where nanopores show unmatched advantages? We tried to use the nanopore to detect specific protein-protein interaction; antigen – antibody binding. Abundance of the antigen beta human chorionic gonadotropin ( $\beta$ -hCG) in women's urine indicates pregnancy. In the first experiments we added monoclonal anti- $\beta$ -hCG

antibody from mouse (IgG) to the *cis* chamber to a final concentration of 4  $\mu\text{g/ml}$  at pH 6, and we measured the current. Then we washed the *cis* chamber and added a solution which both contained  $\beta$ -hCG and the antibody, which was incubated for over 1h at room temperature. To our surprise, only very few spikes were detected. To further investigate the specificity of this phenomenon, we repeated the experiment but this time we first added the antibodies (Fig. 4A), and then we then added OA (Fig. 4A). We observed large valleys -caused by antibody- and smaller valleys -caused by OA-. Then, we added  $\beta$ -hCG to a final concentration of 1  $\mu\text{g/ml}$ , at which point the large valleys could not be detected, whereas the small spike associated with OA remained (Fig. 4 C). From this latter experiment, we conclude first that the pore still remained functional after antigen addition, because we observed translocations of OA. Second, while the addition of OA did not affect the IgG translocation, the antigen strongly decreased the number of large valleys. Hence, the absence of valleys was caused by a specific interaction between antibody and antigen. Since,  $\beta$ -hCG has a molecular weight of about 20 kDa and IgG about 150 kDa, and there are 2 binding sites per IgG, then we would expect full saturation of the antibody (4  $\mu\text{g/ml}$ ) at around 1  $\mu\text{g/ml}$  of antigen. Therefore, we added small amounts of antigen in a step-wise fashion to observe the dose-response. The number of valleys with current drop above 0.4 nA was counted during 1 min and plotted in Fig. 4 D. As hypothesized, we observed that the number of valleys decreased with increasing concentrations of  $\beta$ -hCG; furthermore, above 1  $\mu\text{g/ml}$  of  $\beta$ -hCG, the change approached saturation. Because the size of the complex is still expected to be smaller than the nanopore, we speculate that the absence of antibody-associated valleys upon addition of antigen is due to a change of  $\mu_e$  of the antibody when bound to  $\beta$ -hCG. While IgGs have a pI about pH 6, the pI for  $\beta$ -hCG is about 3, it is likely that upon IgG binding to two  $\beta$ -hCG the  $\mu_e$  is strongly increased such that our electronics were not able to detect the fast translocating complex. For translocation experiments of IgG at pH 7, we only counted 45 valleys compared to the 500 valleys at pH 6, which supports our explanation that the complex has increased mobility compared to free antibody at the pH tested. Since binding to another protein with more mobility appears to increase the mobility of the protein, our assay can be compared to *mobility shift assays*, which is a frequently used gel-based assay, *e.g.* to investigate the binding of gene regulating proteins to DNA (25). Similar assays to determine molecular interactions are also found in capillary electrophoresis (26).

The unmatched and unique advantage of our protein-protein affinity assays is that a label is not needed. In most protein-protein binding assays a labeling process or a subsequent signal generation/amplification step is needed (27). Directly labeling the protein may lead to loss of binding-affinity and sensitivity. Moreover, labeling and signal amplification processes can be very costly and time consuming (27). In contrast, if our postulation is correct, nanopore sensing can

detect single molecules; the number of molecules needed for analysis is equivalent to the statistical reliable count of molecules, *i.e.* less than 1000 molecules. The theoretical sensitivity of nanopores is therefore in the range of zeptomols (10<sup>-21</sup>M). Optimization of such assays could find many biotechnology applications.

The authors would like to thank the technical staff of ComLab, the joint IMT-CSEM clean room facility, Mohammad-Mehdi Dadras and Peter Van der Waal for helpful discussions. Anpan Han also acknowledges the Danish Research Agency for the financial support (Grant: Internationaliseringsstipendium). This project was financially supported by the République and Canton de Neuchâtel.

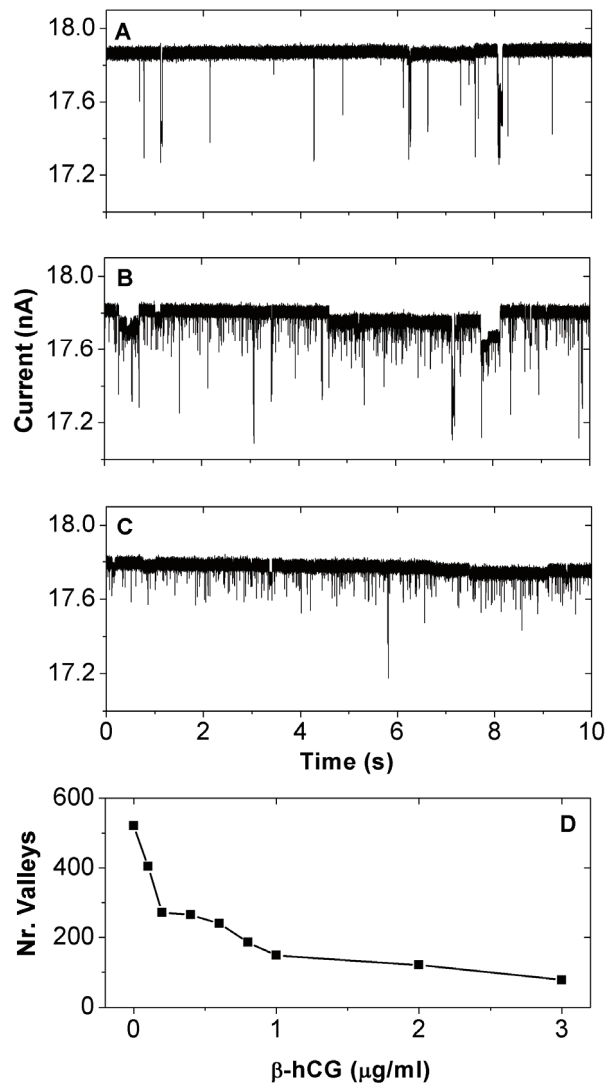


Fig. 4. Antibody-antigen binding experiment. Monoclonal anti- $\beta$ -hCG antibody was added to the *cis* chamber (A). OA added to the *cis* chamber (B).  $\beta$ -hCG was added (C). Dose-response curve is given in D. The line is added to guide the eye.

## Supporting material

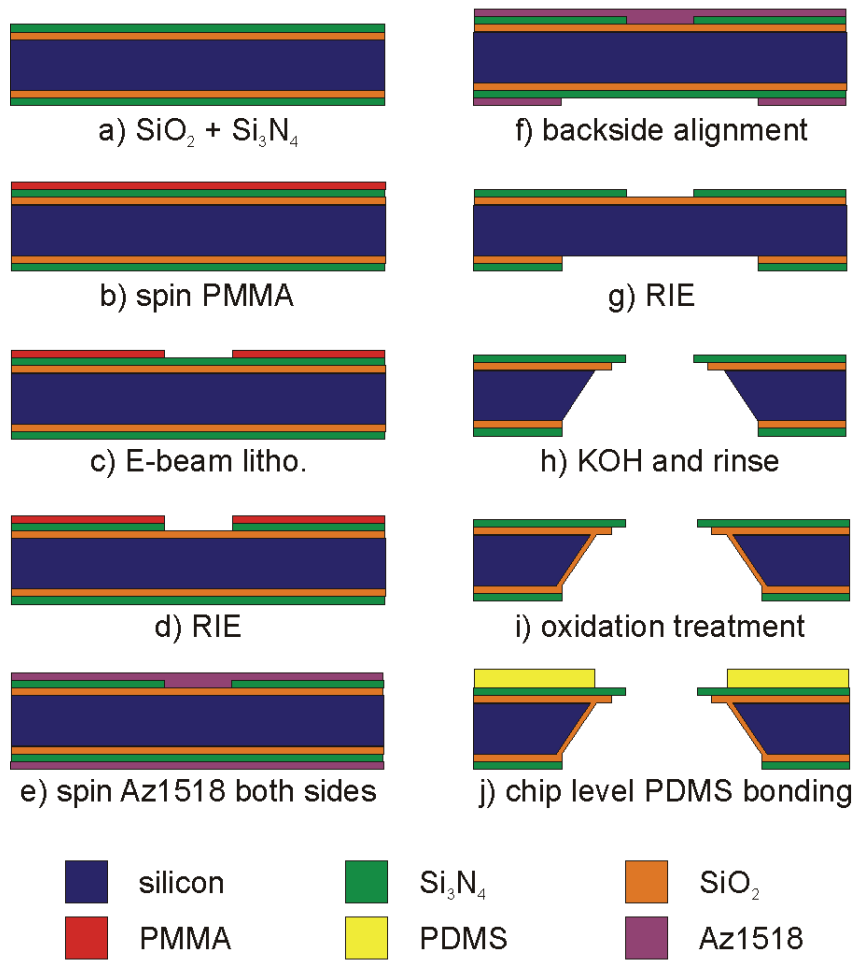


Fig. 5. Nanopore fabrication flow chart, see text for details.

### Nanopore fabrication process

The nanopore fabrication is an optimization of our previously reported work (16). We started with dry thermal oxidation to form a 500-nm-thick silicon dioxide ( $\text{SiO}_2$ ) layer on a 100-mm-diameter,  $\langle 100 \rangle$ , 390- $\mu\text{m}$ -thick, double side polished silicon wafer. Then we coated the wafer on both sides with a layer of 20-nm-thick silicon nitride ( $\text{Si}_3\text{N}_4$ ) (Fig. 5a) by low pressure chemical vapor deposition (LPCVD). The wafer was treated in oxygen plasma (Tepla 132 from PVA Tepla, Feldkirchen, Germany. Parameters: RF power 1000W, pressure 0.73 mbar, 50 °C, 30 min) before spinning a polymethyl methacrylate (PMMA, 2% solid, MW950kD, from MicroChem, MA, USA) layer onto the front side (Fig. 5b). After spinning PMMA, the wafer was baked at 170 °C for 30 min. The e-beam lithography system, Raith 150, from Raith, Dortmund Germany was used for PMMA exposure. To achieve the best wafer uniformity, the acceleration voltage was set to 20 kV, the aperture size was 7.5  $\mu\text{m}$ , and the wafer was clamped onto an electrostatic wafer holder and leveled such that the electron beam was perpendicular to the wafer surface. The pores were patterned using

the *dot* exposure mode (dose: 0.001 pAs) and other structures were written with the *area* mode (dose: 150  $\mu\text{A}/\text{cm}^2$ ). After the exposure, the wafer was developed in 1:3 methylisobutylketone (MIBK) to isopropanol mixture, for 30 s and rinsed briefly in isopropanol and subsequently in deionized water (Fig. 5c). The patterns in the PMMA were transferred into the  $\text{Si}_3\text{N}_4$  by reactive ion etching (RIE), and the etching stopped on the  $\text{SiO}_2$  by timing (Fig. 5d). The RIE (Alcatel GIR 263, Annecy, France) used a  $\text{SF}_6/\text{O}_2$  chemistry. Remaining PMMA was stripped in an oxygen plasma. A standard photolithography process was used to pattern the backside of the wafer: a 2.3- $\mu\text{m}$ -thick AZ1518 photoresist (Shipley, Switzerland) was spun first onto the front side (To protect structures written by E-beam lithography.) and then onto the backside of the wafer (Fig. 5e). The photoresist on the backside served as mask for the subsequently RIE (Fig. 5f), which exposed the silicon on the backside of the wafer (Fig. 5g). After the RIE the photoresist was removed using oxygen plasma and subsequently the wafer was immersed into a 40 % (m/v) KOH etch bath heated to 60 °C. The KOH created a free standing membrane with the pore embedded (Fig. 5h). After the KOH, 10 nm of  $\text{SiO}_2$  was thermally grown at 950 ° before wafer dicing (Fig. 5g). The membrane was situated in the middle of an 8 × 8 mm chip. To reduce the noise during current measurements, a 300- $\mu\text{m}$ -thick polydimethylsiloxane (PDMS) sheet with a 200- $\mu\text{m}$ -diameter hole was prepared and sealed onto the silicon chip such that the membrane was under the hole (Fig. 5i). Just before experiments the chips were treated with a short (2 min) oxygen plasma to render the surface hydrophilic such that water was able to wet and fill the lumen of the nanopore. Immediately after the oxygen plasma the chips were immersed into water, since the PMDS will lose its hydrophilic character upon exposure with air.



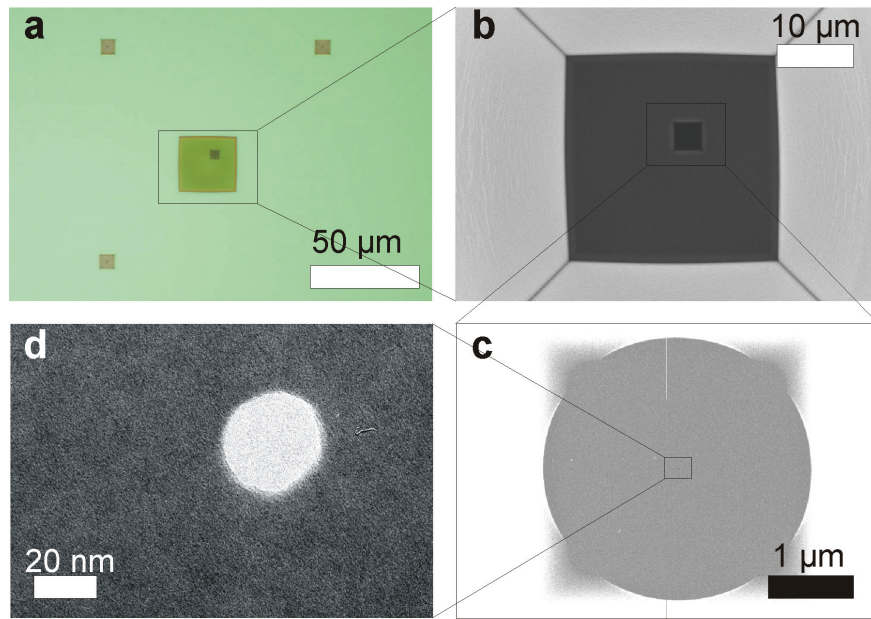


Fig. 6. Fabrication results. (a) An optical microscope image of the  $\text{SiO}_2 / \text{Si}_3\text{N}_4$  membrane (front side of the wafer). A small dark square on the membrane equidistant from the 3 small squares is the membrane in  $\text{Si}_3\text{N}_4$ . (b) is the  $\text{SiO}_2 / \text{Si}_3\text{N}_4$  membrane observed using SEM from the backside. Zooming into the membrane in  $\text{Si}_3\text{N}_4$  we observed a nanopore embedded in its center (c). A high resolution TEM (200 keV) image of a characteristic pore is shown in (d).

The fabrication results are shown in Fig. 6. The pore diameter was measured to be between 20 and 30 nm using transmission electron microscopy (TEM).

### Experiment procedure

A chip was mounted into a in-house designed cell and both chambers were filled with buffer solution. The immersed Ag/AgCl electrodes were connected to a patch clamp amplifier (Axopatch 200B, Axon Instruments, USA). Control experiments were performed such that we were certain that the current we measured was through the nanopore (16). By measuring the current we could calculate the diameter of the pore (16). The average diameter calculated for wafer A was  $24.4 \pm 2.8$  nm (14 chips), and  $27.9 \pm 1.4$  nm (12 chips) for wafer B, which was in agreement with TEM measurements.

Ovalbumin (OA) from chicken white (pn: A7641) and bovine serum albumin (BSA) (pn: A0281) and all chemicals were from Sigma unless specified. Avidin (AV) was from Belovo SA, Belgium (23) and the preparation of recombinant streptavidin from *Escherichia coli* (SAV) is described by Humbert et al. (19). The antigen human chorionic gonadotropin  $\beta$  ( $\beta$ -HCG) from human pregnancy



urine and the monoclonal anti- $\beta$ -HCG antibody (pI 6.4) were from Fitzgerald, MA, USA. For OA experiments pores from wafer A were used, and wafer B was used for all other experiments. First experiments were performed using pores from wafer A. Since we were in the learning phase of our experiments many pores were clogged. Hence, they were not included in this report. Proteins were dissolved in 1M KCl to 0.1 mg/ml and kept at 4 °C. 1 M KCl buffers with different pH were adjusted to the same resistivity (9.09  $\Omega$ cm) using a conductivity meter (Orion 150, conductivity cell 012210, Boston, USA). We used 100 mM citrate buffer for pH 2, 3, 4, 5 and 6, 100 mM bis-tris propane for pH 7 and 8. The buffer pH was fine adjusted using a sensitive pH meter (Orion 610, Boston, USA).

We investigate the solubility of SAV, AV, OA and BSA at different pH. This was carried out by preparing 0.1 mg/ml proteins solutions in buffers with different pH. If the proteins were not soluble at all, sedimentations were formed within an hour. Such pH conditions were unsuitable for nanopore experiments, since the risk of clogging the pores was very large.

Only one protein was analyzed per chip to avoid cross-contamination. Each nanopore experiments started with a clean chip. With the *trans* electrode biased at 50 mV, if the current for a clean chip was stable and the noise was below 20 pA (root mean square, 10 ms window, 100 kHz low-pass filter) the chip could be used. More than 50% of the chips were suitable for experiments, a yield of more than 50% on a wafer level is considered as good for a prototype. Proteins were then added to the *cis* chamber such that the final concentration was between 1 and 10  $\mu$ g/ml, i.e. the stock protein solution was diluted 10 to 100 times. Current recordings were made with different voltage bias. Before changing the pH we washed the chambers and made current recordings to see if the protein was indeed removed by washing. The number of spikes decreases by more than 90% after washing. For the pH sweeps, we started from pH 6 and stepped down to pH 2. To get a reasonable number of spikes higher protein concentrations (up to 10  $\mu$ g/ml) were needed at lower pH. By starting at low concentrations carry-over of proteins between experiments was less problematic. Then we performed experiments at pH 7 and 8. The number of spikes detected was proportional with the protein concentration (results not shown), which justified the use of normalization. We did not use higher concentrations than 10  $\mu$ g/ml, since the carry-over between experiments could be very large.

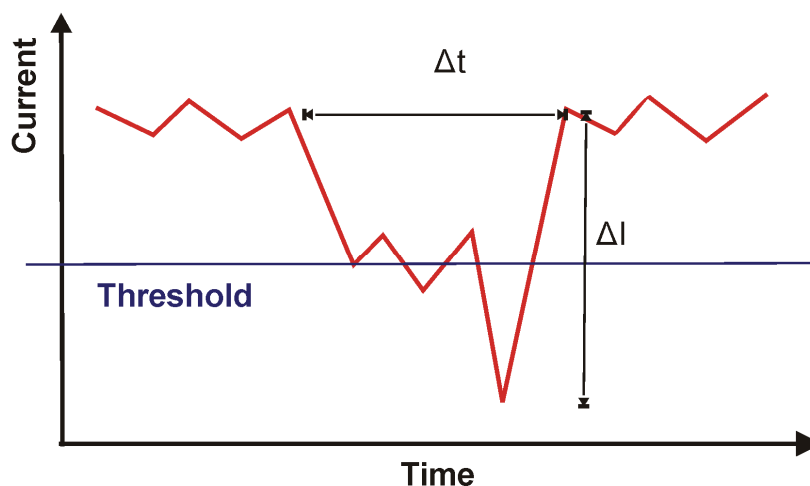


Fig. 7. Data analysis, see text for details.

The analogue signal from the patch clamp amplifier was digitized using a data acquisition card from National Instruments (PCI 6052E), and Labview software (LV) was used to control the data acquisition card and later on to perform signal processing. The acquisition rate was set to 300 kHz, and the data was directly saved to the hard drive. During data processing the following routine was used. The data from the hard-drive was read and the data was globally leveled such that minor drifts of the experiment were eliminated. Spikes were extracted from the leveled data. The duration,  $\Delta t$ , and maximal current drop,  $\Delta I$ , was obtained (Fig. 7). To use the maximal current drop was very simple from a data processing point of view. However, it is also very noisy, since the background noise is directly added. A less noisy method is to average of data points at the bottom of a well, however this is very complicated due to the many different shapes of the spikes.

## Supporting material for Fig. 2

### 2A

During 60s, setting the *trans* electrode to  $\pm 50$  mV, all spikes that have larger absolute value than 0.1 nA were counted. The Nr. of valley is normalized to the protein concentration and measurement time. The unit in full is Nr. of valley/min/( $\mu\text{g}$  protein/ml) .

### 2B

The time duration of each spike was extracted and the averaged duration was obtained. The average spike duration was calculated using the valleys, i.e. *trans* electrode was positively biased, except for BSA at pH 2, 3 and AV at all pH, where average peak durations were used.

Data for FIG. 2

**OA**

**50 mV**

pH	nr. spikes	SD	$\Delta t$ (ms)	SD (ms)
4	136	55	0.26	0.19
5	261	152	0.54	0.17
6	285	70	0.53	0.24
7	21	27	0.09	0.04
8	7	4	0.07	0.04

**-50 mV**

4	21	7	0.22	0.15
5	14	10	0.31	0.02
6	29	9	0.21	0.05
7	0	0	0.02	0.01
8	1	1	0.03	0.01

**SAV**

**50 mV**

pH	nr. spikes	SD	$\Delta t$ (ms)	SD (ms)
2	14	9	0.08	0.05
3	32	24	0.10	0.09
4	190	11	0.25	0.07
5	515	320	0.68	0.22
6	143	65	0.23	0.06
7	79	59	0.07	0.03
8	11	2	0.04	0.00

**-50 mV**

2	8	9	0.08	0.07
3	15	12	0.09	0.03
4	67	41	0.27	0.10
5	172	93	0.49	0.17
6	115	14	0.27	0.02
7	33	48	0.07	0.03
8	21	18	0.04	0.01

**BSA**

**50 mV**

pH	nr. spikes	SD	$\Delta t$ (ms)	SD (ms)
2	2	2	0.14	0.04
3	11	8	0.14	0.08
4	3	1	0.14	0.12
5	328	75	0.54	0.34
6	569	238	0.47	0.12
7	183	135	0.06	0.04
8	42	34	0.04	0.01

**-50 mV**

2	33	7	0.17	0.06
3	33	14	0.20	0.11
4	-	-	-	-
5	27	8	0.42	0.09
6	33	5	0.36	0.09
7	13	18	0.05	0.03
8	1	2	0.04	0.02

**AV**

**50 mV**

pH	nr. spikes	SD	$\Delta t$ (ms)	SD (ms)
4	48	17	0.18	0.16
5	98	45	0.22	0.14
6	90	21	0.24	0.06
7	181	72	0.23	0.07
8	70	9	0.14	0.03

**-50 mV**

4	57	36	0.19	0.13
5	131	47	0.25	0.18
6	230	60	0.31	0.14
7	194	48	0.24	0.13
8	436	35	0.24	0.15

### Coulter Counter model and calculations

By combining Ohm's law and Maxwell's approximation for the conductivity of liquids with suspended insulating particles, Deblois and Bean (28) and later on Ito et. al derived an expression for the current change ( $\Delta I$ ) caused by the translocation of a particle with the diameter,  $d_m$ , through a pore with diameter  $d_p$  and length  $l_p$  (29).

$$\Delta I = S(d_p, d_m) \frac{\kappa \pi U}{4(l_p + 0.8d_p)^2} d_m^3 \quad \text{Eq. 1}$$

Where the  $U$  is the applied voltage,  $\kappa$  is the conductivity of the electrolyte solution and  $S(d_p, d_m)$  is a parameter depending on  $d_m$  and  $d_p$ . The current change is proportional to the square of the dimensions of the pore. In our calculations we set the parameter  $S(d_p, d_m)$  to unity. Although the models for the  $\Delta I$  are well established, we could not find models for the translocation time. This is probably due to that the time resolution was never a problem, since  $l_p$  were often above 10  $\mu\text{m}$  (28, 29). However, in our case where  $l_p$  was about 20 nm, time resolution becomes a critical issue. At very high ionic strength (1M KCl) the main transport mechanism of charged molecules subjected to an external electric field is electrophoresis (30). Assuming a particle with the electrophoretic mobility  $\mu_e$  passing through the pore at a velocity of  $v = \mu_e U/l$  (30) the time,  $t$ , needed for translocation is

$$t = \frac{l}{v} = \frac{l^2}{\mu_e U} \quad \text{Eq. 2}$$

For 5-nm-large proteins dissolved in 1M KCl, where the size of the particle is larger than the Debye length ( $L_D$ ),  $\mu_e$  is given by the Smoluchowski equation (30)

$$\mu_e = \frac{\varepsilon \zeta}{\eta} \approx \frac{\sigma L_D}{\eta} \quad \text{Eq. 3}$$

Where  $\zeta$  is the zeta potential,  $\varepsilon$  is the dielectric permittivity,  $\sigma$  is the surface charge density and  $\eta$  is the viscosity. Menon *et al.* measured  $\mu_e$  values for BSA at 10 mM NaCl, pH 8, to be  $22 \times 10^{-5} \text{ cm}^2/\text{Vs}$ .  $L_D$  at 1 M KCl is 0.3 nm which is 10 times smaller than at 10 mM (30). Hence, according to Eq. 3, the mobility is reduced by a factor of 10. Inserting 20 nm for  $l$ , 0.1 V for  $U$ , and  $2 \times 10^{-5} \text{ cm}^2/\text{Vs}$  for  $\mu_e$ , a BSA molecule will pass through the pore in 2  $\mu\text{s}$ .

## Reference

1. S. Weiss, *Nat. Struct. Mol. Bio.* **7**, 724 (2000).
2. A. D. Mehta, M. Rief, J. A. Spudich, D. A. Smith, R. M. Simmons, *Science* **283**, 1689 (1999).
3. R. Rigler, M. Orrit, T. Basche, *Single molecule spectroscopy, nobel conference lectures*. Springer series in chemical physics (Springer, Berlin, 2001).
4. C. Bustamante, J. C. Macosko, G. J. Wuite, *Nat. Rev. Mol. Cell Bio.* **1**, 130 (2000).
5. H. Itoh *et al.*, *Nature* **427**, 465 (2004).
6. H. Noji, R. Yasuda, M. Yoshida, K. Kinosita, Jr., *Nature* **386**, 299 (1997).
7. J. J. Kasianowicz, E. Brandin, D. Branton, D. W. Deamer, *Proc. Natl. Acad. Sci. USA* **93**, 13770 (1996).
8. J. Li *et al.*, *Nature* **412**, 166 (2001).
9. W. H. Coulter. (1953). US Patent 2.656.508 (1953)
10. H. Bayley, C. R. Martin, *Chem. Rev.* **100**, 2575 (2000).
11. A. Meller, L. Nivon, E. Brandin, J. Golovchenko, D. Branton, *Proc. Natl. Acad. Sci. USA* **97**, 1079 (2000).
12. R. M. Smeets *et al.*, *Nano Lett.* **6**, 89 (2006).
13. D. Fologea, J. Uplinger, B. Thomas, D. S. McNabb, J. Li, *Nano Lett.* **5**, 1734 (2005).
14. J. B. Heng *et al.*, *Biophys. J.* **90**, 1098 (2006).
15. E. A. Heins, Z. S. Siwy, L. A. Baker, C. R. Martin, *Nano Lett.* **5**, 1824 (2005).
16. A. Han *et al.*, *Appl. Phys. Lett.* **88**, 093901 (2006).
17. A. J. Storm, J. H. Chen, H. W. Zandbergen, C. Dekker, *Phys. Rev. E* **71**, 051903 (2005).
18. J. L. Li, M. Gershow, D. Stein, E. Brandin, J. A. Golovchenko, *Nat. Mater.* **2**, 611 (2003).
19. N. Humbert, A. Zocchi, T. R. Ward, *Electrophoresis* **26**, 47 (2005).
20. W. Norde, J. Lyklema, *J. Colloid Interface Sci.* **66**, 277 (1978).
21. M. K. Menon, A. L. Zydney, *Anal. Chem.* **70**, 1581 (1998).
22. G. Scatchard, J. S. Coleman, A. L. Shen, *J. Am. Chem. Soc.* **79**, 12 (1957).
23. Y. Hiller, J. M. Gershoni, E. A. Bayer, M. Wilchek, *Biochem. J.* **248**, 167 (1987).
24. F. Cabre, E. I. Canela, M. A. Canela, *J. Chromatogr. A* **472**, 347 (1989).
25. M. G. Fried, *Electrophoresis* **10**, 366 (1989).
26. N. H. H. Heegaard, *Electrophoresis* **24**, 3879 (2003).
27. L. J. Kricka, D. Wild, in *The Immunoassay Handbook*, D. Wild, Ed. (Elsevier, Amsterdam, 2005), pp. 192-230.
28. R. W. Deblois, C. P. Bean, *Rev. Sci. Instrum.* **41**, 909 (1970).
29. T. Ito, L. Sun, R. M. Crooks, *Anal. Chem.* **75**, 2399 (2003).
30. D. Shaw, J. *Introduction to colloid and surface chemistry*. (Butterworth-Heinemann, Oxford, ed. fourth, 1989).

*I understand those that lack of learning,  
but I dislike those that pretend of knowledge*

## Chapter 6 : Nanochannel devices – applications and fabrication

Unlike the development of nanopores, which is driven by the goal of DNA sequencing, the development of nanochannel devices has been significantly broader. The two main applications of nanochannel devices are in single molecule analysis and colloid science. In a recent review, Eijkel and van den Berg pointed out the main applications as well as the physics and chemistry of fluids and molecules contained in nanochannels (Eijkel, 2005). In this chapter I will concentrate on the experimental work carried out in nanochannels with emphasis on single molecule analysis as well as one topic in colloid science: the filling of nanochannels by capillary force.

### **Single molecule analysis**

As with experiments in nanopores, studies in nanochannels have mostly involved DNA. In their entropically favorable native state, long DNA molecules behave like *random-coils*. For example the genomic  $\lambda$ -DNA has a radius of gyration of 730 nm, when it is stretched out, it has a length of 22  $\mu\text{m}$  (Perkins, 1997). If the depth or the width of a nanochannel is smaller than the radius of gyration,  $\lambda$ -DNA can not enter the channel unless it is somehow uncoiled. Indeed, DNA is stretched out during its entry into nanochannels (Cao, 2002; Guo, 2004; Li, 2003b). The entry of DNA into nanochannels could be facilitated by capillary force (Guo,

2004) or by electrophoresis (Tegenfeldt, 2004). One of the application of DNA stretching is to measure the length of genomic DNA, which in turn could be used to determine its molecular weight (Tegenfeldt, 2004). Established methods used to determine the molecular weight of genomic DNA, such as pulsed field gel electrophoresis, are extremely time and reagent consuming. Han and Craighead reported the separation of long DNA molecules. They used a fluidic chip with channels with periodically varying depth between 100 nm and 3  $\mu\text{m}$ , an *entropic trap array* (Han, 2000). DNA, in the channel sections where the depth is 3  $\mu\text{m}$ , is in its entropically favorable random-coil state. As it approaches the nanochannel, it is shortly trapped. Larger DNA has a higher probability to enter the narrow nanochannels than smaller DNA. This difference in the trapped time allows size dependent DNA separation. Another efficient method for DNA separation, based on the coiling and uncoiling of DNA, is to use fluidic chips with nanofabricated pillar arrays (Kaji, 2004). Foquet et al. reported possible applications of nanochannel in fluorescence correlation spectroscopy (Foquet, 2004). The results showed that the molecules are confined to move in one dimension, i.e. along the nanochannel, the effective diffusion is reduced. Reduced diffusion increases the observation time, and more photons are collected from a

single molecule, which enhances the signal to noise ratio.

Analysis using nanochannels which only need a few molecules could prove to be a good future alternative or supplement to the existing analytical techniques in biochemistry. In addition to superior biochemical analysis methods, Wang et al. reported that it is possible to detect the binding sites of gene regulating proteins on a stretched out DNA (Wang, 2005b). To map such binding sites could help us to better grasp complex protein-DNA interactions which regulate gene expression.

### **Applications in colloid science**

Applications of nanopores and nanochannels in analytical biochemistry are numerous and show great potentials. Colloid science is another scientific field where nanofluidics also greatly contributes. Despite numerous studies, established theory and published textbooks (Probstein, 2003; Shaw, 1989), nanochannels could contribute to novel advancements in the field. Nanochannels could be fabricated with good reproducibility and high yield, providing idealized colloidal systems with well defined dimensions. This was not available to previous investigators that often had to work with highly heterogeneous systems.

Many recent reports concern the study of overlapping electrical double layer (Chapter 2), i.e. if the distance between the walls of the nanochannel is smaller than the Debye length,  $L_D > d$ . The Debye-Hückel potential states that

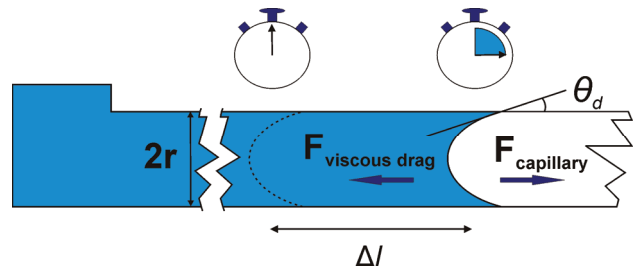


Figure 6-1. Illustration of capillary filling - Washburn kinetics. Please refer to text for details.

charged molecules carried by the ionic solution will be attracted or repelled to the surface if it enters the EDL. Molecules with the same charge as the wall, co-ions, can not enter the EDL due to the electrostatic repulsion, while opposite charged molecules, counter-ions, could enter with ease. Plecis et. al investigated the permeability of ions in nanochannels at different EDL thickness (Plecis, 2005). The permeability for co-ions diminished while it was enhanced up to 3 times for counter-ions. At very large EDL overlap, the conductivity of solutions diverges from the bulk behavior (Schoch, 2005; Stein, 2004a). The ionic conductivity of a channel is the sum of the conductivity of the ions in the bulk, and the charges in the diffusive part of the double layer (Figure 2-1). For channels where the  $L_D \ll d$ , the main contribution is the bulk conductivity, however, if the  $L_D \gg d$ , the charges in the diffusive layer would dominate the ion transport. Stein et al. and Schoch et al. observed that the conductance converged to a finite constant value as the concentration of ions decreased (Schoch, 2005; Stein, 2004a).



### Filling of nanochannels by capillary force.

An interesting subject in colloid science is capillarity (Figure 6-1). As a liquid plug enters a channel three phases are in contact, the inner surfaces of the channel, the liquid itself, and the air-vapor. The surface energy of this contact creates a capillary force. This force will drag the liquid into the capillary if the contact angle of the interface is smaller than  $90^\circ$ , i.e. if the liquid is wetting the surface. The capillary pressure is given as  $p = 2\gamma\cos\theta_d/r$ , where  $r$  is the capillary inner radius,  $\gamma$  and  $\theta_d$  are the surface tension of the liquid and the dynamic contact angle respectively. The magnitude of the capillary pressure in a 100 nm diameter channels filled with water is in the order of 10 bars. The drag acting on the liquid plug, given by the Poiseuille's equation (Eq. 2), will gradually slow the capillary filling of channels. The length of the liquid plug  $\Delta l$  relates with the filling time  $t$ , following the Washburn relation  $\Delta l \sim \sqrt{t}$  (Washburn, 1921). The relation states that, to fill a channel twice as long takes four times more time. Chapter 7 describes in detail the kinetics of filling and other peculiar effects which take place in nanochannels. During the time of reviewing the article, a related paper by Tas et al. also described the filling kinetics of liquids in nanochannels, however, studies were only restricted to water (Tas, 2004). Recently, Hanevald reported the filling kinetics of water in channels down to 5 nm deep. Amazingly, at 5

nm, the Washburn filling kinetics was still valid. (Haneveld, 2006)

### Fabrication strategies

As the author has pointed out, nanochannels provide a novel tool for studying single molecules, and they act as a new technological platform for colloid sciences. There are two major approaches to fabricate nanochannels devices: the use of sacrificial layers, which is also referred to as surface micromachining, or constructing the nanochannels into the bulk of the substrate itself (Figure 6-2).

### Surface machining

The first stage of fabrication is to deposit the structural and sacrificial layer (SL) (Figure 6-2a). The materials selected for the SL and the structural layer are based on the etching selec-

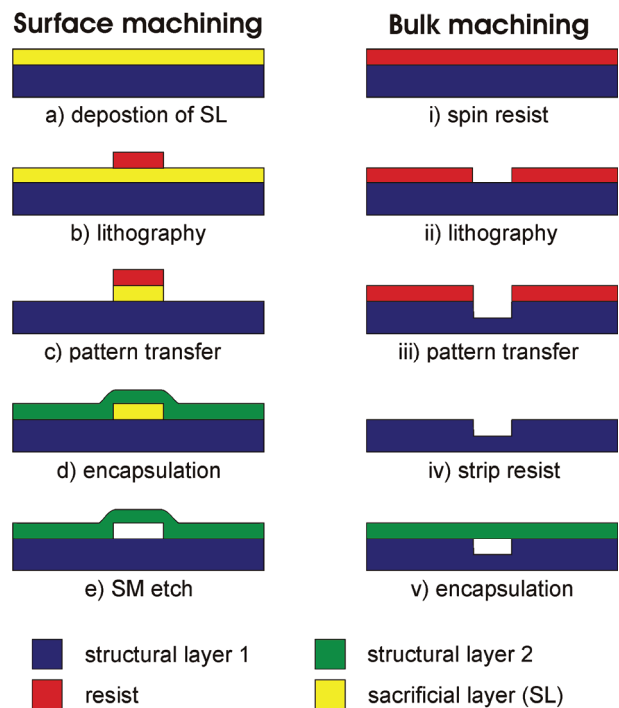


Figure 6-2. Nanochannel fabrication strategies, surface and bulk machining.

tivity between the two layers. Since the removal of the SL through nanochannels is often diffusion limited, the etching time is often very long. Therefore high etch selectivity is necessary. A lithography step defines the width and the length of nanochannels (Figure 6-2b). The width of the channels is often limited by the resolution of the patterning technique. Lithography technologies with sub-micrometer resolution such as nanoimprinting (Li, 2003b), e-beam lithography (Foquet, 2002) and electrospinning (Czaplewski, 2003) have been reported. The next steps are the pattern transfer (Figure 6-2c) and the subsequent encapsulation (Figure 6-2d). After the encapsulation, openings are made in the end of the nanochannels, and the SL is removed by a selective etch (Figure 6-2e). An example of material combinations are polycrystalline silicon (SL) and SiO<sub>2</sub> (structural layer) with tetra-methylammonium hydroxide (TMAH) as etchant (Foquet, 2002).

### **Bulk machining**

Bulk machining starts with the channel definition by lithography (Figure 6-2i). Nanolithography techniques such as focused ion-beam milling (Alarie, 2003), nanoimprinting lithography (Cao, 2002) and electron beam lithography (Kaji, 2004) have been reported. Nanochannels with the width in the micrometer range, also referred as nanoslits or 1-D nanochannels (Haneveld, 2003; Schoch, 2005; Stein,

2002) are very popular for studies in colloid science. The patterns are transferred into the substrate using dry or wet etching (Figure 6-2ii, iii, iv). The encapsulation (Figure 6-2v) of the open conduct is done by bonding (Han, 2000; Haneveld, 2003; Stein, 2002) or non-uniform thin-film deposition (Cao, 2002).

The two fabrication strategies have their advantages and disadvantages, e.g. in the sacrificial layer method, diffusion limited removal of the sacrificial layer in nanochannels could be very time consuming, channels 0.64 mm long required 15 h of etching (Tas, 2002). To reduce the etching time, dedicated irrigation holes for the etchant had to be made (Foquet, 2002), or heat decomposable polymer was used as the sacrificial layer (Czaplewski, 2003; Li, 2003b). The bulk machining approach is often more simple from a technological point of view. However, in certain applications the channels have to be very close to the device surface, e.g. constrains caused by low working distance microscope objectives. It is then more favorable to take the surface machining approach, since only a submicrometer film separates the liquid inside the nanochannel and the device surface.

To circumvent some of the above limitations of surface machining, such as lithography resolution limited channel dimensions, long etching time, a novel nanochannel fabrication process was developed (Chapter 8).

## **Chapter 7 :**

### **Paper 2,**

# **Filling Kinetics of Liquids in Nanochannels as Narrow as 27nm by Capillary Force**

A. Han, G. Mondin, N.G. Hegelbach, N.F. de Rooij, and U. Staufer.

Journal of Colloid and Interface Science, 2005, 293, 151-158.

*in a group of three,  
I find mentors,  
learn from their strength,  
and avoid their mistakes.*



## Filling kinetics of liquids in nanochannels as narrow as 27 nm by capillary force

Anpan Han, Giampietro Mondin, Nicole G. Hegelbach, Nicolaas F. de Rooij, Urs Staufer\*

*Institute of Microtechnology, University of Neuchâtel, Rue Jaquet-Droz 1/C.P. 3, CH-2007 Neuchâtel, Switzerland*

Received 25 November 2004; accepted 11 June 2005

Available online 14 July 2005

### Abstract

We report the filling kinetics of different liquids in nanofabricated capillaries with rectangular cross-section by capillary force. Three sets of channels with different geometry were employed for the experiments. The smallest dimension of the channel cross-section was respectively 27, 50, and 73 nm. Ethanol, isopropanol, water and binary mixtures of ethanol and water spontaneously filled nanochannels with inner walls exposing silanol groups. For all the liquids the position of the moving liquid meniscus was observed to be proportional to the square root of time, which is in accordance with the classical Washburn kinetics. The velocity of the meniscus decreased both with the dimension of the channel and the ratio between the surface tension and the viscosity. In the case of water, air-bubbles were spontaneously trapped as channels were filled. For a binary mixture of 40% ethanol and water, no trapping of air was observed anymore. The filling rate was higher than expected, which also corresponds to the dynamic contact angle for the mixture being lower than that of pure ethanol. Nanochannels and porous materials share many physicochemical properties, e.g., the comparable pores size and extremely high surface to volume ratio. These similarities suggest that our nanochannels could be used as an idealized model to study mass transport mechanisms in systems where surface phenomena dominate.

© 2005 Elsevier Inc. All rights reserved.

*Keywords:* Ethanol; Isopropanol; Water; Ethanol–water mixture; Capillary force; Wetting; Filling kinetics; Nanochannels; Porous materials

### 1. Introduction

For bionanotechnology, studying single molecules, and physicochemical phenomena of liquids in the nanometer scale nanofluidic devices provide a novel tool [1–6]. Downsizing of fluidic systems is attractive for fundamental studies as well as biosensing [7–9]. For example, nanometer-sized entropic traps were used to separate long, genomic DNA [2,3]. Nanochannels combined with near-field microscopy could be used to locate genes [10]. Furthermore, by using nanofluidic systems extremely small measurement volumes, which provide enhanced detection of enzymatic reactions, could be obtained [5]. Novel and interesting physicochemical and thermodynamic phenomena associated with liquids confined in nanofluidic systems such as double-

layer overlap [11], negative pressure induced by capillary force [6], and ion enrichment–depletion effects [12], have been reported.

A less studied physicochemical effect, which is inherent for all nanofluidic devices, is the spontaneous filling by capillary force. The kinetics of filling by capillary force was first reported by Washburn in 1921 [13]. The position of the moving liquid menisci during filling was found to be proportional to the square root of the filling time. Many reported nanofluidic systems fabricated by micro- and nanolithography have rectangular cross-section and channel walls are often composed of silicon nitride and silicon dioxide [6,14,15]. The filling kinetics of channels with non-cylindrical cross-section was also studied [16–19]. To our knowledge, the smallest capillary used for kinetic studies was pulled quartz capillaries with inner diameter of 80 nm [20]. In this article we report how different liquids fill silicon nitride/dioxide nanochannels, which inner surface

\* Corresponding author. Fax: +41 (0) 32 7250711.  
E-mail address: [urs.staufer@unine.ch](mailto:urs.staufer@unine.ch) (U. Staufer).

chemistry mainly consists of hydrophilic silanol groups, by capillary force. The filling kinetics of wetting liquids followed the classical Washburn kinetics. Filling studies using water and binary mixtures of ethanol and water show phenomena similar to that observed in porous material such as trapping of the non-wetting phase.

## 2. Theory

A simple model for the filling kinetics by capillary force in capillaries with rectangular cross-section is used for this study. For a capillary with circular cross-section and inner radius of  $r$ , the capillary pressure is given as  $p = 2\gamma \cos\theta_d/r$ , where  $\gamma$  and  $\theta_d$  are the surface tension of the liquid and the dynamic contact angle, respectively. According to White [21], this equation can be used to calculate the capillary pressure in capillaries with rectangular cross-section if  $r$  is substituted with the hydraulic radius,  $r_H = A/s = r/2$ , where  $A$  is the cross-section area and  $s$  is the wetted perimeter. For a rectangular channel  $r_H = A/s = wd/2(w + d)$ , where  $w$  is the width and  $d$  is the depth (Figs. 1 and 2). For our nanochannels,  $d$  is small compared to  $w$ , and we approximated  $r_H \approx d/2$ . Hence, the capillary pressure in a rectangular channel is  $p = 2\gamma \cos\theta_d/d$ . We neglect the effects of the static pressure ( $<1$  mbar), which is justified since the capillary pressure in our nanochannels was calculated to be above 3 bar. The dynamic filling of a capillary with circular cross-section by capillary pressure, assuming the non-slip condition, is given by the Washburn equation [13]. The meniscus velocity,  $v$ , also referred as the filling rate is given by

$$v = \frac{r\gamma \cos\theta_d}{4\eta} \frac{1}{l}, \quad (1)$$

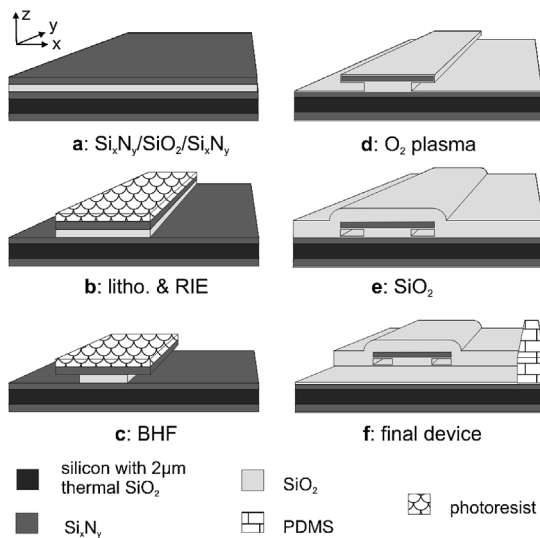


Fig. 1. Pseudo 3-D and cross-section representation of the fabrication process of a pair of nanochannels. Details are given in Section 3. Note that the dimensions of the illustration are neither scale nor proportions.

where  $l$  is the distance between the capillary meniscus and the capillary inlet, and  $\eta$  is the viscosity of the liquid. To obtain the meniscus velocity for a capillary with rectangular cross-section, we substituted the radius with the hydraulic radius,  $r = 2r_H \approx d$ ,

$$v \approx \frac{d\gamma \cos\theta_d}{4\eta} \frac{1}{l} = \frac{D}{2l}, \quad (2)$$

$$D = \frac{d\gamma \cos\theta_d}{2\eta}. \quad (3)$$

The meniscus velocity is higher for larger surface tension to viscosity ratios and channel depth. Integrating the velocity with respect to time we get

$$l = \sqrt{\frac{d\gamma \cos\theta_d}{2\eta}} \sqrt{t} = \sqrt{D} \sqrt{t}. \quad (4)$$

The position of the meniscus relates with time as  $l \sim t^{1/2}$  which is universal for conduits with arbitrary shape, including capillaries with rectangular cross-section [17]. The parameter  $D$ , which is independent of time and the meniscus

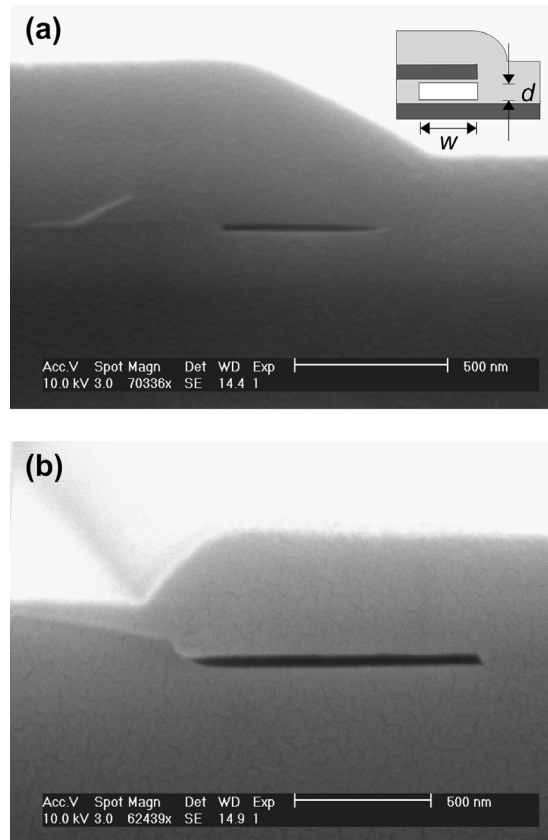


Fig. 2. Scanning electron microscopy (SEM) images of cross-sections through nanochannels fabricated by partial etching of a sacrificial layer. The figure inset in (a) corresponds to a zoom in Fig. 1e, where  $d$  is the channel depth and  $w$  is the width. Channel depth and width were measured by SEM. The black and thin “bars” about 500 nm long (a) and 900 nm long (b) are the inner cavities of the capillary, and the gray area on the picture is the wall material. The channels in (a) and (b) are respectively 27 and 50 nm deep.



position, can be determined by plotting  $l$  versus  $t^{1/2}$  values. The  $l \sim t^{1/2}$  scaling law originates from the capillary pressure which pulls the liquid into the channel, and which remains constant, while the flow resistance increases linearly irrespectively of the geometry of the channel cross-section. Other parameters, such as the degree of roundness of the corners of rectangular channels [17,19], the layered structure of the channel walls [22,23], and the time dependency of the dynamic contact angle [24] that influence the filling rate are not included in Eq. (2). How these issues influence the filling kinetics are going to be presented in the discussions.

### 3. Materials and methods

#### 3.1. Microfabrication process of nanochannels

The nanochannel fabrication process is based on partial etching of a sacrificial layer [25]. The fabrication process only requires established micromachining techniques and does not require any nanolithography. The starting substrates were 525- $\mu\text{m}$ -thick, 100-mm-diameter (100) silicon (Si) wafers polished on one side. The Si wafer was cleaned in a mixture of  $\text{H}_2\text{SO}_4$  and peroxide ( $(\text{NH}_4)_2\text{S}_2\text{O}_8$ ) at 120 °C for 10 min, followed by buffered HF (BHF;  $\text{NH}_4\text{F}:\text{HF} = 7:1$ ) for 1 min, and finally in 70%  $\text{HNO}_3$  at 115 °C for 10 min. The wafers were rinsed in doubly deionized (DI) water between the acid treatments. A layer of 2- $\mu\text{m}$ -thick thermal silicon dioxide was grown. A sandwich of silicon nitride (300 nm) deposited by low-pressure chemical vapor deposition ( $\text{Si}_x\text{N}_y$ ) and silicon dioxide deposited by chemical vapor deposition ( $\text{SiO}_2$ ) was deposited (Fig. 1a). The depth of the nanochannels depends on the thickness of the  $\text{SiO}_2$  layer. Process parameters for  $\text{Si}_x\text{N}_y$  deposition: temperature: 800 °C, gases:  $\text{SiH}_2\text{Cl}_2$  and  $\text{NH}_3$ , pressure 200 mTorr; for  $\text{SiO}_2$  deposition: temperature: 400 °C, gases: 2%  $\text{SiH}_4$  in  $\text{N}_2$ , and  $\text{O}_2$ , pressure: atmospheric. The fabrication required two photolithography processes; the wafers were dehydrated at 200 °C for 30 min and subjected to a silanization treatment with hexamethyldisilazane. A layer of 1.8- $\mu\text{m}$ -thick positive photoresist was spin-coated onto the Si wafer and prebaked for 1 min at 100 °C on a hot plate. A chromium mask with the channel features was aligned to the Si wafer. During the first photolithography, the mask patterns were transferred to the resist by exposure with UV, followed by development. After development (1 min) the photoresist was postbaked for 30 min at 125 °C in an oven. The photoresist served as a mask during the following reactive ion etching (RIE) process where the patterns were transferred into the wafer. Etching was stopped on the second layer of  $\text{Si}_x\text{N}_y$  (Fig. 1b). The sacrificial  $\text{SiO}_2$  layer was partially under etched by BHF followed by rinsing using DI water (Fig. 1c). The width of the nanochannels was determined by the timed etch (about 200 nm/min) of the sacrificial layer. The remaining photoresist was removed by oxygen plasma. Before the encapsulation of the nanochannels, the silicon nitride was

treated with oxygen plasma (Tepla 132 from PVA Tepla, Feldkirchen, Germany. Parameters: RF power 1000 W, pressure 0.73 mbar, 100 °C, 60 min) to create a surface composed mainly of silicon dioxide [26,27]. The inner surface of our nanochannels consisted of a few monolayers of silicon dioxide exposing silanol groups (Fig. 1d). To seal the channels, a fresh layer of  $\text{SiO}_2$  (400 nm) was deposited (Fig. 1e). A second photolithography and RIE process were used to pattern the access openings to the nanochannels. A second oxygen plasma process was used to remove photoresist and create a thin layer of silicon dioxide on the wafer surface. Polydimethylsiloxane (PDMS) O-rings were prepared [28] and sealed reversibly to the access openings to serve as liquid reservoirs (Fig. 1f). Fig. 2 shows a cross-section of the fabricated nanochannels.

#### 3.2. Experimental procedure of the filling kinetic studies

Isopropanol (VLSI grade from Rockwood, Avenches, Switzerland), ethanol (analytical grade from VWR, Le Lignon, Switzerland), mixtures of ethanol and deionized water of clean room quality (resistivity > 10  $\text{M}\Omega/\text{cm}$ ) and Tris (Fluka, Buchs, Switzerland) buffers spontaneously filled array of channels by capillary force. We observed the horizontally positioned nanochannel arrays using a stereomicroscope (MZ8 from Leica) with ring-illumination. We pipetted a few micromilliliters of a liquid into the PDMS reservoir located on one of the two access openings of a nanochannel array. As the array of nanochannels filled, we were able to see a change in color and contrast because of the difference between the refractive index of air in the vacant channels and the refractive index of the liquid (Fig. 3). Pictures and real-time movies were taken through a digital camera (CoolPix 5400 from Nikon, 5.1 million pixels, resolution:

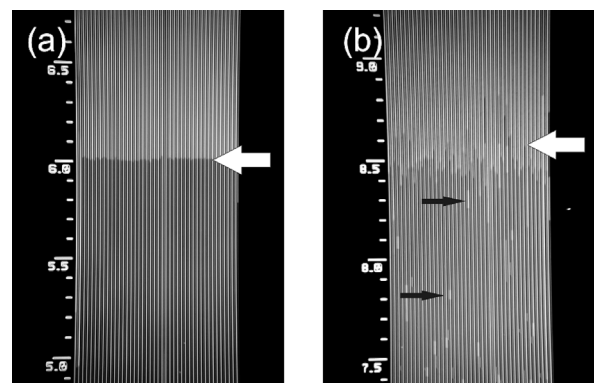


Fig. 3. Optical microscope image showing the filling of channel arrays. Each array consists of 40 pairs (Fig. 1), a total of 80 parallel nanochannels. Each channel is 900 nm wide, 50 nm deep and 15 mm long. The position of the meniscus,  $l$ , could be read from the integrated scale (8.5 indicate  $l = 8.5$  mm, each minor division is 100  $\mu\text{m}$ ). (a) A channel array is filled with isopropanol. The thick white arrow indicates the meniscus position. The darker area below the white arrow is filled and the brighter area is empty. A few channels were not filled, e.g., middle and left. (b) Water was introduced into the channel array and bubbles were trapped during filling (thin black arrows).

2592 × 1944 pixels, 24 bit color) mounted on the stereomicroscope. Computer software Pinnacle Studio, Ver. 8.12.7.0, from Pinnacle Systems and Corel Draw 11 from Corel was respectively used for video and image analysis. For the case of the 27-nm-deep nanochannels it was necessary to digitally enhance the contrast to determine the position of the meniscus. By reviewing the real-time movies the position of the meniscus could be read from an integrated scale beside the nanochannel array, and the associated time could be read from the computer software. For ethanol, 40% ethanol, and isopropanol the position of the common meniscus was clearly defined (Fig. 3a). It was more difficult to evaluate the common meniscus for water since there was not a uniform filling of the channel arrays (Fig. 3b). Time was set to 0 s as the droplet of liquid entered the PDMS reservoir. The ( $t^{1/2}$ ,  $l$ ) values were read and plotted.

### 3.3. Scanning electron and fluorescence microscopies

For fluorescence microscopy the channels were filled with 10 mM rhodamine B (Sigma, Buchs, Switzerland) dissolved in ethanol, or 10 mM fluorescein (Fluka, Buchs, Switzerland) in 10 mM Tris buffer, pH 7.2. The fluorescence signal in the nanochannels was imaged with a cooled CCD camera (CF 8/4 DXC from Kappa, Gleichen, Germany) mounted on an inverted fluorescence microscope with integrated filter sets (Axiovert S100 from Zeiss).

The depth and width of nanochannels were measured by scanning electron microscopy (SEM). The instrument was a XL30 ESEM-FEG from Philips. Samples for SEM imaging were prepared by cleaving a part of a processed wafer, such that the cut ran across the nanochannels, exposing a cross-section of the nanochannels (Fig. 2). To decrease charging effects a thin layer of AuPd (5 nm) was sputtered onto the sample before SEM.

## 4. Results

The kinetics of filling is determined by the liquid, the surface properties, and the geometry of the channel. We performed two sets of experiments by changing either the liquid or the channel geometry while we kept the other parameters constant.

For the first set of experiments, we investigated the filling in channel arrays using water, ethanol, isopropanol, and a two-component ethanol and water mixtures. A channel array has 80 parallel channels and it is at least 15 mm long. The individual channels in an array are 50 nm deep and 900 nm wide. The experiments were done under ambient condition (21–25 °C) without using temperature control. During water filling experiments, bubbles spontaneously appeared inside the channels (Figs. 3 and 4). Apart from water, the variation of the meniscus position within a channel array was about 1% of the filled length. Each filling experiment was

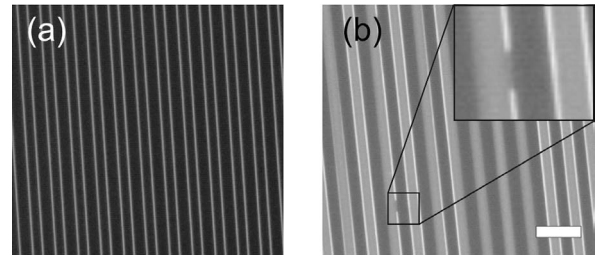


Fig. 4. Arrays of channels were filled using 10 mM rhodamine B dissolved in ethanol (a) and 10 mM fluorescein in 10 mM Tris buffer, pH 7.2 (b). Picture inset in (b) shows a magnification of a bubble trapped inside a channel. The distance between two adjacent channels (thin bright lines) is 10  $\mu\text{m}$ . The scale bar is 40  $\mu\text{m}$ . The pictures were taken with a cooled CCD camera using 640 ms of integration time, maximum gain and same contrast settings. The fluorescein filter set has a higher fluorescence background, and it is more sensitive to scattered light than the rhodamine set. Since the surface of the substrate is not flat because of the fabrication process (Fig. 1) the elevated surfaces are brighter than the lower surfaces.

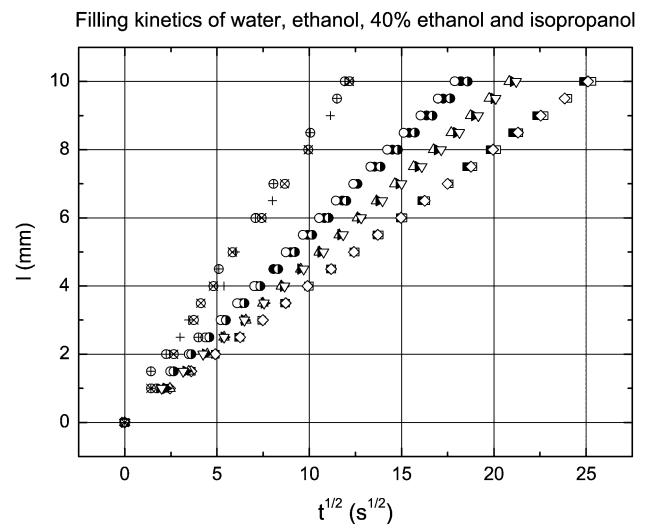


Fig. 5. Filling kinetics of water, ethanol, 40% ethanol, and isopropanol. For each liquid three channel arrays were filled. As each channel array was filled the meniscus position and associated time values were recorded. The three circular legends ( $\circ$ ,  $\bullet$ ,  $\ominus$ ) are filling experiments using ethanol, and each legend represents data from one filling experiment. The triangular ( $\Delta$ ,  $\blacktriangleright$ ,  $\nabla$ ), the square legends ( $\blacksquare$ ,  $\square$ ,  $\diamond$ ) and the legends ( $+$ ,  $\otimes$ ,  $\oplus$ ) correspond to filling experiments using 40% ethanol, isopropanol, and water, respectively.

performed in a fresh channel array to avoid any contamination. The meniscus position  $l$  and the associated time were read as the channels filled (Fig. 3a). The square root of time and the associated meniscus position data were plotted, and data points were fitted using a linear function.

For all the liquids we tested, the position of the meniscus was observed to be proportional to the square root of the time needed to fill the channel array (Fig. 5), which is in accordance with the classical Washburn kinetics. The filling rate, which is proportional to the square of the slope of the linear fit  $D$ , is higher for ethanol than isopropanol. This observation is in agreement with Eq. (2), since the ratio between surface tension and viscosity is higher for ethanol (Table 1).  $D$  was obtained for each filling experiment and the



Table 1  
Summary of filling experiments in Figs. 5 and 6 and tabulated surface tension and viscosity values at 20 °C [29]

Channel depth (nm)	Channel width (nm)	Liquid	Surface tension (dyn/cm)	Viscosity (cP)	$D$ (mm <sup>2</sup> /s)	SD <sup>a</sup>	$\theta_d$	Time to fill 10 mm <sup>b</sup>
50	900	Water	72.9	1.00	0.677	0.02	68	2 min 28 s
50	900	EtOH	22.8	1.20	0.300	0.002	50	5 min 33 s
50	900	Isopropanol	23.8	2.26	0.156	0.01	53	10 min 40 s
50	900	40% EtOH	32.0	2.76	0.229	0.01	38	7 min 17 s
27	500	EtOH	22.8	1.20	0.177	0.004	46	9 min 25 s
73	600	EtOH	22.8	1.20	0.402	0.02	55	4 min 9 s

$D$  is the square of the slope obtained from linear fits of data plotted in Figs. 5 and 6.

<sup>a</sup> Standard deviation of  $D$  is based on three measurements performed on the same day.

<sup>b</sup> The time to fill channels 10 mm is the extrapolated using the fitted  $D$  values.

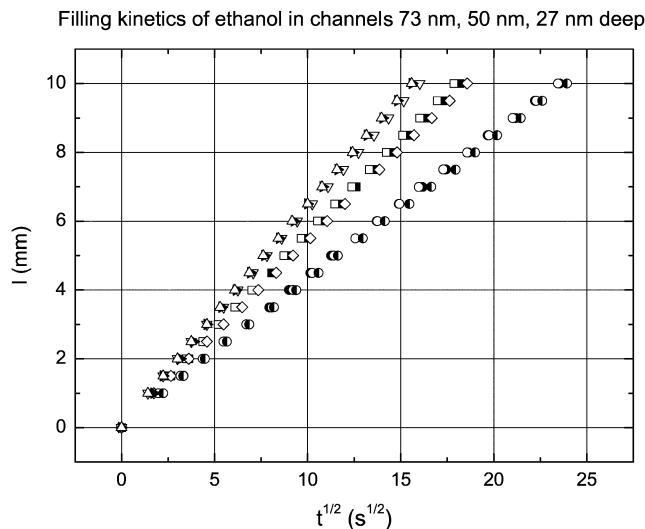


Fig. 6. Filling kinetics of ethanol in channels with different depth. For each channel depth three channel arrays were filled. As each channel array was filled the meniscus position and associated time values were recorded. The three triangular legends ( $\Delta$ ,  $\blacktriangleright$ ,  $\nabla$ ) are filling experiments using 73-nm-deep channels, and each legend represents data from one filling experiment. The rectangular ( $\blacksquare$ ,  $\square$ ,  $\diamond$ ) and the circular legends ( $\circ$ ,  $\bullet$ ,  $\ominus$ ) correspond to filling experiments using 50- and 27-nm-deep channels, respectively.

dynamic contact angle,  $\theta_d$ , was calculated using Eq. (3) and tabulated values (Table 1). The tabulated values are valid for 20 °C [29]. Each measured  $D$  given in Table 1 is an average of three filling experiments performed on the same day. The standard variation of  $D$  for each liquid is less than 4%. For water,  $\theta_d$  is 68°. For ethanol and isopropanol,  $\theta_d$  is respectively 51° and 54°, and for a 40% (v/v) mixture of ethanol and water,  $\theta_d$  is 38°.

In the second set of experiments, we selected ethanol as the test liquid, and studied channels of 27, 50, and 73 nm deep. The experimental conditions were the same as in the first set of experiments. Washburn kinetics was observed for all channel depths. In agreement with Eq. (1) the filling rate decreased with channel depth. Data sets of  $l$  and  $t^{1/2}$  were plotted in Fig. 6, and the obtained  $D$  values are listed in Table 1. The dynamic contact angle is 46° for 27-nm-deep channels and 54° for 73-nm-deep channels.

The time needed to fill the channels using different liquids and channel depth is also given in Table 1. Depending on the

particular liquid and channel depth the time to fill 10-mm-long channels tooks from 2 to 10 min.

## 5. Discussion

### 5.1. Filling kinetics of isopropanol, ethanol, and 40% ethanol in water

We quantitatively studied ethanol, isopropanol, and a two-component mixture (40% ethanol (v/v) in water) in 50-nm-deep and 900-nm-wide channels. The results we obtained were in accordance with the classical Washburn relation, the  $l \sim t^{1/2}$  scaling law. This result also implied that the dynamic contact angles remained independent from time for our experiments. For many times our results were in agreement with studies in nanometer-sized quartz capillaries [20]. Sobolev et al. showed that the dynamic contact angle in nanometer-sized quartz capillaries remained independent from time for meniscus velocities larger than 5  $\mu\text{m/s}$ , which is three times smaller than the lowest meniscus velocity (15.6  $\mu\text{m/s}$  for ethanol in 27-nm-deep channels,  $l = 10$  mm) in our studies. Since our time scale is far above the seconds, dynamic contact angle changes during the initial filling, studied using large-scale molecular dynamic simulation of pore imbibition [24], could not be observed in our experiments.

We calculated the dynamic contact angle by inserting the fitted  $D$  values, and the tabulated values for surface tension and viscosity, into Eq. (3). The values we obtained for the dynamic contact angles were all significantly larger than the equilibrium contact angles measured using a drop shape analysis system from Krüss (Germany). We could only form standing droplets using water on silicon nitride and silicon oxide surfaces. The equilibrium contact angle was about 10° for water and close to zero for the other liquids. Experiments performed by Sobolev et al. [20] showed also a huge difference between the equilibrium and dynamic contact angle. It was observed in capillaries with radii of about 50 nm, that the dynamic contact angle of water increased from 30° to 70° as the meniscus velocity increased from 0 to 8  $\mu\text{m/s}$  which is slightly smaller than our smallest meniscus velocity (15.6  $\mu\text{m/s}$  for ethanol in 27-nm-deep channels,  $l = 10$  mm). In our experiments,  $\theta_d$  was 68° for water, which

agrees well with the experimental data obtained in quartz capillaries [20]. For ethanol,  $\theta_d$  was smaller than the dynamic contact angle for water which was in accordance with measurements made in glass capillaries with an inner radius of 0.295 mm [30]. The  $\theta_d$  for the 40% ethanol water mixture was  $38^\circ$ , which was significantly smaller than  $\theta_d$  for both water and ethanol. We would expect the  $\theta_d$  for the mixture to be between that of ethanol and water. There are two possible explanations, either  $\theta_d$  is really larger than expected, or the other parameters in the  $D$  of Eq. (2) changed. The dynamic contact angle between a fluid and a surface is dependent on the van der Waals forces. Hence, both the silicon dioxide, which is in a direct contact with the liquid, and the underlying silicon nitride influence  $\theta_d$  [22,23]. However, it would be very surprising if the layered silicon oxide/nitride surface had a profound effect for the mixture compared with pure liquids. We look at Eq. (2) for other explanations. Firstly, as mentioned by Dong and Chatzis [17], the filling rate is dependent on the roundness of the corners of capillaries with rectangular cross-section. For the filling of water, ethanol, isopropanol, and 40% ethanol the same set of channels (50 nm deep) was used, and therefore the influence due to the roundness of the corners was the same for all the liquids. Hence, the geometry of the cross-section could not explain the relatively higher filling rate. The remaining parameters which influence  $D$  are the depth, the viscosity, and the surface tension. The depth of our channels, like the roundness of the corners, which only depend on the geometry, would not explain the deviation. Finally, an increase of the ratio between the surface tension and the viscosity,  $\gamma/\eta$ , would also increase the filling rate. According to tabulated viscosity and surface tension values for ethanol–water mixtures [29], 30% ethanol in water mixture has a larger  $\gamma/\eta$  value than the 40% ethanol we used to fill our nanochannels. This might hint that the ethanol content inside the nanochannels is lower than in the initial mixture, which implies a chemical selectivity of the nanochannel toward water. Porous membranes, that are used to separate mixtures of ethanol and water by pervaporation, exhibit similar properties as our nanochannels [31]. Such membranes are more permeable for water than ethanol, and of more water than ethanol entering the membrane. Also our channels and these membranes both have hydrophilic inner surface and similar pore size. The geometry of our nanochannels is uniform while pores in membranes are less well-defined. Arrays of nanochannels could hence serve as an idealized model system to achieve a better understanding of complicated transport and separation mechanisms in membrane materials.

### 5.2. Filling long nanochannels with water and trapping air

We also filled nanochannels using different aqueous solutions. In contrast to ethanol and isopropanol, the filling was very inhomogeneous and bubbles appeared spontaneously. With time the size of the bubbles diminished. Inhomogeneous filling and bubbles were also observed using fluores-

cence microscopy (Fig. 3b). The position of the common meniscus evolved with time corresponds to the Washburn kinetics, however, we do not know how individual channels are filled. Channels were also filled using other mixtures of ethanol and DI water (9%, 18%, ethanol) for which we still observed bubble formation. We were able to fill the channels uniformly without introducing bubbles using 40% ethanol, which generates a lower capillary pressure than pure water when introduced in our nanochannels.

Hibara et al. also observed inhomogeneous filling of water, but they did not observe any air trapping. This is not in contradiction to our observations, since their channels were only 100  $\mu\text{m}$  long [16], and we only observed a few bubbles for every millimeter after the channels were filled (Fig. 3b). Similar trapping of the non-wetting phase (air in our case) during imbibition (injecting a wetting fluid) is a well-known phenomenon in porous media [32,33]. In the range of intermediate to high flow rates, the amount of the trapped non-wetting phase decreases with capillary pressure [33], which is in accordance to our observations. The dimensions between adjacent particles in porous media are comparable to the depth and width of our channels. Therefore, nanochannels could also prove useful as a model system for studying wetting of porous materials under this aspect.

### 5.3. Washburn kinetics in channels with different depth

To our knowledge, 27-nm-deep channels are the smallest channels where filling kinetics by capillary force was studied. This was only possible because of the recent advances in the innovative development of cost-effective fabrication methods of nanochannels [15,25,34–36]. The filling rate decreased with diminishing channel depth (Fig. 5), which is in accordance with Eq. (2). The  $l \sim t^{1/2}$  relation was observed for channels down to about 27 nm. Other filling kinetics studies of channels with rectangular cross-section were performed with much larger channels. Yang et al. reported the marching velocity of capillary menisci in 500-nm-deep silicon nitride channels [18]. Hibara et al. reported filling kinetics in 300-nm-deep channels fabricated in fused silica [16]. Both investigated channels of rectangular cross-section and they also observed the  $l \sim t^{1/2}$  relation. Sobolev et al. made kinetics studies in channels with circular cross-section using pulled quartz capillaries with diameters so small as 80 nm [20]. None of the filling studies in nanochannels including ours showed any clear signs of abrupt physicochemical changes such as phase transitions [37].

## 6. Conclusions

Using a novel and inexpensive technique, we fabricated nanochannels with which we performed filling kinetics studies using different liquids in capillaries down to 27 nm. The position of the moving liquid meniscus during filling was observed to be proportional to the square root of time

needed for filling, which corresponded to the classical Washburn filling kinetics. For pure liquids such as ethanol and isopropanol the experimental results agreed with the theoretical model based on filling by capillary force. For two-component ethanol–water mixtures significant deviation toward higher filling rates were observed. We conclude therefore that nanochannels may have a chemical selectivity toward water compared to ethanol. However, we cannot exclude that the deviation may also be caused by the dynamic contact angle of the mixture being smaller than that of pure ethanol or water. Moreover, we observed trapping of the non-wetting phase (air) during filling with water, which was also observed by others in porous materials. The extreme surface to area ratio of our nanochannel is comparable to pores in membrane materials. The high uniformity of the presented nanochannels could be used as an idealized model to study highly complex mass transport mechanisms in porous materials.

### Acknowledgments

The authors thank the technical staff of ComLab, the joint IMT–CSEM clean room facility. The authors also thank the reviewers of the Journal of Colloid and Interface Science for suggestions and constructive critics. Anpan Han also acknowledges the Danish Research Agency for the financial support (Grant: Internationaliseringsstipendium) for his Ph.D. studies at IMT, University of Neuchâtel.

### References

- [1] S.R. Quake, A. Scherer, *Science* 290 (2000) 1536.
- [2] J. Han, H.G. Craighead, *Science* 288 (2000) 1026.
- [3] N. Kaji, Y. Tezuka, Y. Takamura, M. Ueda, T. Nishimoto, H. Nakanishi, Y. Horiike, Y. Baba, *Anal. Chem.* 76 (2004) 15.
- [4] M.B. Stern, M.W. Geis, J.E. Curtin, *J. Vac. Sci. Technol. B* 15 (1997) 2887.
- [5] M.J. Levene, J. Korfach, S.W. Turner, M. Foquet, H.G. Craighead, W.W. Webb, *Science* 299 (2003) 682.
- [6] N.R. Tas, P. Mela, T. Kramer, J.W. Berenschot, A. van den Berg, *Nano Lett.* 3 (2003) 1537.
- [7] J.L. Li, M. Gershow, D. Stein, E. Brandin, J.A. Golovchenko, *Nat. Mater.* (2003) 611.
- [8] A. Mara, Z. Siwy, C. Trautmann, J. Wan, F. Kamme, *Nano Lett.* 4 (2004) 497.
- [9] H. Bayley, C.R. Martin, *Chem. Rev.* 100 (2000) 2575.
- [10] W.L. Li, J.O. Tegenfeldt, L. Chen, R.H. Austin, S.Y. Chou, P.A. Kohl, J. Krotine, J.C. Sturm, *Nanotechnology* 14 (2003) 578.
- [11] J.M. Ramsey, J.P. Alarie, S.C. Jacobsen, N.J. Peterson, in: Y. Baba, S. Shoji, A. van den Berg (Eds.), *Micro Total Analysis Systems 2002*, vol. 1, Kluwer Academic, Dordrecht, 2002, p. 314.
- [12] Q.S. Pu, J.S. Yun, H. Temkin, S.R. Liu, *Nano Lett.* 4 (2004) 1099.
- [13] E.W. Washburn, *Phys. Rev.* 17 (1921) 273.
- [14] M. Foquet, J. Korfach, W. Zipfel, W.W. Webb, H.G. Craighead, *Anal. Chem.* 74 (2002) 1415.
- [15] H. Cao, Z.N. Yu, J. Wang, J.O. Tegenfeldt, R.H. Austin, E. Chen, W. Wu, S.Y. Chou, *Appl. Phys. Lett.* 81 (2002) 174.
- [16] A. Hibara, T. Saito, H.B. Kim, M. Tokeshi, T. Ooi, M. Nakao, T. Kitamori, *Anal. Chem.* 74 (2002) 6170.
- [17] M. Dong, I. Chatzis, *J. Colloid Interface Sci.* 172 (1995) 278.
- [18] L.J. Yang, T.J. Yao, Y.C. Tai, *J. Micromech. Microeng.* 14 (2004) 220.
- [19] T.C. Ransohoff, C.J. Radke, *J. Colloid Interface Sci.* 121 (1988) 392.
- [20] V.D. Sobolev, N.V. Churaev, M.G. Velarde, Z.M. Zorin, *J. Colloid Interface Sci.* 222 (2000) 51.
- [21] F.M. White, *Fluid Mechanics*, fourth ed., McGraw–Hill, Singapore, 1999.
- [22] A.W. Adamson, A.P. Gast, *Physical Chemistry of Surfaces*, sixth ed., Wiley, New York, 1997.
- [23] G.W. Wang, Y. Zhang, Y.P. Zhao, G.T. Yang, *J. Micromech. Microeng.* 14 (2004) 1119.
- [24] G. Martic, F. Gentner, D. Seveno, J. De Coninck, T.D. Blake, *J. Colloid Interface Sci.* 270 (2004) 171.
- [25] A. Han, G. Mondin, N.G. Hegelbach, N.F. de Rooij, U. Stauffer, in: T. Laurell, J. Nilsson, K. Jensen, D.J. Harrison, J.P. Kutter (Eds.), *Micro Total Analysis Systems 2004*, vol. 1, The Royal Society of Chemistry, Malmö, Sweden, 2004, p. 309.
- [26] G.P. Kennedy, S. Taylor, W. Eccleston, W.M. Arnoldbik, F. Habraken, *Microelectron. Eng.* 28 (1995) 141.
- [27] S. Weichel, R. de Reus, S. Bouaidat, P.A. Rasmussen, O. Hansen, K. Birkelund, H. Dirac, *Sens. Actuators A Phys.* 82 (2000) 249.
- [28] D.C. Duffy, J.C. McDonald, O.J.A. Schueller, G.M. Whitesides, *Anal. Chem.* 70 (1998) 4974.
- [29] R.C. Weast, *CRC Handbook of Chemistry and Physics*, CRC, Boca Raton, 1988.
- [30] A. Hamraoui, K. Thuresson, T. Nylander, V. Yaminsky, *J. Colloid Interface Sci.* 226 (2000) 199.
- [31] X.S. Feng, R.Y.M. Huang, *Ind. Eng. Chem. Res.* 36 (1997) 1048.
- [32] F.A.L. Dullien, *Porous Media, Fluidic Transport and Pore Structure*, second ed., Academic Press, New York, 1992, p. 117.
- [33] M. Blunt, M.J. King, H. Scher, *Phys. Rev. A* 46 (1992) 7680.
- [34] N.R. Tas, J.W. Berenschot, P. Mela, H.V. Jansen, M. Elwenspoek, A. van den Berg, *Nano Lett.* 2 (2002) 1031.
- [35] D.A. Czaplowski, J. Kameoka, R. Mathers, G.W. Coates, H.G. Craighead, *Appl. Phys. Lett.* 83 (2003) 4836.
- [36] C. Lee, E.H. Yang, N.V. Myung, T. George, *Nano Lett.* 3 (2003) 1339.
- [37] J. Klein, E. Kumacheva, *J. Chem. Phys.* 108 (1998) 6996.

## **Chapter 8 :**

### **Paper 3,**

# **Design and fabrication of nanofluidic devices by surface micromachining**

A. Han, N.F. de Rooij, and U. Staufer.

Nanotechnology, 2006, 17, 2498 - 2503.

*to have knowledge is good,*

*to possess curiosity is better,*

*to learn as a hobby is best.*

# Design and fabrication of nanofluidic devices by surface micromachining

Anpan Han, Nicolaas F de Rooij and Urs Staufer<sup>1</sup>

Institute of Microtechnology, University of Neuchâtel, Rue Jaquet-Droz 1/C.P. 3,  
CH-2007 Neuchâtel, Switzerland

E-mail: [urs.staufer@unine.ch](mailto:urs.staufer@unine.ch)

Received 27 January 2006, in final form 13 March 2006

Published 24 April 2006

Online at [stacks.iop.org/Nano/17/2498](http://stacks.iop.org/Nano/17/2498)

## Abstract

Using surface micromachining technology, we fabricated nanofluidic devices with channels down to 10 nm deep, 200 nm wide and up to 8 cm long. We demonstrated that different materials, such as silicon nitride, polysilicon and silicon dioxide, combined with variations of the fabrication procedure, could be used to make channels both on silicon and glass substrates. Critical channel design parameters were also examined. With the channels as the basis, we integrated equivalent elements which are found on micro total analysis ( $\mu$ TAS) chips for electrokinetic separations. On-chip platinum electrodes enabled electrokinetic liquid actuation. Micro-moulded polydimethylsiloxane (PDMS) structures bonded to the devices served as liquid reservoirs for buffers and sample. Ionic conductance measurements showed Ohmic behaviour at ion concentrations above 10 mM, and surface charge governed ion transport below 5 mM. Low device to device conductance variation (1%) indicated excellent channel uniformity on the wafer level. As proof of concept, we demonstrated electrokinetic injections using an injection cross with volume below 50 attolitres ( $10^{-18}$  l).

## 1. Introduction

Fluidic devices with channels in the nanometre range, nanochannels, provide a novel tool for studying single molecules and bionanotechnology [1–4]. Exciting studies on the unique physical chemical properties of fluids in nanochannels have been reported. For example, Stein *et al* described the surface charge governed ion transport, where the ionic conductance of nanochannels strongly deviates from the bulk conductance at low ion concentrations [5]. Daiguji *et al* reported that mechanical energy could be converted to electrochemical energy [6]. As for applications, nanometre-sized entropic traps are used to separate long, genomic DNA [1, 2]. Based on the unique electrokinetic trapping mechanism in nanochannels, Wang *et al* reported million-fold preconcentration of peptides [7]. For a recent review on the nature of nanofluidics and application please refer to Eijkel and van den Berg [8].

Hence, there is an increasing demand for nanofluidic devices. There are two major approaches to fabricate

nanochannels, which serve as the basis of such devices: the use of sacrificial layers, which is also referred to as surface micromachining, or constructing the nanochannels into the bulk of the substrate itself. The first stage for both types of fabrication is to pattern the nanochannel structures. Nanolithography techniques such as focused ion-beam milling [9], nanoimprinting lithography [10] and electron beam lithography [2] have been reported. The width of the channels is often limited by the resolution of the patterning technique. Nanochannels with the width in the micrometre range, also referred to as nanoslits or 1D nanochannels, are fabricated by transferring micrometre wide lines into the bulk of a glass or silicon substrate [1, 3, 11]. It is relatively simple to control the depth of the channels, since established pattern transfer techniques such as wet-etching and reactive ion etching processes could be controlled very well in the nanometre range. For surface machining strategies, the next step would be the encapsulation and the subsequent removal of the sacrificial layer. Taking the bulk machining approach, the second step of fabrication would be to seal the open conduit by bonding [11] or non-uniform thin-film deposition [10]. The two fabrication strategies have

<sup>1</sup> Author to whom any correspondence should be addressed.



their advantages and disadvantages, e.g. diffusion limited removal of the sacrificial layer in nanochannels could be very time consuming, e.g. channels 0.64 mm long required 15 h of etching [12]. To reduce the etching time, dedicated irrigation holes for the etchant have to be made [13], or heat decomposable polymer are used as the sacrificial layer [14, 15]. In certain applications the channels have to be very close to the device surface, e.g. constraints caused by low working distance microscope objectives. It is then more favourable to take the surface machining approach, since only a submicron film separates the liquid inside the nanochannel and the device surface.

Inspired by the innovative work of Lee *et al* [16] and Tas *et al* [12], we developed a new surface machining strategy to fabricate nanochannels with a width up to ten times smaller than the resolution of our photolithography system [17, 18]. The partial etching of the sacrificial layer from the side of the channel shortened the etch time to below 30 min. Applying non-uniform thin-film deposition for encapsulation, our nanochannels have the advantage of being situated just a few hundred nanometres below the device surface.

In this report we investigated the critical design parameters. We fabricated channels with depth between 10 nm and 100 nm and width between 200 nm and 2  $\mu\text{m}$ . By exchanging the different layer materials and adapting the fabrication process, we demonstrated three different material combinations. We also implemented on-chip supporting elements found in micro total analysis systems ( $\mu\text{TAS}$ ) [19, 20]: platinum electrodes and polydimethylsiloxane (PDMS) liquid reservoirs. Ionic conductance experiments in nanochannels showed excellent channel uniformity across a 10 cm silicon wafer. As proof of concept, we performed attolitre electrokinetic injections.

## 2. Materials and methods

### 2.1. Fabrication of nanochannels

**2.1.1. Silicon nitride/silicon dioxide channels on silicon substrates.** The nanochannel fabrication process is based on partial etching of a sacrificial layer [17]. The fabrication process only required established micromachining techniques and did not require any nanolithography. The starting substrates were 525  $\mu\text{m}$  thick, 100 mm diameter (100) silicon (Si) wafers polished on one side. Since electrokinetic experiments were carried out under high electrical fields, an insulation layer of 2  $\mu\text{m}$  thick thermal silicon dioxide ( $\text{SiO}_2$ ) was grown. A sandwich of two silicon nitride ( $\text{Si}_3\text{N}_4$ ) layers deposited by low-pressure chemical vapour deposition (LPCVD) and a  $\text{SiO}_2$  layer in the middle deposited by chemical vapour deposition (CVD) served as the base for further processing (figure 1(a)). The depth of the nanochannels was defined by the thickness of this  $\text{SiO}_2$  layer. For thin  $\text{SiO}_2$  films, a plasma enhanced CVD process with superior thickness control was used instead of CVD. In the first photolithography, features, e.g. lines, were patterned into a positive-tone photoresist. The nanochannels were fabricated along the edges of these features as will be explained further below. The exposed areas of the top  $\text{Si}_3\text{N}_4$  layer were etched by reactive ion etching (RIE). RIE was stopped on the  $\text{SiO}_2$  (figure 1(b)). The exposed sacrificial  $\text{SiO}_2$  layer was partially

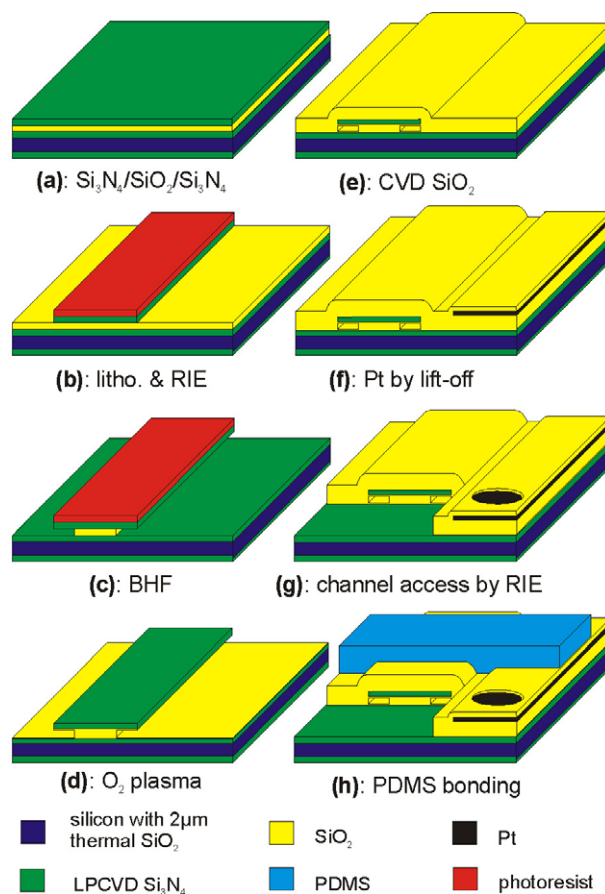


**Figure 1.** Nanochannel system fabrication processes. See section 2 for details.

(This figure is in colour only in the electronic version)

under-etched by buffered hydrofluoric acid (BHF) followed by rinsing using deionized (DI) water (figure 1(c)). In most surface machining processes the sacrificial layer is entirely removed. In our process only a very small portion of it was removed, creating a cavity between the two layers of  $\text{Si}_3\text{N}_4$ . The width of the cavity was determined by the timed etch (about 200 nm  $\text{min}^{-1}$ ) of the sacrificial layer. Before forming the nanochannels by encapsulating these cavities, the  $\text{Si}_3\text{N}_4$  was treated with oxygen plasma (Tepla 132 from PVA Tepla, Feldkirchen, Germany. Parameters: RF power 1000 W, pressure 0.73 mbar, 100  $^\circ\text{C}$ , 60 min) to create a surface composed mainly of  $\text{SiO}_2$  (figure 1(d)) [21, 22]. To seal the channels, a layer of non-uniform CVD  $\text{SiO}_2$  was deposited (figure 1(e)). CVD  $\text{SiO}_2$  deposition: temperature 400  $^\circ\text{C}$ , gases 2%  $\text{SiH}_4$  in  $\text{N}_2$ , and  $\text{O}_2$ , pressure atmospheric.

**2.1.2.  $\text{SiO}_2$  channels.** Instead of using  $\text{Si}_3\text{N}_4$  layers we used 300 nm thick LPCVD polysilicon layers. After the BHF etch of sacrificial  $\text{SiO}_2$ , the substrate was put into an oxidation furnace to convert the polysilicon into  $\text{SiO}_2$ . The channels were encapsulated using the same non-uniform CVD process. Channels in  $\text{SiO}_2$  have extremely low autofluorescence, hence they are very suitable for experiments which require low background fluorescence.

**2.1.3. Silicon nitride/dioxide channels on Pyrex substrates.** For Pyrex substrates we used 300 nm thick PECVD  $\text{Si}_x\text{N}_y$  as top and bottom layers due to the incompatibility between Pyrex and high temperature LPCVD processing. The transparency of Pyrex substrates allows working in optical transmission mode, which could increase the flexibility of the experimental set-up. Furthermore, Pyrex is an insulator; hence nanochannels fabricated on Pyrex substrates could be used for experiments involving electrokinetically driven flow at extremely high electrical fields.

## 2.2. Integration of on-chip support elements

After channel encapsulation, platinum (Pt) electrodes were integrated using a *lift-off* process. For the Pt electrodes, 1300 Å of Pt was evaporated on top of 200 Å of a tantalum adhesion layer. Pt electrodes were covered with another 200 nm of CVD  $\text{SiO}_2$  (figure 1(f)). A third photolithography and RIE process was used to pattern the access openings to the nanochannels and to expose the Pt where needed (figure 1(g)). An advantage of our fabrication strategy was that after the encapsulation the channels remained closed until access openings were made. This allowed subsequent processes, e.g. in our case lift-off of Pt to form electrodes. Polydimethylsiloxane (PDMS) structures were prepared by SU-8 moulding [23] and sealed irreversibly to the access openings to serve as liquid reservoirs (figure 1(h)). The final die was glued and wire-bonded to a printed circuit board (PCB). The PCB had two major functions; the on-chip electrodes could be easily interfaced with off-chip electronics, and the PCB had size equivalent to a standard 3 inch microscope slide. It was convenient to handle and compatible with most microscopes.

## 2.3. Ionic conductance measurements

We prefilled the nanochannels by adding a DI water–ethanol mixture (40% ethanol) to one of the two reservoirs to avoid air bubbles [17]. After the prefilling process, phosphate buffer (pH 8) solution prepared from  $\text{Na}_2\text{H}_2\text{PO}_4$  and  $\text{Na}_3\text{HPO}_4$  (Sigma, Buchs, Switzerland) was added to the liquid reservoirs to replace the water–ethanol mixture. The on-chip electrodes were connected to a voltage–current source–measure unit (236, Keithley, OH, USA), controlled by a computer program in Labview (National Instruments, USA). Voltage sweeps were made by stepping the voltage from  $-100$  to  $+100$  V in steps of 10 V with 10 s duration. The current was measured and the slopes of the voltage/current data plots were obtained. After the exchange of buffer, the first sweeps were not stable and produced a slope which was too high or too low depending on the previous buffer. We discarded these first sweeps. The conductance was then calculated from the average slope value of three sweeps.

## 2.4. Electrokinetic injections

After the initial prefilling, 50 mM borate buffer, pH 9 (Fluka, Buchs, Switzerland) was added to the liquid reservoirs in PDMS to replace the water–ethanol mixture. The on-chip Pt electrodes were connected to an in-house constructed high voltage power supply [24]. We used 10 mM fluorescein

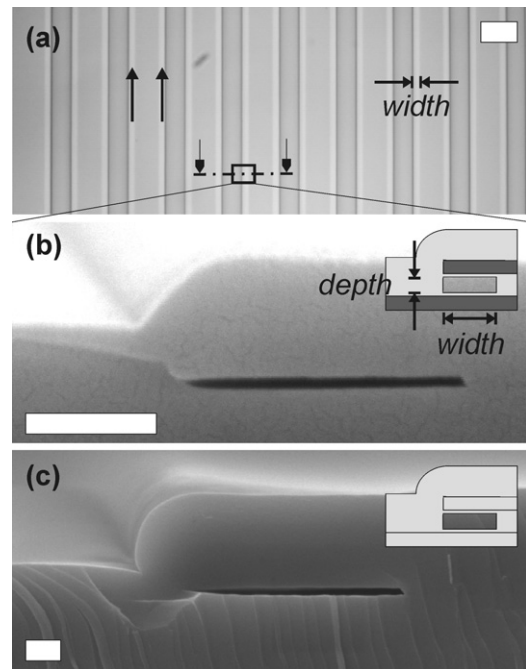


**Figure 2.** Optical microscopy image of 18 parallel nanochannels in LPCVD  $\text{Si}_3\text{N}_4/\text{SiO}_2$  (a), and cross-sectional scanning electron microscopy (SEM) images of nanochannels in LPCVD  $\text{Si}_3\text{N}_4/\text{SiO}_2$  (b), and  $\text{SiO}_2$  (c) on silicon substrates. Scale bar: 10  $\mu\text{m}$  in (a) and 500 nm in (b) and (c). The two parallel arrows in (a) pointing upwards indicate a pair of nanochannels seen as bright lines about 2  $\mu\text{m}$  wide. (b) is a cross-sectional image of one of the parallel nanochannels in (a). The dark thin slits in (b) and (c) are the cross-sections of nanochannels being respectively 2  $\mu\text{m}$  and 600 nm wide and less than 100 nm deep. Samples for SEM imaging were prepared by cleaving a part of a processed wafer, such that the cut ran across the nanochannels, exposing the cross-section. To decrease charging effects a thin layer of AuPd (5 nm) was sputtered onto the sample before imaging.

(Fluka, Buchs, Switzerland) dissolved in borate buffer as the sample for our proof of concept injection experiments. The fluorescence signal in the nanochannels was imaged with a cooled CCD camera (CF 8/4 DXC from Kappa, Gleichen, Germany) mounted on an inverted fluorescence microscope with integrated filter-sets (Axiovert S100 from Zeiss). Computer software Pinnacle Studio, version 8.12.7.0, from Pinnacle Systems and Corel Draw 11 from Corel were respectively used for video and image analysis.

## 3. Results and discussions

### 3.1. Fabrication

Using a surface machining technique (figure 1), we fabricated parallel channels in different materials with width dimensions smaller than our lithography resolution (figure 2). Figure 2(a) shows an optical microscopy image of 18 parallel nanochannels about 2  $\mu\text{m}$  wide. Corresponding to figure 1(e), a pair of nanochannels was formed for a line patterned using standard photolithography. Using this technique we fabricated  $\text{Si}_3\text{N}_4/\text{SiO}_2$  nanochannels with width between 200 nm and 2  $\mu\text{m}$ , and depth between 10 and 100 nm. By combining different materials and adapting the fabrication



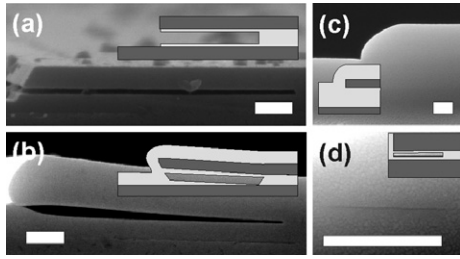


**Figure 3.** Critical processing parameters. Scale bar: 500 nm. By changing the thickness of the LPCVD  $\text{Si}_3\text{N}_4$  and the sacrificial  $\text{SiO}_2$  layers, different channel cross-sectional geometries could be fabricated. If the partial sacrificial etch was large ((a) before encapsulation), the upper  $\text{Si}_3\text{N}_4$  layer bent upward during the encapsulation with  $\text{SiO}_2$ , which had compressive stress ((b) the same structure as (a) after encapsulation). If the sacrificial layer was too thick, the non-uniform encapsulation layer could enter and fill the cavity (c). Channels 10 nm deep were fabricated using a very thin sacrificial layer (d).

process, we were also able to fabricate nanochannels entirely in  $\text{SiO}_2$  on silicon substrates (figure 2(c)), and PECVD  $\text{Si}_x\text{N}_y/\text{SiO}_2$  on Pyrex substrates (not shown). Under conditions where the channel depth was large, the non-uniform deposition of CVD  $\text{SiO}_2$ , used to encapsulate the channels, entered the cavity, resulting in certain cases in a slightly triangular cross-section (figure 2(c)). To further investigate and refine the nanochannel fabrication process we performed a set of experiments using  $\text{Si}_3\text{N}_4/\text{SiO}_2$  nanochannels on silicon substrates as a model.

We varied the thickness of the top structural  $\text{Si}_3\text{N}_4$  layer (200 and 300 nm), the thickness of the sacrificial layer (10, 50, 100, 500 nm) and the time of the partial sacrificial etch (up to 20 min). The thickness of the sacrificial layer determined the depth of our nanochannels, while the channel width was controlled by the timed etch. Due to the compressive stress accumulated during the CVD deposition, the suspended  $\text{Si}_3\text{N}_4$  bent up if it was too thin or if the cavity was too wide (figures 3(a) and (b)). In figure 3(b) we see that the non-uniform CVD  $\text{SiO}_2$  also entered the cavity. The up-bending could be controlled by using a thicker  $\text{Si}_3\text{N}_4$  layer, a narrower channel or a stiffer material. In the extreme case, if the thickness of the sacrificial layer was too large (500 nm), i.e. the gap between the two structural layers was too big, the CVD deposition filled the entire cavity (figure 3(c)). On the other hand, depositing very thin sacrificial layers, channels approximately 10 nm deep were fabricated (figure 3(d)). To reproducibly fabricate nanochannels, we derived from our set of experiments that if a 300 nm thick  $\text{Si}_3\text{N}_4$  top layer was used the width to depth aspect ratio should be kept between 5 and 20. The achievable width to depth aspect ratio depended on the stress in the deposited encapsulation layer and its non-uniformity. Hence, by reducing the stress and increasing the non-uniformity of the encapsulation layer, narrower and wider channels could be fabricated.

Apart from parallel channels we were also able to fabricate crosses, which connected four channels. During the first photolithography process, we designed two squares with a slight overlap of 500 nm to 2  $\mu\text{m}$ . This overlap was transferred into the  $\text{Si}_3\text{N}_4$ , and after the partial sacrificial etch

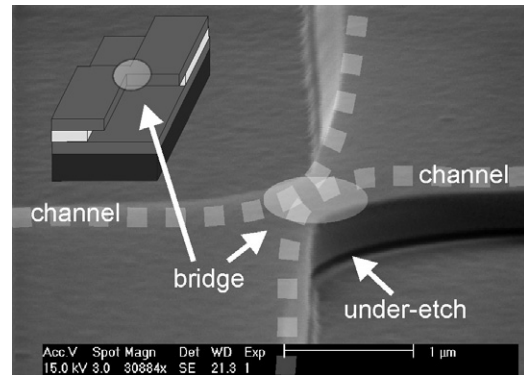


**Figure 4.** Injection-cross structure before channel encapsulation using non-uniform CVD  $\text{SiO}_2$  deposition. Two squares with a small overlap were transferred into the  $\text{Si}_3\text{N}_4$ . After the partial sacrificial etch, a free standing bridge connecting four channels was formed.

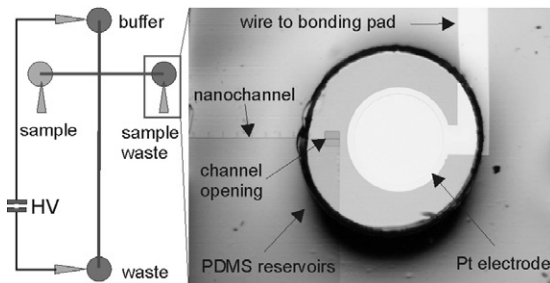


**Figure 5.** Functional elements on the nanofluidic chip. On-chip platinum electrodes fabricated by lift-off were connected to an in-house constructed high-voltage (HV) power supply or a source measurement unit. Solutions were pipetted into the PDMS reservoirs moulded using SU8. The nanochannel and its opening are also shown. The distance between the sample and the sample waste reservoirs was 10 mm, and the distance between the buffer and the waste reservoirs was 20 mm.

a free standing bridge connecting four channels was formed (figure 4).

### 3.2. Ionic conductance measurements

By combining nanochannels in  $\text{Si}_3\text{N}_4/\text{SiO}_2$  on silicon substrates together with on-chip platinum electrodes fabricated by lift-off and PDMS reservoirs, we could design simple nanofluidic devices (figure 5). In the subsequent experiments, channels were 50 nm deep and 2  $\mu\text{m}$  wide unless stated otherwise. We measured the ionic conductance by plotting data from voltage–current measurements in nanochannels fabricated on a single wafer. The ionic conductance was proportional to the number of parallel channels (figure 6), and inversely proportional to the channel length. By measuring the conductance as a function of buffer concentration we observed Ohmic behaviour at concentrations between 10 and 500 mM (equivalent to about 20 and 1000 mM KCl), but as the concentration decreased to 1 mM we approached a conductance plateau. Our observations were consistent with previous reports. Stein *et al* and Schoch *et al* showed that for channels about 50–100 nm deep the ion transport due to surface charge takes place at concentrations below 5 mM KCl [5, 25].

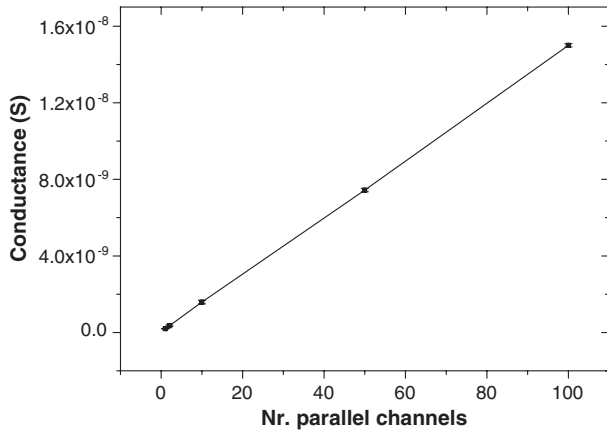


**Figure 6.** Ionic conductance of chips with parallel channels 50 nm deep, 2  $\mu\text{m}$  wide and 5 mm long, filled with 0.5 M phosphate buffer (pH 8). Each data point with error bar was based on the conductance measured on three different chips.

### 3.3. Channel uniformity on the wafer level

For chips with 50 and 100 parallel channels the variance of the conductance measurement of three chips was 1% (figure 6). Large conductance variance of a single channel (7%) is explained by our measurement set-up, which was not optimized to measure impedances in the 10 G $\Omega$  range. The low chip to chip variation confirmed the high wafer level uniformity of our nanochannels [17]; filling experiments in Si<sub>3</sub>N<sub>4</sub>/SiO<sub>2</sub> nanochannels on silicon substrates showed that, as we filled 80 parallel nanochannels with isopropanol or ethanol, the variation between the filling was less than 1% of the filled length, i.e. if the meniscus front was 10 mm from the liquid reservoir, the variation among the 80 parallel channels was less than 100  $\mu\text{m}$  [17]. From the filling kinetic studies different channel-arrays positioned across the 10 cm diameter wafer were analysed and found to show similar filling rates. Since the filling rate is dependent on the channel geometry and the surface chemistry, the nanochannels proved to be extremely uniform across the wafer.

### 3.4. Electrokinetic measurements and attolitre injections

Using the current monitoring method [26], we investigated the electro-osmotic flow (EOF) mobility in chips with 100 parallel channels, each being 5 mm long. The channels were filled with 50 mM phosphate buffer (pH 8). The EOF mobility was determined to be  $1.5 \times 10^{-8} \text{ m}^2 \text{ V}^{-1} \text{ s}^{-1}$ , which was slightly smaller than reported values ( $2.8 \times 10^{-8} \text{ m}^2 \text{ V}^{-1} \text{ s}^{-1}$ ) in channels about 200 nm deep [27].

We were able to perform electrokinetic injections of fluorescein (figure 7). We used pinched injection to minimize the sample plug [28, 29]. The switching time needed to redirect the sample plug into the separation channel took about 1 s, which was about the same as the switching time of our electronics. The plug broadened slightly by diffusion during the switching. In figure 7, we see that the width of the fluorescence image of the channels is significantly wider than its physical dimensions. This is because the fluorescence images do not give accurate dimensions of the nanochannels

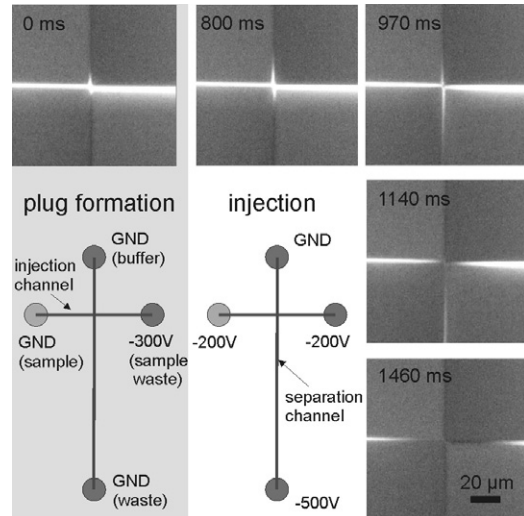


**Figure 7.** Pinched injection. Five image frames were taken from a video recording of the injection of fluorescein. The sample plug was formed (0 ms) by setting all the reservoirs to ground except the sample waste reservoir (300 V). The sample was confined to the injection channel; only a minimal amount of sample entered the separation channel by diffusion. During the injection itself, the waste reservoir was set to  $-500 \text{ V}$ , the sample and sample waste to  $-200 \text{ V}$ , while the buffer was set to ground. The plug broadened slightly during the switching of the electronics (800 ms), and it moved towards the waste reservoir (970 ms). At 1140 ms, the plug moved entirely into the separation channel, before leaving the field of observation (1460 ms). We clearly see that the pinched injection procedure pushed the sample back into the injection channels during injection.

due to emission of fluorescence in all directions. The size of the moving injection plug image was larger than its actual dimension, since the integration time of the CCD camera caused streaking effects.

## 4. Conclusions and outlook

We fabricated nanofluidic chips using a simple process which only required three photolithography steps. The fabrication of nanochannels using the partial sacrificial etching technique proved to be very flexible and a range of material combinations and substrates could be used. This flexibility could be advantageous in specific applications; e.g. in many nanofluidic applications, fluorescence detection is preferred due to the availability of different labels and the wide range of sensitive detection methods [1, 2, 4]. For these applications the nanochannels made entirely in SiO<sub>2</sub> could be used due to the low fluorescence background. The selected material combinations were restricted by the availability in our laboratory. We believe that other material combinations are possible. In our process, we could grow thick, up to several  $\mu\text{m}$ , silicon oxide layers onto silicon wafers for electrical insulation, which is needed for electrokinetic experiments. We could therefore operate our chips safely at high voltages compared to e.g. channels fabricated using anodic bonding of silicon to Pyrex [1]. At the moment all channels in our device have the same cross-section; however, we could perform several lithography and partial

sacrificial etching steps to include channels with different widths. The depth could also be varied by selectively removing or adding sacrificial layers in certain areas before depositing the second structural layer. The wafer level homogeneity of nanochannels proved to be excellent by ionic conductance as well as filling experiments [17]. As Eijkel and van den Berg [8] pointed out, the high uniformity achieved using nanofabrication technologies could be for example used as a matrix for chemical separation. Since our nanochannels have the same dimensions as the pores inside the silica packing for high performance liquid chromatography, HPLC, they could serve as a new separation matrix. The resolution of HPLC is limited by the band broadening effect due to e.g. the fact that molecules take different pathways inside a separation column, *eddy diffusion* [30]. The high uniformity of the channels could increase the resolution, since all molecules have the same pathway and eddy diffusion is removed. In the future we would like to investigate if liquid chromatography separation in nanochannels, which corresponds to separation inside a pore of a silica packing particle, can increase the resolution of separation.

### Acknowledgments

The authors would like to thank the technical staff of ComLab, the joint IMT-CSEM clean room facility. AH also acknowledges the Danish Research Agency for the financial support (grant Internationaliseringsstipendium) for his PhD studies at IMT, University of Neuchâtel.

### References

- [1] Han J and Craighead H G 2000 *Science* **288** 1026
- [2] Kaji N, Tezuka Y, Takamura Y, Ueda M, Nishimoto T, Nakanishi H, Horiike Y and Baba Y 2004 *Anal. Chem.* **76** 15
- [3] Stern M B, Geis M W and Curtin J E 1997 *J. Vac. Sci. Technol. B* **15** 2887
- [4] Levene M J, Korfach J, Turner S W, Foquet M, Craighead H G and Webb W W 2003 *Science* **299** 682
- [5] Stein D, Kruijthof M and Dekker C 2004 *Phys. Rev. Lett.* **93** 1
- [6] Daiguji H, Yang P D, Szeri A J and Majumdar A 2004 *Nano Lett.* **4** 2315
- [7] Wang Y C, Stevens A L and Han J Y 2005 *Anal. Chem.* **77** 4293
- [8] Eijkel J and van den Berg A 2005 *Microfluidics and Nanofluidics* **1** 249
- [9] Alarie J P, Hmelo A B, Jacobsen S C, Baddor A P, Feldman L and Ramsey J M 2003 *Conf. Proc. of Micro Total Analysis Systems (Squaw Valley, CA, USA)* vol 1, p 9
- [10] Cao H, Yu Z N, Wang J, Tegenfeldt J O, Austin R H, Chen E, Wu W and Chou S Y 2002 *Appl. Phys. Lett.* **81** 174
- [11] Haneveld J, Jansen H, Berenschot E, Tas N and Elwenspoek M 2003 *J. Micromech. Microeng.* **13** S62
- [12] Tas N R, Berenschot J W, Mela P, Jansen H V, Elwenspoek M and van den Berg A 2002 *Nano Lett.* **2** 1031
- [13] Foquet M, Korfach J, Zipfel W, Webb W W and Craighead H G 2002 *Anal. Chem.* **74** 1415
- [14] Li W L, Tegenfeldt J O, Chen L, Austin R H, Chou S Y, Kohl P A, Krotine J and Sturm J C 2003 *Nanotechnology* **14** 578
- [15] Czaplowski D A, Kameoka J, Mathers R, Coates G W and Craighead H G 2003 *Appl. Phys. Lett.* **83** 4836
- [16] Lee C, Yang E H, Myung N V and George T 2003 *Nano Lett.* **3** 1339
- [17] Han A, Mondin G, Hegelbach N G, Rooij N F and Stauffer U 2006 *J. Colloid Interface Sci.* **293** 151
- [18] Han A, Mondin G, Hegelbach N G, de Rooij N F and Stauffer U 2004 *Conf. Proc. Micro Total Analysis Systems (The Royal Society of Chemistry, Malmö, Sweden)* vol 1, p 309
- [19] Vilknær T, Janásek D and Manz A 2004 *Anal. Chem.* **76** 3373
- [20] Bruin G J 2000 *Electrophoresis* **21** 3931
- [21] Kennedy G P, Taylor S, Eccleston W, Arnoldbik W M and Habraken F 1995 *Microelectron. Eng.* **28** 141
- [22] Weichel S, de Reus R, Bouaidat S, Rasmussen P A, Hansen O, Birkelund K and Dirac H 2000 *Sensors Actuators A* **82** 249
- [23] Duffy D C, McDonald J C, Schueller O J A and Whitesides G M 1998 *Anal. Chem.* **70** 4974
- [24] Linder V, Verpoorte E, Thormann W, de Rooij N F and Sigrüst H 2001 *Anal. Chem.* **73** 4181
- [25] Schoch R B and Renaud P 2005 *Appl. Phys. Lett.* **86** 253111
- [26] Huang X H, Gordon M J and Zare R N 1988 *Anal. Chem.* **60** 1837
- [27] Mela P, Tas N R, Berenschot E J, van Nieuwkasteel J and van den Berg A 2004 *Electrophoresis* **25** 3687
- [28] Shultz-Lockyear L L, Colyer C L, Fan Z H, Roy K I and Harrison D J 1999 *Electrophoresis* **20** 529
- [29] Jacobson S C, Hergenroder R, Koutny L B, Warmack R J and Ramsey J M 1994 *Anal. Chem.* **66** 1107
- [30] Skoog D A, West D M and Holler F J 1991 *Fundamentals of Analytical Chemistry* 7th edn (Fort Worth: Saunders College Publishing)

## Chapter 9 : Summary and outlook

The greatest dream of scientists and engineers is to construct new tools to look at nature at the molecular level. In this thesis the author presents some of the efforts in that direction by the use of nanopores and nanochannels. The struggle towards the distant goal seems very difficult. Nevertheless, efforts by many brilliant scientists, have planted numerous milestones. Examples are real-time observation of rotating molecular motors (Noji, 1997) and counting single DNA or protein molecules using molecular Coulter counters, which is the main topic of this thesis. Using synthetic nanopores fabricated at IMT it is possible to determine the size of protein molecules as well as extract information on their net charge. Such information is very important for fundamental studies of proteins, but it could also be useful in biochemical analysis. Nanopore experiments at IMT also showed that it is possible to detect specific molecular binding without the use of labels which is a major cost factor of biochemical assays. Since nanopore sensing is a single molecule method, the number of molecule needed for analysis is equivalent to the statistical reliable count of molecules, i.e. less than 1000 molecules. The theoretical sensitivity of nanopores is therefore in the range of zeptomols ( $10^{-21}$ ). Optimization of such assays could find many biotechnology applications.

A new nanochannel fabrication process has been developed at IMT which showed superior uniformity and at the same time being relatively

simple from the fabrication point of view. At IMT studies of filling kinetics by capillary force in channels down to 30 nm deep were made. While the over-all filling kinetics followed the classical Washburn description, more unexpected results such as spontaneous bubble formation have been observed. The greatest strength of microfabricated nanochannels is its superior uniformity compared to previous colloidal systems. This makes them the ideal experimental platforms to study physiochemical effects in the nanometer range. Experiments in nanochannels reported by other investigators, suggested that nanochannels also have great potentials in biochemical analysis on the single molecule level.

Taking the advantage of nanopores and channels which have the same dimensions as single biomolecules, new and outperforming devices were constructed to study and analyze one molecule at a time. Numerous unique applications have been presented. I am thrilled to read the next milestones towards the ultimate goal of looking at how the nanomachines of nature work together. To my personal belief, the H. C. Andersen picture is likely to repeat itself, however much more civilized than Copenhagen in the 19th century. The DNA is being read by a number of proteins, and somehow they are arguing like construction workers about how and where to start the work, while the engineer is trying to figure out

if his team is on the right chromosome. To make things more chaotic small and disturbing ions are always getting in the way.

Anything else would be too boring and disappointing.

*the persistence to memorize,  
the endurance to learn,  
and the patience to describe and teach,*

*if only I had one.*



## Appendix, Critical steps of nanopore fabrication

The nanopore fabrication process is given in Chapter 4 and Chapter 5. The fabrication process is apparently simple and straightforward. However, the author will point out several important critical steps in the following sections.

### **LPCVD $\text{Si}_3\text{N}_4$**

The first step was very important since elevated defects (also referred to as pinholes) in the 20-nm-thin layer could totally damage the wafer in the KOH process. The  $\text{Si}_3\text{N}_4$  served as a mask in the KOH etching process, any defect in the 20-nm-thick mask would be transferred into the underlying 500-nm-thick  $\text{SiO}_2$ .  $\text{SiO}_2$  is slowly etched in KOH (50 nm/h). To create the free standing membranes, the total etch time was about 24h. Hence, the KOH will penetrate the  $\text{SiO}_2$  and etch the underlying silicon. Due to the orientation of the crystallographic planes of silicon, small pyramidal pits about a few  $\mu\text{m}$  large were created for every defect in the  $\text{Si}_3\text{N}_4$  layer. At 40 $\times$  magnification such pits were visible as dark squares. The area density of such pits is a direct measure of the density of the pinholes in the  $\text{Si}_3\text{N}_4$  layer.

### **Pretreatment of $\text{Si}_3\text{N}_4$ before PMMA spinning:**

The PMMA layer served as the etch mask for structuring the  $\text{Si}_3\text{N}_4$  layer. Defects in the PMMA layer were hence also transferred into the  $\text{Si}_3\text{N}_4$  during the RIE. A high defect density in the PMMA layer would be equivalent to poor

LPCVD  $\text{Si}_3\text{N}_4$ . To decrease the density of defects in the PMMA layer a surface treatment of the wafer proved to be very effective. A 30 minute oxygen plasma treatment decreased defects by 80%. Note that during spinning of PMMA any contact with polymers should be avoided, since the PMMA solvent is not compatible with many polymers.

### **E-beam writing process.**

For an introduction to e-beam lithography please refer to (McCord, 1997). The e-beam lithography process is very dependent on the employed equipment. In this thesis the Raith 150 was employed, hence many of the information below was based on this specific equipment. I try to give a general description of the lithography process. In certain cases special machine specific procedures are also mentioned.

During the manufacturing of silicon wafers, a *bow* is created, i.e. the wafer is not entirely flat. On the  $\mu\text{m}$  range it has a bowl shape. The bow parameter is in the range of 40  $\mu\text{m}$ . As a wafer was written by the e-beam with a fixed focus, the wafer would be at certain areas out of focus, decreasing the definition of the objects being written. To achieve a good uniformity on the wafer level, it is very important that the wafer was fixed on a very flat surface. To achieve this, an electrostatic chuck was used to fix the wafer. Using the electrostatic chuck from Raith, it was necessary to contact the silicon of the wa-

fer to the electrodes, which was done by scratching locally on the wafer by a diamond knife for removing the insulating oxides. The wafer was also adjusted such that it was perpendicular to the beam using the *sample leveling* procedure in the Raith software.

To achieve the smallest pores, according to McCord and Rooks, the highest acceleration voltage should be combined with the smallest aperture size and the thinnest possible PMMA layer. In the best case where secondary electron scattering dominates, the practical resolution is 20 nm (McCord, 1997). Different aperture size, 7.5, 10, 20 and 30  $\mu\text{m}$  were tested. Using the 20 kV and 7.5  $\mu\text{m}$  aperture settings, the quality of the images at 200000 $\times$  magnification changed little if the focus distance was changed by  $\pm 5 \mu\text{m}$ . While using the 20 and 30  $\mu\text{m}$  apertures, the tolerance of focus was reduced to  $\pm 2 \mu\text{m}$ . For the 10  $\mu\text{m}$  aperture the tolerance was  $\pm 3 \mu\text{m}$ . Since the total thickness variation of a 10 cm diameter silicon wafer was typically 5  $\mu\text{m}$ . The best wafer level uniformity could be achieved by using the 7.5  $\mu\text{m}$  aperture. It is very important to keep the substrate in focus for a good wafer level uniformity. Another feature of the Raith machine, *height control*, which moves the stage up and down to maintain focus, should be switched on.

Having selected the acceleration voltage and aperture size, the shape of the beam has to be optimized by adjusting the aperture alignment and the stigmation. In case of astigmatic image

errors pores with an elliptical shape were fabricated.

The next step of writing was to *align the write-field* which was 100  $\mu\text{m} \times 100 \mu\text{m}$  large. In the same write-field as the pore three 1  $\mu\text{m}$  large squares were written to facilitate the location of the nanopore during optical and scanning electron microscopy.

The Raith software offers three different writing modes, *area*, *line*, and *dot*. The nanopores were defined using the dot mode, where the e-beam moved to the coordinates of the nanopore and the PMMA was exposed to e-beam radiation for a defined period of time. The other features were exposed using the area mode, where the beam scanned in a vector fashion covering the designed area. The dot dose was about 0.001 pAs, and the area dose was about 150  $\mu\text{A}/\text{cm}^2$ .

### ***Pattern transfer from PMMA to $\text{Si}_3\text{N}_4$ by reactive ion etching***

The features in the PMMA were transferred into the  $\text{Si}_3\text{N}_4$  by RIE. The Alcatel machine had two etching modes, a  $\text{SF}_6$  chemistry operating at low power and low pressure (RIE low) or a  $\text{CF}_4$  chemistry operating at high power and high pressure process (RGV low). The RGV low process has a more physical etching character than the RIE mode due to the high operating power (Madou, 2002). To achieve the smallest pores a physical pattern transfer is more attractive, and indeed after numerous test the smallest



## *Appendix*

pores fabricated using the RGV low mode were 15 nm, while 20 nm for the RIE low mode.

## References

- Alarie, J.P., Hmelo, A.B., Jacobsen, S.C., Baddor, A.P., Feldman, L. and Ramsey, J.M. (2003) Fabrication and evaluation of 2D confined nanochannels. *Micro Total Analysis Systems 2003*, Squaw Valley, California, USA, pp. 9-12.
- Alberts, B., Bray, D., Johnson, A., Lewis, L., Raff, M., Roberts, K. and Walter, P. (1998) *Essential cell biology*. Garland, New York.
- Bayley, H. and Martin, C.R. (2000) Resistive-pulse sensing - From microbes to molecules. *Chemical Reviews*, **100**, 2575.
- Bustamante, C., Macosko, J.C. and Wuite, G.J. (2000) Grabbing the cat by the tail: manipulating molecules one by one. *Nature Reviews Molecular Cell Biology*, **1**, 130.
- Butler, T.Z., Gundlach, J.H. and Troll, M.A. (2006) Determination of RNA orientation during translocation through a biological nanopore. *Biophysical Journal*, **90**, 190.
- Cao, H., Yu, Z.N., Wang, J., Tegenfeldt, J.O., Austin, R.H., Chen, E., Wu, W. and Chou, S.Y. (2002) Fabrication of 10 nm enclosed nanofluidic channels. *Applied Physics Letters*, **81**, 174.
- Chang, H., Kosari, F., Andreadakis, G., Alam, M.A., Vasmatazis, G. and Bashir, R. (2004) DNA-mediated fluctuations in ionic current through silicon oxide nanopore channels. *Nano Letters*, **4**, 1551.
- Chen, P., Mitsui, T., Farmer, D.B., Golovchenko, J., Gordon, R.G. and Branton, D. (2004) Atomic layer deposition to fine-tune the surface properties and diameters of fabricated nanopores. *Nano Letters*, **4**, 1333.
- Constans, A. (2003) Beyond Sanger: toward the \$1,000 genome. *The Scientist*, **17**, 36.
- Coulter, W.H. (1953) Means of counting particles suspended in a fluid. US Patent 2.656.508
- Czaplewski, D.A., Kameoka, J., Mathers, R., Coates, G.W. and Craighead, H.G. (2003) Nanofluidic channels with elliptical cross sections formed using a nonlithographic process. *Applied Physics Letters*, **83**, 4836.
- Davenport, R.J., Wuite, G.J., Landick, R. and Bustamante, C. (2000) Single-molecule study of transcriptional pausing and arrest by E. coli RNA polymerase. *Science*, **287**, 2497.
- Deblois, R.W. and Bean, C.P. (1970) Counting and sizing of submicron particles by resistive pulse technique. *Review of Scientific Instruments*, **41**, 909.
- Deblois, R.W., Uzgiris, E.E., Cluxton, D.H. and Mazzone, H.M. (1978) Comparative measurements of size and polydispersity of several insect viruses. *Analytical Biochemistry*, **90**, 273.
- Eijkel, J. and van den Berg, A. (2005) Nanofluidics: what is it and what can we expect from it. *Microfluidics and Nanofluidics*, **1**, 249.
- Fologea, D., Gershow, M., Ledden, B., McNabb, D.S., Golovchenko, J.A. and Li, J. (2005a) Detecting single stranded DNA with a solid state nanopore. *Nano Letters*, **5**, 1905.
- Fologea, D., Uplinger, J., Thomas, B., McNabb, D.S. and Li, J. (2005b) Slowing DNA translocation in a solid-state nanopore. *Nano Letters*, **5**, 1734.
- Foquet, M., Korlach, J., Zipfel, W., Webb, W.W. and Craighead, H.G. (2002) DNA fragment sizing by single molecule detection in submicrometer-sized closed fluidic channels. *Analytical Chemistry*, **74**, 1415.
- Foquet, M., Korlach, J., Zipfel, W.R., Webb, W.W. and Craighead, H.G. (2004) Focal volume confinement by submicrometer-sized fluidic channels. *Analytical Chemistry*, **76**, 1618.
- Guo, L.J., Cheng, X. and Chou, C.F. (2004) Fabrication of size-controllable nanofluidic channels by nanoimprinting and its application for DNA stretching. *Nano Letters*, **4**, 69.
- Han, J. and Craighead, H.G. (2000) Separation of long DNA molecules in a microfabricated entropic trap array. *Science*, **288**, 1026.
- Haneveld, J. (2006) Nanochannel fabrication and characterization using bond micromachining. Twente.

## References

- Haneveld, J., Jansen, H., Berenschot, E., Tas, N. and Elwenspoek, M. (2003) Wet anisotropic etching for fluidic 1D nanochannels. *Journal of Micromechanics and Microengineering*, **13**, S62.
- Heins, E.A., Siwy, Z.S., Baker, L.A. and Martin, C.R. (2005) Detecting single porphyrin molecules in a conically shaped synthetic nanopore. *Nano Letters*, **5**, 1824.
- Heng, J.B., Ho, C., Kim, T., Timp, R., Aksimentiev, A., Grinkova, Y.V., Sligar, S., Schulten, K. and Timp, G. (2004) Sizing DNA using a nanometer-diameter pore. *Biophysical Journal*, **87**, 2905.
- Ho, C., Qiao, R., Heng, J.B., Chatterjee, A., Timp, R.J., Aluru, N.R. and Timp, G. (2005) Electrolytic transport through a synthetic nanometer-diameter pore. *Proc Natl Acad Sci U S A*, **102**, 10445.
- Hunter, R.J. (1981) *Zeta potential in colloid science, principles and applications*. Academic press, London.
- Ito, T., Sun, L., Bevan, M.A. and Crooks, R.M. (2004) Comparison of nanoparticle size and electrophoretic mobility measurements using a carbon-nanotube-based coulter counter, dynamic light scattering, transmission electron microscopy, and phase analysis light scattering. *Langmuir*, **20**, 6940.
- Ito, T., Sun, L. and Crooks, R.M. (2003) Simultaneous determination of the size and surface charge of individual nanoparticles using a carbon nanotube-based coulter counter. *Analytical Chemistry*, **75**, 2399.
- Itoh, H., Takahashi, A., Adachi, K., Noji, H., Yasuda, R., Yoshida, M. and Kinosita, K. (2004) Mechanically driven ATP synthesis by F1-ATPase. *Nature*, **427**, 465.
- Kaji, N., Tezuka, Y., Takamura, Y., Ueda, M., Nishimoto, T., Nakanishi, H., Horiike, Y. and Baba, Y. (2004) Separation of long DNA molecules by quartz nanopillar chips under a direct current electric field. *Analytical Chemistry*, **76**, 15.
- Kasianowicz, J.J., Brandin, E., Branton, D. and Deamer, D.W. (1996) Characterization of individual polynucleotide molecules using a membrane channel. *Proc Natl Acad Sci U S A*, **93**, 13770.
- Krapf, D., Wu, M.Y., Smeets, R.M., Zandbergen, H.W., Dekker, C. and Lemay, S.G. (2006) Fabrication and characterization of nanopore-based electrodes with radii down to 2 nm. *Nano Letters*, **6**, 105.
- Kricka, L.J. and Wild, D. (2005) Signal generation and detection systems (excluding homogeneous assays). In Wild, D. (ed.), *The Immunoassay Handbook*. Elsevier, Amsterdam, pp. 192-230.
- Lewin, B. (2000) *Genes VII*. Oxford University Press, New York.
- Li, J., Stein, D., McMullan, C., Branton, D., Aziz, M.J. and Golovchenko, J.A. (2001) Ion-beam sculpting at nanometre length scales. *Nature*, **412**, 166.
- Li, J.L., Gershow, M., Stein, D., Brandin, E. and Golovchenko, J.A. (2003a) DNA molecules and configurations in a solid-state nanopore microscope. *Nature Materials*, **2**, 611.
- Li, W.L., Tegenfeldt, J.O., Chen, L., Austin, R.H., Chou, S.Y., Kohl, P.A., Krotine, J. and Sturm, J.C. (2003b) Sacrificial polymers for nanofluidic channels in biological applications. *Nanotechnology*, **14**, 578.
- Lines, R.W. (1992) The electrical sensing zone method. In Stanley-Wood, N.G. and Lines, R.W. (eds.), *Particle Size Analysis*. The Royal Society of Chemistry, Cambridge, pp. 350-374.
- Madou, M.J. (2002) *Fundamentals of microfabrication: the science of miniaturization*. CRC.
- Mara, A., Siwy, Z., Trautmann, C., Wan, J. and Kamme, F. (2004) An asymmetric polymer nanopore for single molecule detection. *Nano Letters*, **4**, 497.
- McCord, M.A. and Rooks, M.J. (1997) Electron beam lithography. In Rai-Choudhury, P. (ed.), *Handbook of microlithography, micromachining and microfabrication*. SPIE press, IEE, London, Vol. 1: Microlithography, pp. 139-249.
- Meller, A., Nivon, L., Brandin, E., Golovchenko, J. and Branton, D. (2000) Rapid nanopore discrimination between single polynucleotide molecules. *Proc Natl Acad Sci U S A*, **97**, 1079.
- Molleman. (2003) *Patch clamping*. John Wiley & Sons, LTD.

- Noji, H., Yasuda, R., Yoshida, M. and Kinosita, K., Jr. (1997) Direct observation of the rotation of F1-ATPase. *Nature*, **386**, 299.
- Peng, C., Gu, J.J., Brandin, E., Kim, Y.R., Qiao, W. and Branton, D. (2004) Probing single DNA molecule transport using fabricated nanopores. *Nano Letters*, **4**, 2293.
- Perkins, T.T., Quake, S.R., Smith, D.E. and Chu, S. (1994) Relaxation of a single DNA molecule observed by optical microscopy. *Science*, **264**, 822.
- Perkins, T.T., Smith, D.E. and Chu, S. (1997) Single polymer dynamics in an elongational flow. *Science*, **276**, 2016.
- Plečis, A., Schoch, R.B. and Renaud, P. (2005) Ionic transport phenomena in nanofluidics: Experimental and theoretical study of the exclusion-enrichment effect on a chip. *Nano Letters*, **5**, 1147.
- Probstein, R.F. (2003) *Physicochemical hydrodynamics, an introduction*. Wiley-Interscience, New Jersey.
- Schenkel, T., Radmilovic, V., Stach, E.A., Park, S.J. and Persaud, A. (2003) Formation of a few nanometer wide holes in membranes with a dual beam focused ion beam system. *Journal of Vacuum Science & Technology B*, **21**, 2720.
- Schoch, R.B. and Renaud, P. (2005) Ion transport through nanoslits dominated by the effective surface charge. *Applied Physics Letters*, **86**, 253111.
- Shaw, D., J. (1989) *Introduction to colloid and surface chemistry*. Butterworth-Heinemann, Oxford.
- Sherman-Gold, R. (1993) *The Axon guide for electrophysiology and biophysics laboratory techniques*. Axon Instruments, Inc.
- Siwy, Z., Dobrev, D., Neumann, R., Trautmann, C. and Voss, K. (2003) Electro-responsive asymmetric nanopores in polyimide with stable ion-current signal. *Applied Physics a-Materials Science & Processing*, **76**, 781.
- Smeets, R.M., Keyser, U.F., Krapf, D., Wu, M.Y., Dekker, N.H. and Dekker, C. (2006) Salt dependence of ion transport and DNA translocation through solid-state nanopores. *Nano Letters*, **6**, 89.
- Smith, D.E. and Chu, S. (1998) Response of flexible polymers to a sudden elongational flow. *Science*, **281**, 1335.
- Stein, D., Kruithof, M. and Dekker, C. (2004a) Surface-charge-governed ion transport in nanofluidic channels. *Physical Review Letters*, **93**, 1.
- Stein, D., Li, J. and Golovchenko, J.A. (2002) Ion-beam sculpting time scales. *Physical Review Letters*, **89**, 276106.
- Stein, D.M., McMullan, C.J., Li, J.L. and Golovchenko, J.A. (2004b) Feedback-controlled ion beam sculpting apparatus. *Review of Scientific Instruments*, **75**, 900.
- Stolz, M., Raiteri, R., Daniels, A.U., VanLandingham, M.R., Baschong, W. and Aebi, U. (2004) Dynamic elastic modulus of porcine articular cartilage determined at two different levels of tissue organization by indentation-type atomic force microscopy. *Biophysical Journal*, **86**, 3269.
- Storm, A.J., Chen, J.H., Ling, X.S., Zandbergen, H.W. and Dekker, C. (2003) Fabrication of solid-state nanopores with single-nanometre precision. *Nature Materials*, **2**, 537.
- Storm, A.J., Chen, J.H., Zandbergen, H.W. and Dekker, C. (2005a) Translocation of double-strand DNA through a silicon oxide nanopore. *Physical Review E*, **71**, 051903.
- Storm, A.J., Storm, C., Chen, J.H., Zandbergen, H., Joanny, J.F. and Dekker, C. (2005b) Fast DNA translocation through a solid-state nanopore. *Nano Letters*, **5**, 1193.
- Sutherland, T.C., Long, Y.T., Stefureac, R.I., Bediako-Amoa, I., Kraatz, H.B. and Lee, J.S. (2004) Structure of peptides investigated by nanopore analysis. *Nano Letters*, **4**, 1273.
- Tas, N.R., Berenschot, J.W., Mela, P., Jansen, H.V., Elwenspoek, M. and van den Berg, A. (2002) 2D-confined nanochannels fabricated by conventional micromachining. *Nano Letters*, **2**, 1031.

## References

- Tas, N.R., Haneveld, J., Jansen, H.V., Elwenspoek, M. and van den Berg, A. **(2004)** Capillary filling speed of water in nanochannels. *Applied Physics Letters*, **85**, 3274.
- Tegenfeldt, J.O., Prinz, C., Cao, H., Chou, S., Reisner, W.W., Riehn, R., Wang, Y.M., Cox, E.C., Sturm, J.C., Silberzan, P. and Austin, R.H. **(2004)** From the Cover: The dynamics of genomic-length DNA molecules in 100-nm channels. *Proc Natl Acad Sci U S A*, **101**, 10979.
- Tong, H.D., Jansen, H.V., Gadgil, V.J., Bostan, C.G., Berenschot, E., van Rijn, C.J.M. and Elwenspoek, M. **(2004)** Silicon nitride nanosieve membrane. *Nano Letters*, **4**, 283.
- Wang, H., Dunning, J.E., Huang, A.P., Nyamwanda, J.A. and Branton, D. **(2004)** DNA heterogeneity and phosphorylation unveiled by single-molecule electrophoresis. *Proc Natl Acad Sci U S A*, **101**, 13472.
- Wang, Y.C., Stevens, A.L. and Han, J.Y. **(2005a)** Million-fold preconcentration of proteins and peptides by nanofluidic filter. *Analytical Chemistry*, **77**, 4293.
- Wang, Y.M., Tegenfeldt, J.O., Reisner, W., Riehn, R., Guan, X.J., Guo, L., Golding, I., Cox, E.C., Sturm, J. and Austin, R.H. **(2005b)** Single-molecule studies of repressor-DNA interactions show long-range interactions. *Proc Natl Acad Sci U S A*, **102**, 9796.
- Washburn, E.W. **(1921)** The dynamics of capillary flow. *Physical Review*, **17**, 273.
- Weiss, S. **(2000)** Measuring conformational dynamics of biomolecules by single molecule fluorescence spectroscopy. *Nature Structural and Molecular Biology*, **7**, 724.
- Wu, M.Y., Krapf, D., Zandbergen, M., Zandbergen, H. and Batson, P.E. **(2005)** Formation of nanopores in a SiN/SiO<sub>2</sub> membrane with an electron beam. *Applied Physics Letters*, **87**, 113106.

# List of publications

## Refereed articles

A. Han, G. Mondin, N.G. Hegelbach, N.F. de Rooij, and U. Staufer.  
*Filling Kinetics of Liquids in Nanochannels as Narrow as 27nm by Capillary Force*  
Journal of Colloid and Interface Science, 2005, **293**, 151.

A. Han, G. Schürmann, G. Mondin, R. Bitterli, N. Hegelbach, N. F. de Rooij, and U. Staufer  
Sensing Protein Molecules Using Nanofabricated Pores  
Applied Physics Letters, 2006, **88**, 093901

A. Han, N.F. de Rooij, and U. Staufer.  
Design and fabrication of nanofluidic devices by surface micromachining  
Nanotechnology, 2006, **17**, 2498.

## Presentations at international conferences and workshops

A. Han, N.F. de Rooij, U. Staufer  
Fabrication of Nanochannels Systems by Surface Micromachining  
NanoTech 2004, Montreux, Switzerland  
Poster

A. Han, G. Mondin, N.G. Hegelbach, N.F. de Rooij, U. Staufer  
Fabrication of Nanochannels Using Photolithography and Partial Etching of Sacrificial Layer  
Micro Total Analysis Systems 2004, Malmö, Sweden, Proceedings, pp. 309-311  
Poster

A. Han, G. Mondin, N. Hegelbach-Guye, N.F. de Rooij, U. Staufer.  
Filling Kinetics of Liquids in Nanochannels down to 27 nm Deep by Capillary Force  
First International Nanofluidics Workshop, Boekelo, The Netherlands  
Poster

A. Han, L. Ceriotti, J. Lichtenberg, N.F. de Rooij, E. Verpoorte  
DNA Fragmentation in a Microfabricated Microfluidic Device  
Micro Total Analysis System 2003, Squaw Valley, USA, Proceedings, pp. 575-578  
Poster, not related to thesis

E. Verpoorte, G.L. Lettieri, L. Ceriotti, A. Han, J. Lichtenberg, N.F. de Rooij.  
Analyzing Nucleic Acids on Microfluidic Devices.  
25th International Symposium on Chromatography, 2004, in Paris, France.  
Invited oral, not related to thesis

E. Verpoorte, L. Ceriotti, G. L.Lettieri, A. Han, J. Lichtenberg, N. F. de Rooij.  
New approaches for DNA sample preparation in open microchannels.  
55th Pittsburgh Conference on Analytical Chemistry and Applied Spectroscopy (Pittcon), 2004,  
Chicago, USA.  
Invited oral, not related to thesis



## A Non-standard Acknowledgements

I do not know who I should thank first, so I will start from the beginning. Some day, after a night of party and drinking, with my head in my pockets, sitting in a sofa, 2<sup>nd</sup> floor, north wing, Nordisk Kollegium, Copenhagen, Denmark. A boring February afternoon 2002 (like all February afternoons in Denmark), I chatted with Francis Romstad, a PhD student in optical communications at the Technical University of Denmark (DTU). He is one of the many heroes in the acknowledgements. Somehow we diverged from our normal, non-academic, discussion; we talked about how to do a PhD in a non-Danish country, as I was fed up with the far right government in Denmark (I should maybe start thanking them first!). He suggested that I should apply for a scholar ship, Internationaliseringsstipendium, very long word, from the Danish Research Agency. The scholarship required a hosting institute and a candidate.

After consulting some of my colleagues at MIC, DTU, the choice fell on Prof. Sabeth Verpoorte (now at University Groningen) and Prof. Nico de Rooij at Samlab, IMT, Neuchâtel, Switzerland. An e-mail was sent to Sabeth 24/3 2002, the deadline of application being 15/4. I must thank Sabeth being willing to take a total stranger as a possible PhD student, we have never met each other before. All odds were against us, very little time to prepare the project description, and the chance of getting the scholarship being 5-10 %. With some luck the grant was positive July 2002. I must thank the Danish Research Agency for the funding, and support. I also apologize to Prof. Martin Dufva, since I turned a DTU PhD scholarship down that we applied for together. I thank Martin for his great understanding and largeness, and the valuable input during my thesis, he was my *Danish contact*.

Finishing my master studies at MIC, DTU. I packed everything I owned and left for Neuchâtel, Switzerland. I arrived one week before 1/11 2002. The shock was incredible. I knew nothing about Switzerland, and nothing at all about Neuchâtel and what awaited me. I should have done better research! My impression was everything else than great, a total nightmare. What was going to happen was even worse. Sometime between July 2002 and 1/11 2002, Sabeth had got a professorship at the University of Groningen, Groningen, the Netherlands. Her PhDs, Jan Lichtenberg (With whom I did my first experiments at IMT, and shared apartment with the first 2 weeks, really great guy.), Arash Dodge and Gian-Luca Lettieri left the laboratory soon after I arrived. This was not the best start ever for my PhD, fortunately not the worst one. I learned that Winston Sun (funny guy) had to change his thesis topic after his supervisor got brain damage after a car accident. I thank Winston and also Torsten Freltoft the CEO of Sophion who suggested that I should not give up.

I was proposed to pack everything I had, again, and leave for the Netherlands. Having visited the lab of Sabeth in Groningen I was almost convinced to go, nice place, nice people, nice weather and great food. Unfortunately, I went to do some shoe shopping, I ended up in a boat yard! The shoes were like heavy battle cruisers! So partly because of practical reasons, I stayed with Prof. de Rooij, with the subject in nanofluidics. I thank Prof. de Rooij for letting a still total stranger, stay, and work in the great Samlab.

The time between the departure of Sabeth and the meeting with the modern missile cruisers of the Netherlands, I worked together with Sander Koster, Alexandra Homsy, Anna-Maria Déléze (The only Scandinavian in our group, we could talk about anything.), Thomas Hug and Laura Ceriotti who was the only “old” PhD of Sabeth. I enjoyed working with Laura; she kept me going by her energy and sometimes her Italian fury. Later on, Prof. Teruo Fujii joined the group as a visiting scientist. What a mental guidance!

I was under the supervision of Prof. Urs Stauffer for whom I thank the most. Great guidance and pushing in the right direction. My work in nanofluidics started slowly and steadily. Summer walked slowly to Neuchâtel. A great feeling. The waves have settled. There was only laminar flow in nanofluidics.



I would like to give my appreciations to the members of the Nanotools group for their input and feedback. Teru Akiyama who taught me about lithography and knows about almost everything in microfabrication. Laure Aeschmann the happiest and only girl in the group. Maurizio Gullo, the expert in cleanroom safety. Daniel Parrat and Sebastian Gautsch who worked hard on an AFM to be flown to the planet Mars by 2007. Raphaël Imer working towards the goal of eliminating problems with the human knee. Benjamin Chui who designed the worlds most complicated AFM. I thank Kaspar Suter, who has the next most difficult job in the world, and still could find time and patience to introduce me to the Raith 150 e-beam lithography system. Later on Gregor Schürmann joined the team, with the most difficult task in the world sitting in the same office as me. Just ask Patrick Carazzetti and Luca Berdondini. I also thank Gregor for valuable scientific input on the work done in nanopores.

I would like to thank the technical staff, cleanroom family, at the ComLab, where I spend a good part of my PhD, both for their technical and spiritual support. Edith Millotte and Gianni Mondin, the caring parents. Nicole Hegelbach and later on Pierre-André Clerc who pushed the limits of reactive ion etching. José Vaquera with his surrealistic connection with the Karl Suss mask aligner. The dedicated efforts of Stéphane Ischer. Sylviane Pochon who entertained during my ultra low noise current measurements. Finally, M. Jeanneret who kept the cleanroom as one of the most stable, very few equipment was ever broken.

On the academic side I am also grateful towards Massoud Dadras for his many hours at the TEM with me, Peter van der Wal, who is always available with his vast experience in electro-chemistry and sober scientific attitude. Silvia Generelli, Kaspar Suter, Roland Bitterli, Peter van der Wal also helped me with useful input for the thesis, for which I am grateful.

I would also like to thank the rest of the Samlab, giving me good advice on the alpine slopes (Michael Zickar), during lunch (Vincent Linder, Renato Krpoun, Danick Briand, Wilfried Noell, Herbert Shea) even better advice after a few beers (long list), and keeping me alive inside.

Apart people from IMT, I would also like to thank our collaborators at the Department of Chemistry Prof. Thomas Ward and Marc Creus. M. Burri from Nanoworld. I would like to thank my apartmentmate through 3 years Veronique Delaforge, great French teacher. Special thanks and appreciations to my girlfriend Gao Wei (Brenda), no words could be found.

Finally, I would like to give my gratitude's to my loving parents. For bringing me up, setting the bar, giving me the support, taking care of themselves, so that I could concentrate on my studies.

**Probably the best parents in the world.**

## **Biography**

Anpan Han was born 8 pm, 18<sup>th</sup> July 1978, Beijing University Hospital (Former 3<sup>rd</sup> hospital of Beijing) China. Spent first 3 years of his life with grandmother on mother's side.

From 1981 to 1988, lived with parents and grandparents on the father's side at the residence for the 9<sup>th</sup> section of the 2<sup>nd</sup> Machine Ministry. Anpan Han never knew what the neighbors did, until the age of 20: nuclear science and industry, including nuclear arms.

From 1988 to 1991, lived in Stockholm Sweden with mother Chenggong Yu, and father Zhenghe Han. Father conducted research in high temperature superconductivity, at the Royal Technical University. From 1991-1993, lived in Linköping and Mantorp, Sweden. Anpan Han moved with parents to Copenhagen Denmark 1993. 1997, graduated from Marie Kruse High School.

1997, enrolled at the Niels Bohr Institute for Astronomy, Physics and Geophysics, University of Copenhagen with mathematics as side subject. Anpan was admitted to stay at the Nordisk Kollegium, Copenhagen, Denmark based on the criteria of excellent academic record. 2001, started work for master thesis at the Department of Micro and Nanotechnology, the Technical University of Denmark. Under the supervision of Prof. Martin Dufva, efforts were made in the development of immunoassay on bio-array format, with applications in the detection of pesticide contamination of drinking water.

2002, received the title Cand. Scient. in Biophysics from the University of Copenhagen. Awarded several Ph.D grants, among others the Internationaliseringsstipendium from the Danish Research Agency. Joined Sensors, Actuators and Microsystems Laboratory, Institute of Microtechnology, University of Neuchâtel, Switzerland. First under the supervision of Prof. Sabeth Verpoorte and later on under the supervision of Prof. Urs. Staufer and Prof. N. F. de Rooij.

Current member of the Foundation of the Student Residence Sablons, Neuchâtel.